

THESIS

NUMERICAL MODELING OF STREAMFLOW ACCRETION BY CONJUNCTIVE USE AT
TAMARACK RANCH STATE WILDLIFE AREA, COLORADO

Submitted by

Jason A. Roudebush

Department of Ecosystem Science and Sustainability

In partial fulfillment of the requirements

For the Degree of Master of Science

Colorado State University

Fort Collins, Colorado

Fall 2013

Master's Committee:

Advisor: John D. Stednick

Michael J. Ronayne
Steven R. Fassnacht

ABSTRACT

NUMERICAL MODELING OF STREAMFLOW ACCRETION BY CONJUNCTIVE USE AT TAMARACK RANCH STATE WILDLIFE AREA, COLORADO

Conjunctive use of groundwater at Tamarack Ranch State Wildlife Area is used to augment streamflow in the Platte River during low flow periods, critical for aquatic species. As part of a cooperative Tri-State Agreement (TSA) with Nebraska and Wyoming, Colorado's portion of the TSA is to pump alluvial groundwater (up to 1,233 ha-m) during periods of unappropriated flow in the river, to recharge ponds located in upland eolian sand deposits, where the water infiltrates into the ground and returns to the river at a later time.

Understanding the location of these recharge ponds and the timing of streamflow accretion is critical for evaluating the effectiveness of recharge operations at Tamarack but has proven difficult to physically measure. To better understand the streamflow-aquifer system changes, a detailed numerical model was created using the MODFLOW Streamflow-Routing technique to simulate physically based groundwater-surface water interaction from managed groundwater recharge.

The simulation modeled groundwater pumping from December 2012 through March 2013 and showed that managed groundwater recharge at Tamarack is producing a quantifiable contribution to streamflow in the desired period of April to September and on the Tamarack property. Streamflow accretion began ten days after the pumps were turned off and the center of mass arrived at the river 16 days later. The total volume of streamflow accretion simulated in this study at the Red Lion Bridge was 878,000 m³, 13% of the 6,887,000 m³ of groundwater pumped into the recharge ponds in water year 2013. Streamflow accretion had not fully

diminished by the end of model simulation in August 2013, warranting further study to better account for all streamflow accretions.

ACKNOWLEDGMENTS

I would like to express my deepest appreciation to my advisor, Dr. John Stednick, who supported me throughout this academic endeavor with his incredible knowledge and guidance. I have been very fortunate to learn the scientific method under someone with such enthusiasm and passion for Watershed Science.

Special thanks to Dr. Mike Ronayne for his endless patience and first rate knowledge of groundwater modeling. He is one of the best teachers I've ever had, and without his counsel and model diagnostic skills, this project would not have been possible. I am also grateful to Dr. Steven Fassnacht for his contributions to my thesis committee and to Dr. Lee MacDonald whose encouragement, enthusiasm, and faith in me has been extremely helpful.

I would like to thank Erin Donnelly, Reece Lonsert, Levi Kokes of Colorado Parks and Wildlife, and John Altenhofen of the Northern Colorado Water Conservancy District for providing invaluable field data that made this study possible.

Finally I would like to thank my parents, Gary and Sandy, for always believing in me and encouraging me to pursue my dreams. My wife, Lisa, whose constant support and endless encouragement allowed me to finish this journey. She spent countless hours editing manuscripts, listening to presentation rehearsals, and providing excellent advice that shaped my direction. I also would like to thank my in-laws, Tim and Cine, for their unconditional support and encouragement.

This research was funded by the Colorado Water Institute and Colorado Parks and Wildlife through the Species Conservation Trust.

TABLE OF CONTENTS

ABSTRACT.....	ii
ACKNOWLEDGEMENTS.....	iv
LIST OF TABLES.....	vii
LIST OF FIGURES.....	viii
CHAPTER 1: INTRODUCTION.....	1
1.1 Background.....	1
1.2 Study Goal.....	5
1.3 Study Objectives.....	5
CHAPTER 2: METHODOLOGY.....	6
2.1 Site Description.....	6
2.2 Groundwater Modeling.....	8
2.2.1 Model Domain and Grid.....	10
2.2.2 Model Boundary Conditions.....	12
2.2.3 Model Properties.....	16
2.2.4 Model Parameters.....	17
2.3 Steady-State Simulation.....	19
2.4 Steady-State Calibration.....	19
2.5 Transient Flow Simulation.....	20
CHAPTER 3: RESULTS.....	22
3.1 Stream.....	22
3.2 Evapotranspiration.....	24

3.3 General Head Boundaries	24
3.4 Steady-State Model Calibration	25
3.5 Steady State Head Contours.....	29
3.6 Transient Model Simulation	32
3.7 Transient Head Contouring.....	35
3.8 Transient Model Water Budget.....	40
3.9 Stream-Aquifer Interaction	42
3.10 Advective Transport Simulation	53
CHAPTER 4: DISCUSSION.....	56
4.1 Steady-State Model Calibration and the Groundwater Flow Field.....	56
4.2 Transient Model Simulation	57
4.2.1 Transient Water Budget	58
4.2.2 Stream-Aquifer Interaction	59
4.3 Advective Transport.....	61
CHAPTER 5: CONCLUSIONS	62
CHAPTER 6: RECOMMENDATIONS.....	63
LITERATURE CITED	65
APPENDIX A - Detailed Model Input Variables and Transient Water Budget.....	69
APPENDIX B - Groundwater-Surface Water Flux and Stream Depth Plots	73

LIST OF TABLES

Table 1: Evapotranspiration rating factor and rates by month.

Table 2: General Head Boundary (GHB) input variables for the east and west model boundaries. Variables include hydraulic conductivity (m/d), distance to the GHB (m), width of the GHB cell (m), and the range of saturated thickness in GHB cells (m).

Table 3: Simulated heads and observed hydraulic heads for 10 September 2009, used to calibrate the steady-state model. Coordinate system for geographic locations: NAD 1983, UTM 13N.

Table 4: Steady-state calibration statistics including number of observations, minimum residual (m), maximum residual (m), mean error (m), mean absolute error (m), range of data (m), mean absolute error/range, and the Nash-Sutcliffe efficiency coefficient.

Table 5: Calibrated stream properties used to calculate the streambed conductance term including streambed hydraulic conductivity (m/d), streambed thickness (m), stream width (m), length of each stream cell (m), Manning's coefficient, and the stream constant (m^3/d).

Table 6: Total volume (m^3) pumped per stress period for each groundwater recharge well.

Table 7: Total volume (m^3) of water delivered to each recharge pond per stress period.

Table 8: Simulated mean daily streamflow accretion (m^3/s), mean daily streamflow (m^3/s), and streamflow accretion percent contribution to total streamflow for the period 10 April 2013 – 31 August 2013 at the Red Lion Bridge (stream reach 232).

LIST OF FIGURES

Figure 1: Location of model domain within the South Platte River Basin. The Basin is symbolized by elevation in meters.

Figure 2: Points of bedrock interpretation used to develop the confining unit surface. Data include boreholes, surface Electrical Resistivity Tomography surveys, and faux points developed from nearby boreholes.

Figure 3: Map of the study area including recharge ponds, pumping wells, South Platte River, no-flow boundaries, and extent of the riparian area. Recharge pond and pumping well naming convention assigned by the State of Colorado.

Figure 4: Mean daily streamflow at the Crook gaging station for the period 10 July 2009 – 10 September 2009.

Figure 5: Stream depth and streamflow measurement relationships at the Crook streamflow gaging station (data from Donnelly, 2012).

Figure 6: Steady-state plot of simulated vs. observed heads in meters.

Figure 7: Steady-state stream depth for every stream reach in the model. Stream reaches are sequentially numbered from 0, the furthest upstream reach, to 351, the furthest downstream reach.

Figure 8: Location of steady-state model calibration points, recharge ponds, South Platte River, no-flow boundaries and the extent of the riparian area.

Figure 9: Steady-state head contours in 1m increments, calibrated to water levels observations on 10 September 2009. Contours are labeled in meters above sea level.

Figure 10: Daily pumping rates (m^3/d) for the recharge wells at Tamarack, utilized in the transient simulation.

Figure 11: Simulated head contours on 31 March 2013, the last day of recharge operations. Contours are labeled in 1 meter increments on the base map and 0.5 meter increments on the inserts. All contours are labeled meters above sea level.

Figure 12: Simulated head contours on 15 April 2013, two weeks after the end of recharge operations. Contours are labeled in 1 meter increments on the base map and 0.5 meter increments on the inserts. All contours are labeled meters above sea level.

Figure 13: Simulated head contours on 1 June 2013, two months after the end of recharge operations. Contours are labeled in 1 meter increments on the base map and 0.5 meter increments on the inserts. All contours are labeled meters above sea level.

Figure 14: March 2013 transient model water budget with aquifer inflows in blue and outflows in red for the eastern and western boundary underflows, stream leakage, precipitation recharge, aquifer storage, evapotranspiration, pumping wells, and recharge ponds.

Figure 15: July 2013 transient model water budget with aquifer inflows in blue and aquifer outflows in red for the eastern and western boundary underflows, stream leakage, precipitation recharge, aquifer storage, evapotranspiration, pumping wells, and recharge ponds.

Figure 16: Simulated stream depth, with and without pumping, for each stream reach, 31 March 2013. Stream reaches are sequentially numbered from 0, the furthest upstream reach, to 351, the furthest downstream reach.

Figure 17: Simulated groundwater/surface water flux rate, with and without pumping, for each stream reach, 31 March 2013. Stream reaches are sequentially numbered from 0, the furthest upstream reach, to 351, the furthest downstream reach.

Figure 18: Simulated stream depth, with and without pumping, for each stream reach, 31 July 2013. Stream reaches are sequentially numbered from 0, the furthest upstream reach, to 351, the furthest downstream reach.

Figure 19: Simulated groundwater/surface water flux rate, with and without pumping, for each stream reach, 31 July 2013. Stream reaches are sequentially numbered from 0, the furthest upstream reach, to 351, the furthest downstream reach.

Figure 20: Location streamflow gaging stations (Stream Reaches 20, 112, 218, 232, and 351) used to compute streamflow hydrographs with the GAGE package. Also included are the Tamarack property boundary, locations of the recharge ponds, pumping wells, South Platte River, no-flow boundaries and the extent of the riparian community.

Figure 21: Transient hydrographs at stream reach 20 for both the pumping and non-pumping transient models (m^3/d).

Figure 22: Transient hydrographs at the Red Lion Bridge (stream reach 232) for both the pumping and non-pumping transient models (m^3/d).

Figure 23: Change in streamflow (m^3/d) at the Red Lion Bridge (stream reach 232) calculated by subtracting the non-pumping model hydrograph from the pumping model hydrograph (shown in Fig. 22).

Figure 23: Change in streamflow (m^3/d) at Stream Reach 20, calculated by subtracting the non-pumping model hydrograph from the pumping model hydrograph (shown in Fig. 22).

Figure 24: Change in streamflow (m^3/d) at Stream Reach 112, calculated by subtracting the non-pumping model hydrograph from the pumping model hydrograph (shown in Fig. 22).

Figure 25: Change in streamflow (m^3/d) at Stream Reach 218, calculated by subtracting the non-pumping model hydrograph from the pumping model hydrograph (shown in Fig. 22).

Figure 26: Change in streamflow (m^3/d) at the Red Lion Bridge (stream reach 232) calculated by subtracting the non-pumping model hydrograph from the pumping model hydrograph (shown in Fig. 22).

Figure 27: Change in streamflow (m^3/d) at the eastern model boundary (Stream Reach 351), calculated by subtracting the non-pumping model hydrograph from the pumping model hydrograph (shown in Fig. 22).

Figure 28: Total simulated streamflow accretion (m^3/s) at the Red Lion Bridge (stream reach 232) from 10 April 2013 to 31 August 2013.

Figure 29: Transient model forward particle tracking for the period: 1 December 2012 – 31 August 2013. Each arrow represents 30 days of elapsed time.

CHAPTER 1

INTRODUCTION

1.1 Background

Water in Colorado is a precious shared resource requiring optimal usage to sustain population growth and environmental needs. The often semi-arid Colorado climate characterized by low precipitation, high potential evapotranspiration, and frequent drought periods necessitates prudent water resource management. Water resource managers in Colorado are tasked with strategically balancing variable water supplies with increasing demands from agricultural, municipal, industrial, and recreational users. To meet increasing demands, the coordinated use of surface water and groundwater supplies, also known as conjunctive use, has become a promising approach to achieving multiple water resource objectives [Blomquist *et al.*, 2001]. Conjunctive use in a stream-aquifer system requires mathematical modeling to understand streamflow effects. Modern groundwater hydrology began in 1940 when C.V. Theis developed an equation to model aquifer system responses to pumping through time and has expanded to include analytical solutions and more complex numerical modeling [Bredehoeft, 2012]. The utilization of mathematical solutions and models has become an important tool for water resource managers and the increased regulatory decision making process.

The Prior Appropriation Doctrine of “first in time, first in right” governs water usage in Colorado and was originally developed for surface waters [Stenzel and Cech, 2013]. In 1876, when Colorado became a state and the Prior Appropriation Doctrine was written, the amount of groundwater lying beneath the surface was unknown. In 1886 the first documented irrigation well was excavated in the Lone Tree Creek alluvium near Eaton, Colorado, marking the

beginning of groundwater development in Colorado, particularly along the lower South Platte River [Stenzel and Cech, 2013]. Well construction and groundwater pumping rapidly expanded until 1957 when the State Legislature established the Ground Water Commission to address the problem of aquifer depletion on the eastern plains [Hobbs, 1999]. In 1965 the Groundwater Management Act established the framework for governing groundwater use and development in Colorado. After the passage of the 1965 Act, issues regarding groundwater regulation remained. In 1969 the Water Rights Determination Act created seven water divisions along major watershed boundaries and integrated tributary groundwater and surface-water into the same administration system. The 1969 Act also authorized the use of streamflow augmentation plans which allow out-of-priority diversions that would have been curtailed otherwise [Hobbs, 1999].

Along the lower South Platte River in Colorado, where the stream and unconfined alluvial aquifer are hydraulically connected, augmentation plans have become a common conjunctive use method allowing agricultural wells to pump while protecting existing water rights. Augmentation is the replacement of water depleted from a stream system by an out-of-priority diversion (ie. well pumping). When adjudicated and operated to replace depletions to the stream, the out-of-priority diversions are allowed to continue even if a call has been placed on the stream by a senior water right [Stenzel and Cech, 2013]. Currently there are approximately 7,500 high capacity (>190 liters/min) alluvial groundwater wells in Division One (South Platte River Basin). Roughly 5,500 of those wells are tributary groundwater wells permitted or decreed under an augmentation or substitute water supply plans [Heidi Garner, personal communication, 30 April 2013].

Four threatened or endangered species: the whooping crane (*Grus americana*), interior least tern (*Sterna antillarum*), piping plover (*Charadrius melodus*), and pallid sturgeon

(*Scaphirhynchus albus*) on the Platte River in Nebraska, prompted the states of Colorado, Wyoming and Nebraska to enter into a cooperative Tri-State Agreement with the U.S. Fish and Wildlife Service to implement recovery efforts by improving riverine habitats for these species [Freeman, 2010]. This agreement, known as the Platte River Recovery Implementation Program (PRRIP), began on January 1, 2007 while allowing water use and development to continue in the Platte River Basin. Wyoming's obligation under PRRIP is met by operating an environmental account in Pathfinder Reservoir to retine streamflow during periods of target flow shortages. Nebraska operates a similar environmental account in Lake McConaughy to retine flows while also conducting in-channel vegetation removal and providing additional land habitat for aquatic species in the Lexington to Chapman reach of the Platte River [PRRIP, 2013]. Colorado's contribution is the Tamarack artificial groundwater recharge project near the town of Crook. Managed groundwater recharge at Tamarack is designed to meet the state of Colorado's obligation to increase streamflow in the Platte River by an average of 1,200 (hectare-meters) per year [Freeman, 2010]. This obligation is met by pumping alluvial groundwater during winter months of unappropriated streamflow, to recharge ponds located in upland eolian sand deposits, where the water infiltrates into the ground and returns to the river at a later time. Under designed conditions, recharge water flows through the aquifer system with a timing that supplements streamflow during periods of critical low-flow between April and September.

During the Tamarack project design, the physical location of the recharge ponds was determined with United States Geological Survey (USGS) Stream Depletion Factor (SDF) maps [Hurr and Schneider, 1972a]. SDF maps are based on bedrock data collected from a series of boreholes and have been the predominant method used to quantify stream effects from well pumping in Colorado for over 30 years [Hurr and Schneider, 1972a; Miller et al, 2007]. The

SDF is a semi-analytical solution used to analyze depletion to streams caused by well pumping and is defined as the time (days) of the point in which the volume of stream depletion is 28% of the volume pumped for a given location. The solution in a mathematically ideal aquifer is expressed as:

$$\text{SDF} = \frac{a^2 S}{Tt} \quad (\text{Equation 1})$$

where:

a is the perpendicular distance from the well (L), **S** is specific yield (L^3/L^3), **T** is the transmissivity (L^2/T), and **t** is the pumping time [Jenkins 1968]. Numerical modeling is then used to account for impermeable boundaries and other non-ideal aquifer properties [Miller et al., 2007]. At conjunctive use sites like Tamarack, the SDF is used in reverse because volume is added to the stream from recharge ponds [Beckman, 2007].

While, the SDF is a widely accepted method to estimate the effects of groundwater pumping on streamflow, it over-simplifies physical conditions [Fox *et al.*, 2002]. To better quantify relationships within the groundwater flow system at Tamarack, Colorado Parks and Wildlife (CPW), formerly the Colorado Division of Wildlife (CDOW) developed a numerical MODFLOW [Harbaugh *et al.*, 2000] model based on aquifer conditions in the vicinity of the recharge wells to evaluate groundwater-surface water exchange [CPW vs. State of Colorado, 2012]. As a result, Unit Response Functions (URFs) were adapted to take the place of the outdated SDF method of aquifer management. The URF approach is based on the use of an optimization model in ArcGIS, coupled with a numerical groundwater flow model (Larroque *et al.*, 2008).

Much of the aquifer characterization in the CPW model was based on earlier work utilizing borehole data that mapped the presence of a paleo-channel influencing groundwater

flow in the study area [Hurr and Schneider, 1972a]. A recent Electrical Resistivity Tomography (ERT) investigation into the subsurface stratigraphy of the eolian sands, alluvial sediments and bedrock confining units suggests the geometry of the South Platte alluvial aquifer is more complex than previously understood by revealing steeper topographic relief in the area between the recharge ponds and the river. The buried paleo-landscape of incised valley floor depressions, heavily eroded amphitheater channel heads, and steep side walls, potentially act as a preferential flow pathways for recharge water [Lonsert, 2013]. Incorporation of this new confining bedrock topography into a new MODFLOW numerical model should provide a more detailed hydraulic head solution and a better understanding of the location and timing of streamflow accretions due to managed groundwater recharge.

1.2 Study Goal

Determine if managed groundwater recharge at Tamarack increases streamflow in the study area, during periods of target flow shortages, as modeled by MODFLOW, with physically based groundwater-surface water interaction.

1.3 Study Objectives

To determine the timing and location of streamflow accretion, this study had the following objectives:

1. Build and calibrate a steady-state MODFLOW groundwater flow model of the study area to characterize the regional groundwater flow field.
2. Model and evaluate groundwater-surface water interaction with transient simulations in MODFLOW, to determine the location and timing of streamflow accretion and the transient water budget at Tamarack.

CHAPTER 2

METHODOLOGY

2.1 Site Description

The Tamarack Ranch State Wildlife Area is operated by CPW and is located on approximately 48 km² of land, along the lower South Platte River in Logan County, Colorado (Fig. 1). The Tamarack recharge project began in 1997 and consists of ten high capacity wells, four recharge ponds, 22 piezometers, and seven abandoned irrigation wells. In 2013, the project was undergoing expansion to include a total of 16 high-capacity wells and 5 recharge ponds [L. Kokes, personal communication, 2013].

The South Platte River flows from west to east at a gradient of 1.3 m/km in the study area, and is characterized by an incised channel and a flat channel bottom. The incised channel and heavily vegetated banks result in increased depth but not increased width with increased discharge [Donnelly, 2012]. The stream is flanked on both banks by a forest of riparian phreatophytic vegetation, up to one kilometer wide. The riparian forest is dominated by the plains cottonwood (*Populus deltoides*), and to a lesser extent, the peach-leaved willow (*Salix amygdaloides*). The trees are largely confined to swales and low areas on the floodplain where soils are fine textured and water accumulates during runoff. Little to no shrub canopy is present and the undergrowth is primarily tall slough grass (*Spartina pectinata*) [Kittel *et al.*, 1998]. Areas away from the stream channel are vegetated eolian sand deposits consisting of very fine to medium grained sand [Bjorkland and Brown, 1957]. The eolian sand hills provide an ideal location for recharge ponds due to the high permeability of the sands directly overlying the alluvium [Warner *et al.*, 1986].

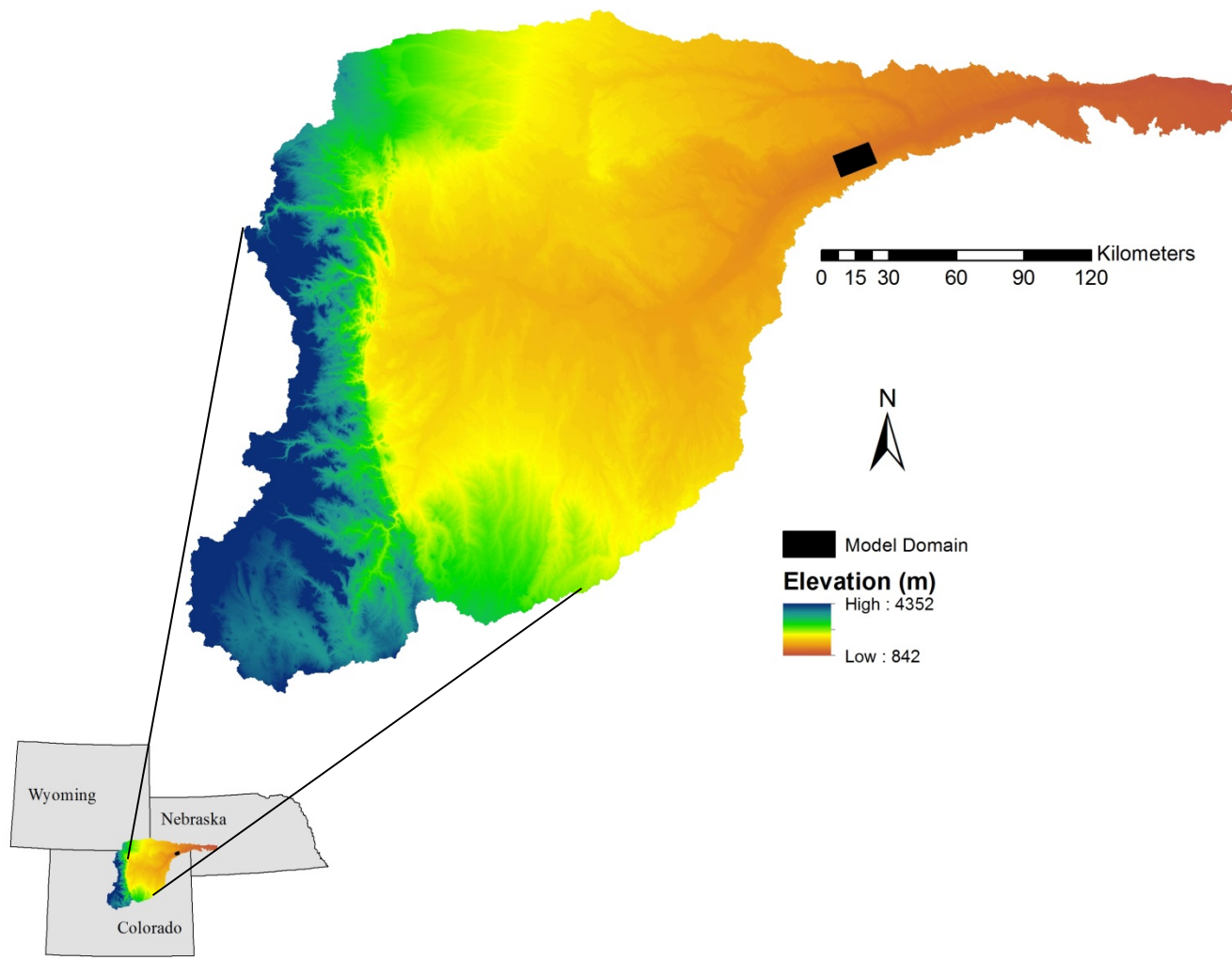


Figure 1: Location of model domain within the South Platte River Basin. Map projection is NAD 1983 UTM 13N. Data sources for the map: nationalatlas.gov and nationalmap.gov.

In the study area, the unconfined alluvial aquifer is underlain by the Tertiary White River Group and the upper Cretaceous Pierre Shale Formation [Lonsert, 2013]. The White River Group is comprised of the Brule and Chadron Formations and consists of poorly cemented beds of silt and clay which are relatively impermeable and form the base of the aquifer [Poceta, 2005; Lonsert, 2013]. Deposited on the White River Group and Pierre Shale, is the valley fill aquifer which consists of Pleistocene and recent alluvium deposited by the South Platte River [Warner *et al.*, 1986]. The alluvium consists of a heterogeneous mixture of well sorted to poorly sorted sand, gravel, and clay lens channel deposits [Bjorkland and Brown, 1957; Warner *et al.*, 1986; Beckman, 2007; Lonsert, 2013]. The alluvium is up to 90 m thick beneath the river and has high hydraulic conductivity values. Aquifer and tracer tests in the alluvium suggest horizontal hydraulic conductivities ranging from 45 to 460 m/d with specific yield values ranging from 10 - 20% [Burns, 1985; Fox, 2003; Halstead and Flory, 2003; Paschall *et al.*, 2006; Donnelly, 2012].

2.2 Groundwater Modeling

Understanding the location and timing of streamflow accretion is critical for evaluating the effectiveness of recharge operations at Tamarack but has proven difficult to physically measure [Donnelly, 2012]. Small aquifer system changes, undetectable with physical measurements are better understood with the help of mathematical models. Mathematical models are a mathematical expression, or group of expressions, that describes the hydraulic relationships within a groundwater flow system [Remson *et al.*, 1971]. MODFLOW, a commonly used computer code for finite difference numerical modeling, is capable of simulating fully three-dimensional groundwater flow in systems that are horizontally and vertically heterogeneous and have complex boundary conditions [Harbaugh *et al.*, 2000]. It was developed

by the USGS [McDonald and Harbaugh, 1983] and solves for groundwater flow with the following partial differential equation:

$$\frac{\partial}{\partial x} \left(K_{xx} \frac{\partial h}{\partial x} \right) + \frac{\partial}{\partial y} \left(K_{yy} \frac{\partial h}{\partial y} \right) + \frac{\partial}{\partial z} \left(K_{zz} \frac{\partial h}{\partial z} \right) + W = S_s \frac{dh}{dt} \quad (\text{Equation 2})$$

where:

K_{xx} , K_{yy} , and K_{zz} are values of hydraulic conductivity (L/T) along the x, y, and z coordinate axes; h is the hydraulic head (L); W is a volumetric flux per unit volume (T^{-1}) representing sources and/or sinks of water; S_s is the specific storage (L^{-1}) of the porous material; and t is time (T) [McDonald and Harbaugh, 1988]. Using the finite difference method, MODFLOW then solves for hydraulic head, everywhere it is unknown, by replacing the continuous derivatives from the governing flow equation with new algebraic expressions at each node in the domain.

Source/sink terms (W in Equation 2) within the model are contributions to/from streamflow, evapotranspiration, precipitation recharge, pumping wells, and injection wells.

Groundwater-surface water interaction, in the form of streamflow accretion or depletion, can be modeled in MODFLOW with the Streamflow-Routing (SFR) package [Prudic *et al.*, 2004]. The SFR package calculates both stream baseflow and groundwater flow at the midpoint of each cell stream cell. Separation of the two distinct water budgets allows for the quantification of streamflow accretions and depletions from managed groundwater recharge.

Model scenarios were developed with Environmental Simulations Inc.'s Groundwater Vistas[©] software (GV) [Rumbaugh and Rumbaugh, 2011]. GV is a commercially available graphical interface for pre- and post-processing of MODFLOW models.

2.2.1 Model Domain and Grid

Three-dimensional models are utilized to simulate unconfined aquifers with significant vertical head gradients [Anderson and Woessner, 1992]. At Tamarack, vertical hydraulic gradients are important in the vicinity of the recharge ponds where water is moving down through the eolian sand into the alluvium, and also at the stream-aquifer interface. The model domain is 17.6 km (east to west) by 9.8 km (north to south) and incorporates the natural physical and hydraulic boundaries of the South Platte alluvial aquifer. It is comprised of two layers, split into 79,554 active cells, arranged in a grid of 262 columns and 179 rows. Grid cells spacing along the x- and y-axes ranges from 25 to 100 m, with the highest density of cells occurring in the area of new confining bedrock topographic interpretations (Fig. 2). There are 351 stream cells, 525 General Head Boundary (GHB) cells, 96 injection wells (transient model), 10 pumping wells (transient model), and 14,242 inactive no-flow cells in the model.

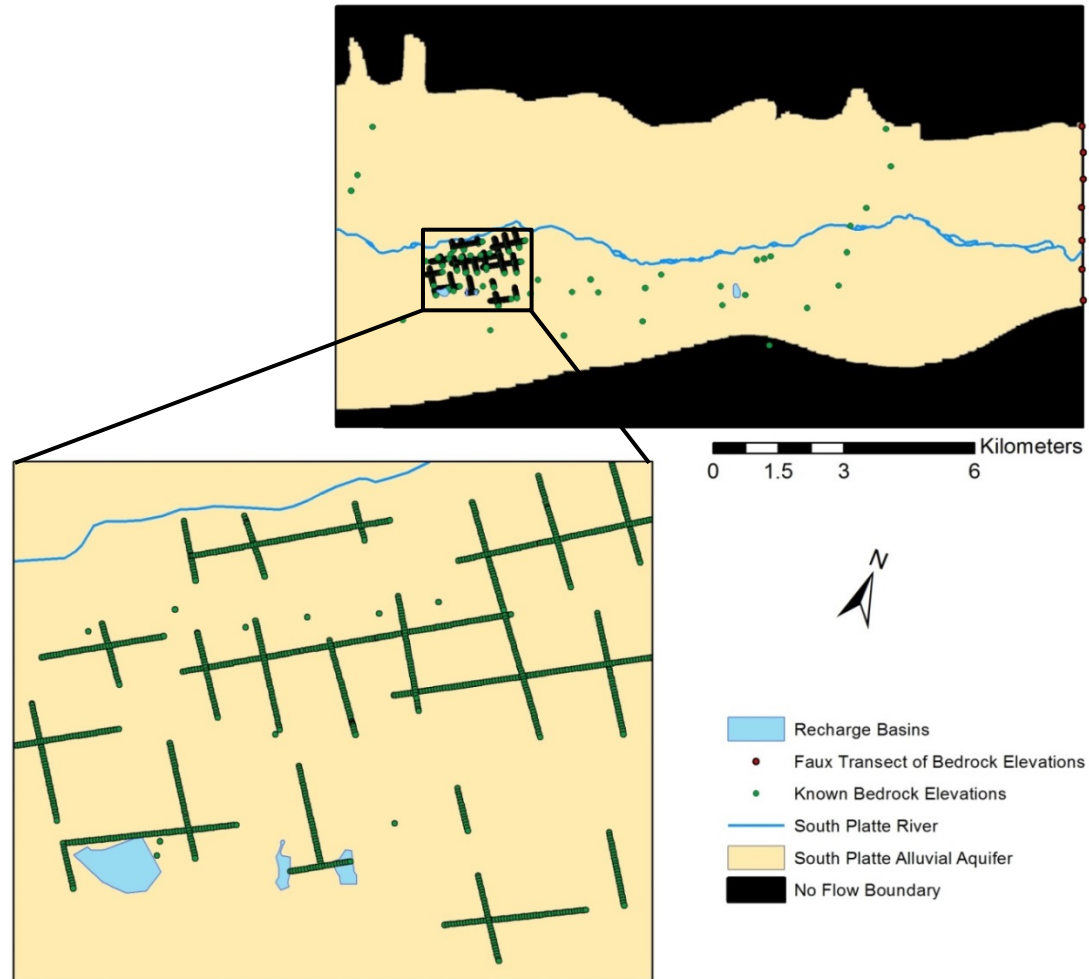


Figure 2: Points of bedrock interpretation used to develop the confining unit surface. Data include boreholes, surface Electrical Resistivity Tomography surveys, and faux points developed from nearby boreholes. Map projection is NAD 1983 UTM 13N. Data sources for the map: Lonsert 2013, Colorado Division of Water Resources and Colorado Parks and Wildlife.

2.2.2 Model Boundary Conditions

The groundwater recharge project at Tamarack consists of ten high-capacity pumping wells, with a maximum individual discharge rate of 7.65 cubic meters per minute (m^3/min), and four recharge ponds. A detailed pumping schedule was obtained from The Northern Colorado Water Conservancy District [J. Altenhofen, personal communication, 2013] and the locations, depths, and screened intervals for the pumping wells were obtained from CPW [Levi Kokes, personal communication, 2013]. All pumping wells are located in the alluvium near the river, in model layers one and two, and were modeled using Analytic Elements (Fig. 3). The four recharge ponds are located south of the stream, in the eolian sand hills (Fig. 3). The ponds range from 0.47 – 5.78 hectares in size, and are located 750 – 1175m away from the river. All four ponds were modeled as injection wells in Layer 1 of the model. Pumping rates for each injection well were averaged based on the number of cells located inside the recharge pond boundary at full capacity.

The South Platte River was simulated as a partially penetrating stream in Layer 1 with the SFR package. The western model boundary is aligned with the CDWR streamflow gaging station and defines the uppermost reach of the river (Stream reach 1). The streamflow gaging records provided for an accurate representation of streamflow entering the model; subsequent contributions to base flow downstream of the gage represent spatially variable groundwater inputs, including streamflow accretions from recharge operations. The period of record for the Crook gaging station dates from September 2007 to present.

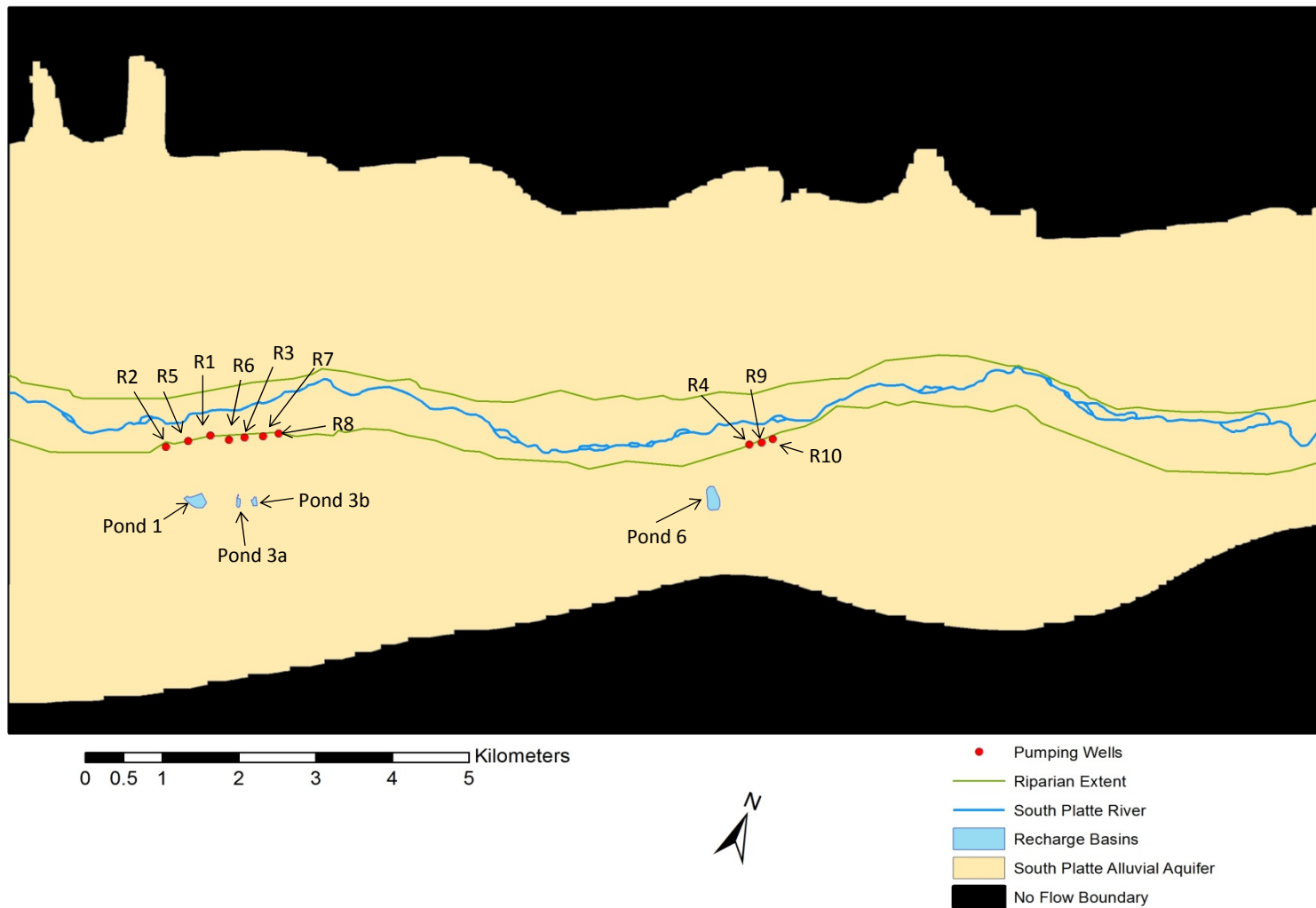


Figure 3: Map of the model domain including recharge ponds, pumping wells, South Platte River, no-flow boundaries, and extent of the riparian area. Recharge pond and pumping well naming convention assigned by the State of Colorado. Map projection is NAD 1983 UTM 13N. Data sources for the map: Colorado Division of Water Resources and Colorado Parks and Wildlife.

To model the stream boundary, variables for streamflow, stream depth, streambed elevation, streambed conductance, and Manning's roughness coefficient must be assigned. Streamflow and stream depth are assigned at the furthest upgradient stream cell as a starting point for the SFR package, which simulates stream depth in the model based on one of five different methods. Channel width did not increase with increased streamflow, indicating an entrenched channel with no lateral expansion, especially at low flows [Donnelly, 2012]. With an entrenched channel and relatively flat stream bottom, the best option for simulating stream depth is SFR package option two which uses Manning's equation to determine depth as a function of flow [Prudic *et al*, 2004]. Field observations of the streambed material suggest consistent particle sizes throughout the study reach and allow the use of a single Manning's roughness coefficient to model the streambed. SFR option two assumes a wide rectangular channel where stream width is much greater than stream depth. With this option, surface water flow between stream cells is computed as:

$$Q = \left(\frac{C}{n}\right) w y^{\frac{5}{3}} S^{\frac{1}{2}} \quad (\text{Equation 3})$$

where:

Q is the stream discharge (L^3/T), C is a constant of 86,400 for units of (m^3/day), n is Manning's roughness coefficient (dimensionless), w is the width of the channel (L), y is the depth of water in the stream (L), and S is slope of the stream channel (L/L) [Prudic *et al*, 2004].

Flow between the stream and the aquifer is computed using Darcy's Law and assumes uniform depth over a given section of stream and corresponding volume of aquifer [Prudic *et al.*, 2004]. The exchange flow is computed with the following equation:

$$Q_L = \frac{KwL}{m} (h_s - h_a) \quad (\text{Equation 4})$$

where:

Q_L is the volumetric flow between a given section of stream and volume of aquifer (L^3/T); K is the hydraulic conductivity of the streambed (L/T); w is the width of stream (L); L is the length of stream (L); m is the thickness of the streambed (L); h_s is the head in the stream determined by adding stream depth to elevation of the streambed (L); h_a is the head in the aquifer beneath the streambed (L) [Prudic *et al.*, 2004].

Regional aquifer recharge from precipitation is difficult to measure and not well known. In the often semi-arid environment of northeastern Colorado, it is thought to be an insignificant component of the total water budget. Previous groundwater modeling of Tamarack [Burns, 1985] suggested a uniform recharge rate of 0.5 cm/y. This recharge rate was used in the model and evaluated in the steady-state sensitivity analysis. During sensitivity analyses, calibrated values are systematically changed within a plausible range to evaluate the magnitude change in hydraulic heads [Anderson and Woessner, 1992]. The results reveal the sensitivity of the model to the specific parameter with regard to the head solution.

The lateral boundaries to the north and south are formed by the edges of the alluvial deposits, digitized from USGS Geologic Maps of the area [Scott, 1978], and are considered to be no-flow boundaries. The western edge of the model is located along State Highway 55 where the Colorado Division of Water Resources (CDWR) operates a streamflow gaging station; the eastern edge is 17.6 kilometers downstream, to the southeast. A head dependent boundary condition was applied to both the inflow (west) and outflow (east) boundaries using MODFLOW's GHB package. The GHB package allows the boundary flux to vary by simulating flow into or out of a cell from an external source in proportion to the difference between head in the cell and head assigned to the external source [Harbaugh *et al.*, 2000].

2.2.3 Model Properties

Land surface elevations were downloaded from the USGS National Elevation Dataset (NED) server as a 1 arc-second Digital Elevation Model (DEM) [U.S. Geological Survey, 2013]. The raw DEM was imported into ArcGIS® 10.0 and projected into the North American Datum 1983 Universal Transverse Mercator 13 North (NAD 83 UTM 13 N) coordinate system. The DEM was then converted into x, y and z coordinate data and imported into GV to define the top of Layer 1.

Surface ERT data were used in combination with drill logs, to create the confining bedrock surface map in ArcGIS® 10.0 [Bjorklund and Brown, 1957; Lonsert, 2013]. Points of bedrock interpretation exhibit a wide range of spatial variability (Fig. 3), therefore the Inverse Distance Weighting (IDW) method of spatial interpolation was utilized to extrapolate bedrock elevations between previously interpreted points. The recent surface ERT data are concentrated in the vicinity of recharge ponds 1 and 3b, and the previous drill log data are spread out in a series of north to south transects (Fig. 3). After initial interpolation of these data, the confining unit surface along the eastern boundary was determined to be too shallow and did not reasonably match the conceptual model, largely due to sparse bedrock data in the area. To better fit the conceptual model, aquifer thickness along the eastern boundary was increased by inserting a transect of faux bedrock points. Seven faux points were created using the nearest bedrock interpretations to the east and west and applying a weighted average of those elevations based on distance. The resulting faux transect was used with existing bedrock interpretations to create the confining unit surface in ArcGIS® 10.0 via IDW.

2.2.4 Model Parameters

Riparian vegetation uses water in evapotranspiration and is an important component of the water budget during the spring, summer and fall months. The spatial discretization of riparian vegetation was accomplished in ArcGIS[®] 10.0 by tracing satellite imagery [ESRI, 2013] of the site with lines (shapefiles) that could be imported into GV. ET is simulated in MODFLOW with the Evapotranspiration (EVT) package [McDonald and Harbaugh, 1988] and calculates water loss from the system based on the simulated hydraulic head in the cell, a maximum ET flux rate, and an extinction depth. The two required model inputs for the EVT package are: ET flux (L/T), and ET extinction depth (L) but these quantities are variable and have to be estimated.

ET flux varies throughout the day depending on weather, vegetation, and soil, so it is necessary to simplify the conceptual model into a single rate for a given stress period. Riparian cottonwood stands in the western U.S. have been shown to transpire 3-6 mm of water per day (mm/d) [Williams and Cooper, 2005]. A maximum ET rate in the model was 3 mm/d during the hot summer months and was decreased for the off-peak months using a scaling factor (Table 4). The scaling factor accounts for time of year and better represents the natural system between May when the cottonwood trees leaf-out, and October when leaves senesce with shorter days and cooler nights [Gazal *et al.* 2006, D.Cooper, personal communication, 2013].

Extinction depth is the depth to which plant roots extend below land surface and evapotranspiration from groundwater ceases. Cottonwood roots can reach depths up to 10 m but experience canopy dieback and mortality when depth to groundwater exceeds 2.5 - 3m [Horton *et al.*, 2001; Landmeyer, 2011]. Extinction depth for the model was set to 3m.

Tracer and aquifer tests at Tamarack indicate a wide range of possible horizontal hydraulic conductivities (45 - 450 m/d) due to the heterogeneous nature of the fluvial sediments [Burns, 1985; Fox, 2003; Halstead, 2003; Paschall *et al.*, 2006; Donnelly, 2013]. The entire range of suggested hydraulic conductivities was investigated during model calibration. The anisotropy ratio was also investigated during calibration because fluvial sediments have been shown to have horizontal conductivity values between two and ten times larger than vertical conductivity values [Freeze and Cherry, 1979].

The storage term for unconfined aquifers is *specific yield* and is defined as the volume of water that it released from storage per unit surface area of aquifer or per unit decline in the water table [Freeze and Cherry, 1979]. Aquifer tests of the study area suggest a specific yield value between 10 - 30% [Fox, 2003; Halstead, 2003; Gehman, 2006; Paschall *et al.*, 2006; CPW vs. State of Colorado, 2012]. Specific yield in the model was set to 20%.

The *specific storage* of a saturated aquifer is defined as the volume of water that a unit volume of aquifer releases from storage under a unit decline in hydraulic head. Although the aquifer is unconfined, the model contains two layers with the bottom layer being fully saturated in most areas. Specific storage is calculated with the following equation:

$$S_S = \rho_w g (\beta_p + n\beta_w) \quad (\text{Equation 5})$$

where:

ρ_w is the density of water (M/L^3), g is the acceleration due to gravity (L/T^2), β_p is the vertical compressibility of the aquifer matrix (L/MLT^{-2}), n is the porosity (L^3/L^3), and β_w is the compressibility of water (L/MLT^{-2}) [Domenico and Schwartz, 1990].

The range of vertical aquifer matrix compressibility is $1 \times 10^{-8} - 5.2 \times 10^{-9} \text{ m}^2/\text{N}$ for dense, sandy gravel [Domenico and Schwartz, 1990]. The range of porosity in sand and gravel

alluvial aquifers is 20-35% [Fetter, 1980]. Using a porosity of 20% and matrix compressibility of $5.2 \times 10^{-9} \text{ m}^2 / \text{N}$, specific storage was set to $7.5 \times 10^{-5} \text{ m}^{-1}$ for the model.

2.3 Steady-State Simulation

Steady-state groundwater flow is the solution of hydraulic heads without a time component. The gradient and flow velocity are constant with no groundwater pumping in the study area. The steady-state model is calibrated by adjusting hydraulic conductivities, streambed conductance, GHB conductance, and precipitation recharge to achieve a reasonable fit between modeled and observed groundwater levels in the network of monitoring wells.

2.4 Steady State Calibration

Model calibration refers to a demonstration that the model is capable of producing field-measured hydraulic heads and fluxes and is accomplished by finding a set of parameters and boundary conditions that produce simulated heads and fluxes that match field measured values within a pre-established range of error [Anderson and Woessner, 1992]. No downstream gaging station exists within the model domain, therefore calibration statistics were only computed for hydraulic head observations. Evaluation of simulated vs. observed hydraulic heads within the model is quantitatively described with three statistical measures:

(1) The Mean Error (ME) is an evaluation of model bias and is the arithmetic mean difference between observed heads (h_m) and simulated heads (h_s) [Anderson and Woessner, 1992]. A ME close to zero indicates no bias within the model and is calculated with the following equation:

$$ME = \frac{1}{n} \sum (h_m - h_s) \quad (\text{Equation 6})$$

(2) The Mean Absolute Error (MAE) measures the average magnitude of the errors in a set of data [Anderson and Woessner, 1992]. It is a measure of accuracy and is the arithmetic mean of the absolute value of the differences between observed (h_m) and simulated (h_s) hydraulic heads. When divided by the range of data, the size of the error is relative to the range in hydraulic head. MAE divided by the range is calculated with the following equation:

$$\frac{\text{MAE}}{\text{Range}} = \frac{\frac{1}{n}\sum|h_m - h_s|}{h_{\max} - h_{\min}} \quad (\text{Equation 7})$$

(3) The Nash-Sutcliffe efficiency (NSE) coefficient is an indicator of the model's goodness of fit to the 1:1 line of observed (h_m) vs. simulated (h_s) hydraulic heads (Nash and Sutcliffe, 1970). NSE values range from $-\infty$ to 1, with values nearing 1 as the model becomes more accurate at predicting heads. NSE is calculated with the following equation:

$$\text{NSE} = 1 - \left[\frac{\sum(h_m - h_s)^2}{\sum(h_m - \bar{h}_m)^2} \right] \quad (\text{Equation 8})$$

Another method for calibrating the steady-state model is to evaluate stream depth. To support the conceptual model, the stream should not have large gaining or losing reaches under steady-state conditions [Donnelly, 2012]. The stream was evaluated by plotting stream depth throughout the model and calibration was achieved by adjusting streambed conductance until stream depth remained relatively stable throughout the model domain.

2.5 Transient Flow Simulation

Transient simulations are necessary when an aquifer stress (e.g. pumping rate, pumping well configuration, or evapotranspiration) changes, in order to model the changing groundwater

flow field. The one year transient simulation was divided into monthly periods of time, referred to as stress periods, where these varying aquifer stresses are held constant. During transient simulation, streamflow accretion and depletion is modeled as the flux between the aquifer and individual stream cells and can be evaluated at various times and locations to understand how the groundwater/surface water interaction affects the aquifer system.

To further evaluate recharge operations in the transient model, particle tracking can be used to trace the pathways of water leaving the recharge ponds. This is accomplished using MODPATH [Pollock, 2012], a post-processor to flow models that accepts the head distribution of a MODFLOW model and uses it to calculate a velocity distribution, which is used to trace flow pathways [Anderson and Woessner, 1992]. Two types of flow tracking can be simulated, forward and backward, and are related to the temporal reference frame [Cypher, 2008]. Forward particle tracking will be used in this study to trace the flow pathways by assigning particles to water pumped into the recharge ponds. MODPATH keeps track of particle travel times via advective transport. Advection is the process by which solutes are transported with the bulk motion of groundwater flow [Freeze and Cherry, 1979]. Advective transport does not account for hydrodynamic dispersion or diffusion. It is the movement of solute at the average linear velocity of groundwater.

CHAPTER 3
RESULTS

3.1 Stream

The steady-state flow simulation incorporated average daily streamflow in the South Platte River from the Crook gaging station and static water levels from 28 monitoring wells at Tamarack on 10 September 2009. During the eight-week period preceding 10 September 2009, streamflow remained relatively stable following the high flows from snow melt runoff, ending in mid-July (Fig. 4). This period allowed groundwater levels to stabilize without any major stream inputs from storms or releases from water storage facilities upstream of Tamarack that could potentially raise groundwater levels and affect calibration.

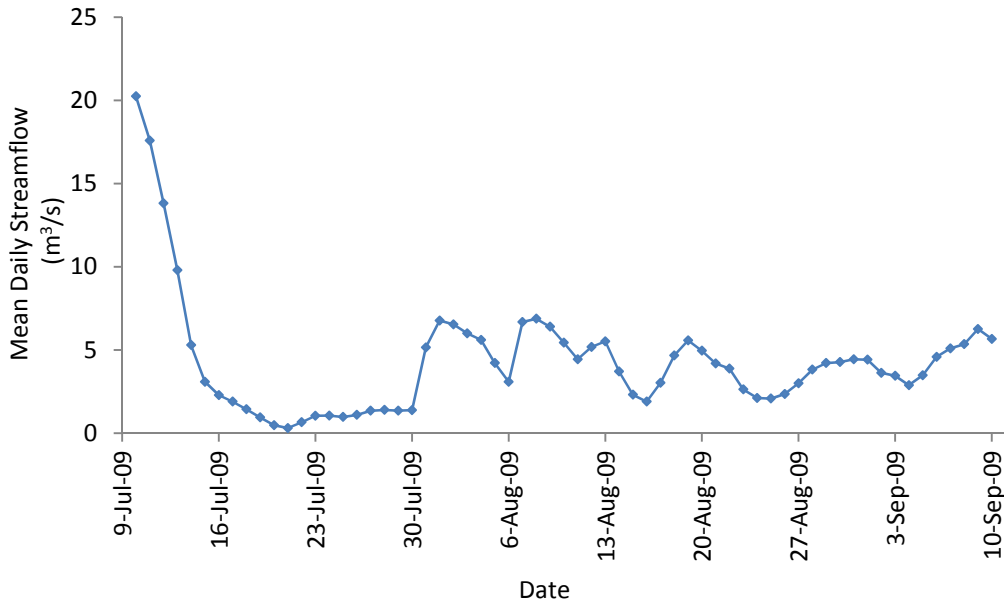


Figure 4: Mean daily streamflow at the Crook gaging station for the period 10 July 2009 – 10 September 2009.

The SFR package used in MODFLOW is a head dependent boundary package; streamflow, stream depth, and stream width are critical input variables for calculating head in the stream, which drives water exchange between the stream and aquifer. Stream depth model input was determined from streamflow measurements at the Crook gaging station from 2010-2011 [Donnelly, 2012]. Streamflow and stream depth were well correlated ($R^2= 0.95$) at this location, as a result a linear relationship was used to estimate stream depth (Fig. 5). Stream width in the 2010-2011 study was 25m at the Crook gaging station and did not increase with increased streamflow, indicating an entrenched channel [Donnelly, 2012]. Stream length was measured in ArcGIS[®] 10.0 for each stream cell and is the only variable term in the conductance calculation. The stream was simulated using the average daily streamflow of 5.66 m³/s on 10 September 2009 and a calculated stream depth of 0.43m [CDWR, 2013].

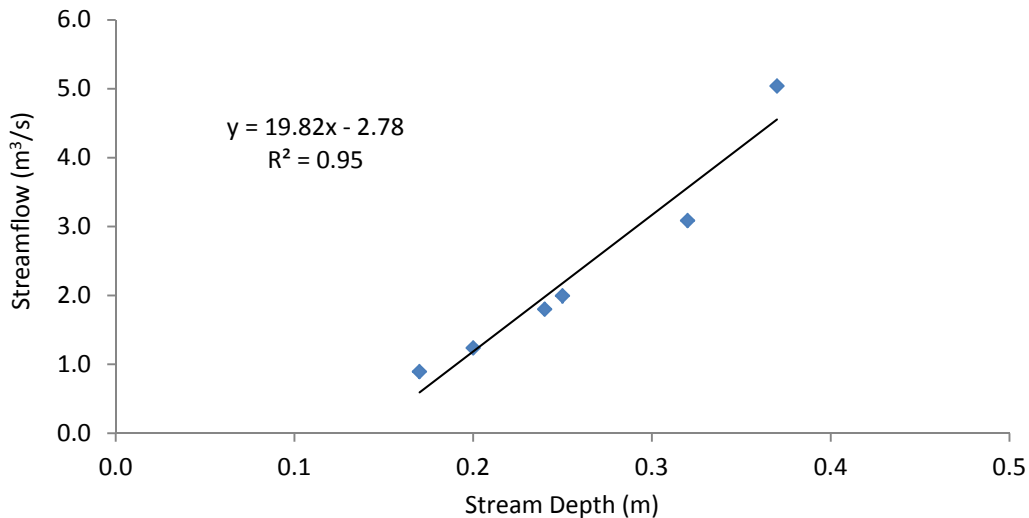


Figure 5: Stream depth and streamflow measurement relationships at the Crook streamflow gaging station (data from Donnelly, 2012).

3.2 Evapotranspiration

Evapotranspiration (ET) in the model was confined to the riparian zone, directly adjacent to the South Platte River (Fig. 2), and simulates ET from Plains Cottonwood trees with a maximum ET rate of 3.0 mm/day. For the steady-state model, ET rates were set to 70% of peak summertime ET (2.1 mm/day) by using a time factoring method (Table 1), which accounts for seasonal differences in temperature and day length. Meadow grasses were not included in the model because they only draw water from the shallow soils and not groundwater for ET. The extinction depth of ET was held constant at 3m for all ET cells. Aerial coverage of cottonwood trees in the riparian zone was estimated at 10% using the live map feature in ArcGIS® 10.0.

Table 1: Evapotranspiration rating factor and rates by month.

Month	Sep	Oct	Nov	Dec	Jan	Feb	Mar	Apr	May	Jun	July	Aug
ET Rate Factor	0.7	0.1	0	0	0	0	0	0	0.4	0.9	1.0	1.0
ET Rate (m/d)	0.0021	0.0003	0	0	0	0	0	0	0.0012	0.0027	0.003	0.003

3.3 General Head Boundaries

A head dependent boundary condition was applied to both the inflow (west) and outflow (east) boundaries using MODFLOW’s General Head Boundary Package (GHB). Hydraulic conductivity and distance to the GHB (external to the model), remained constant for every GHB cell. Distance to the GHB was determined in ArcGIS by measuring the distance between known static groundwater levels and determining the head gradient. The saturated thickness of each GHB cell varies with the simulated head in the cell and was calculated automatically in GV (Table 2).

Table 2: General Head Boundary (GHB) input variables for the east and west model boundaries. Variables include hydraulic conductivity (m/d), distance to the GHB (m), width of the GHB cell (m), and the range of saturated thickness in GHB cells (m).

Boundary	Hydraulic Conductivity (m/d)	Distance to GHB (m)	Width of GHB Cell (m)	Range of Saturated Thickness in GHB Cells (m)
West	90	500	25-100	0.05 - 36.09
East	90	500	25-100	0.04 - 32.09

3.4 Steady-State Model Calibration

The model was quantitatively evaluated for sensitivity using the GV auto-sensitivity analysis tool for parameter and boundary condition changes, and found to be most sensitive to changes in GHB conductance, horizontal aquifer hydraulic conductivity and vertical aquifer hydraulic conductivity. Model calibration was then achieved through trial and error adjustment of these sensitive parameters and quantitative evaluation with the use of hydraulic head residual statistics. Calibration can also be qualitatively evaluated by visually examining the head contour map. Unexpected deviations in head contours provide indication of areas in the model that do not support the conceptual model and require further investigation and calibration.

Model calibration was achieved through comparisons of simulated groundwater levels to groundwater levels observed in the monitoring wells on 10 September 2009 (Table 3 and Figs. 6 and 8). The calibration statistics reported by GV are based on the difference between simulated head in the model and measured head in the monitoring wells and are referred to as head residuals. The average of the head residual differences is then used to quantify the average error in the calibration [Anderson and Woessner, 2002]. The objective of calibration is to minimize the average error in the model by getting as close to zero as possible.

Table 3: Simulated heads and observed hydraulic heads for 10 September 2009, used to calibrate the steady-state model. Coordinate system for geographic locations: NAD 1983, UTM 13N

Monitoring Well	X Coordinate (m)	Y Coordinate (m)	Model Layer	Observed Hydraulic Head (m)	Simulated Hydraulic Head (m)	Residual
R1	687728	4523920	1	1125.16	1125.49	-0.33
R2	687248	4523560	1	1126.21	1126.44	-0.23
R3	688154	4524060	1	1124.59	1124.83	-0.24
R4	694317	4526390	1	1114.24	1114.44	-0.20
R5	687484	4523740	1	1125.72	1125.99	-0.27
R6	687973	4523950	1	1124.80	1125.11	-0.31
R7	688375	4524160	1	1124.12	1124.57	-0.45
R8	688548	4524270	1	1123.83	1124.31	-0.48
R9	694457	4526470	1	1113.98	1114.20	-0.22
R10	694573	4526570	1	1113.63	1114.01	-0.38
DOW4	688693	4523500	1	1125.41	1124.65	0.76
DOW5	689763	4523730	1	1123.36	1123.27	-0.01
DOW6	690641	4524120	2	1121.33	1121.89	-0.56
DOW7	691207	4524330	1	1120.05	1120.65	-0.60
DOW10	694372	4525510	1	1115.71	1114.94	0.77
T2	687810	4523030	1	1126.08	1126.11	-0.03
T3	687722	4523300	1	1126.67	1126.01	0.66
T5	687934	4523580	1	1125.79	1125.52	0.27
T6	688183	4523960	1	1124.84	1124.86	-0.02
T7	687790	4523930	1	1125.19	1125.38	-0.19
T8	687657	4523890	1	1125.33	1125.63	-0.30
T9	687753	4523820	1	1125.43	1125.54	-0.11
T10	687762	4523720	1	1125.64	1125.61	0.03
T11	687854	4523970	1	1125.07	1125.26	-0.19
T12	687761	4523920	1	1125.22	1125.44	-0.22
T13d	687986	4523100	1	1126.58	1125.87	0.71
T17d	687977	4523150	1	1125.87	1125.83	0.04
T18d	688002	4523170	1	1125.73	1125.79	-0.06

Table 4: Steady-state calibration statistics including number of observations, minimum residual (m), maximum residual (m), mean error (m), mean absolute error (m), range of data (m), mean absolute error/range, and the Nash-Sutcliffe efficiency coefficient.

Number of Observations	Minimum Residual (m)	Maximum Residual (m)	Mean Error (m)	Mean Absolute Error (m)	Range of Data (m)	Mean Absolute Error/Range	Nash-Sutcliffe efficiency coefficient
28	-0.60	0.77	-0.08	0.31	13.04	0.024	0.99

The simulated vs. observed heads data fall on or near to the 45 degree line indicating good accuracy between simulated and observed values (Fig. 6). The deviation of points above the line indicate model bias toward over simulating heads, particularly in monitoring wells near the river (Table 3).

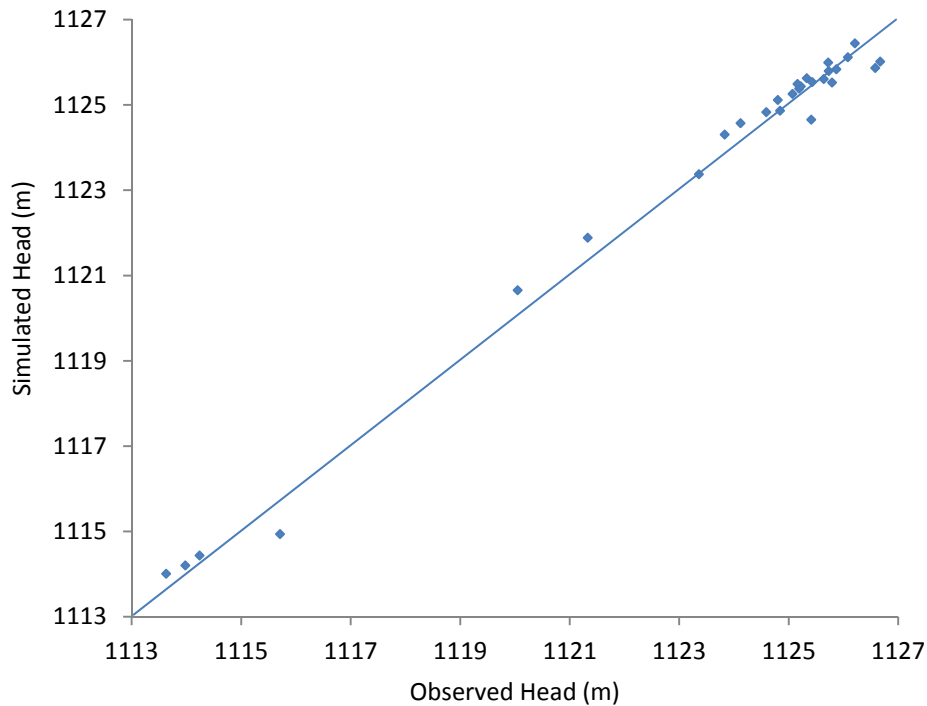


Figure 6: Simulated vs. observed heads for the calibrated steady-state model.

The Nash-Sutcliffe efficiency (NSE) was applied to the observed and simulated heads to quantitatively describe the accuracy of model outputs (Nash and Sutcliffe, 1970). The NSE coefficient of 0.99 indicates a good fit between observed and simulated data to the 1:1 line (Fig. 6).

To calibrate the stream, simulated stream depth was plotted for each stream cell (Fig. 7) under various streambed hydraulic conductivities until the simulated stream depth remained

relatively constant throughout the model. Final calibrated stream depth fluctuated little around .038m.

Table 5: Calibrated stream properties used to calculate the streambed conductance term including streambed hydraulic conductivity (m/d), streambed thickness (m), stream width (m), length of each stream cell (m), and Manning’s coefficient.

Streambed Hydraulic Conductivity (m/d)	Streambed Thickness (m)	Stream Width (m)	Stream Cell Length (m)	Manning’s Coefficient
18	1	25	25-100	0.035*

* Manning’s roughness coefficient for a clean, straight, natural sandy bed [Maidment, 1993].

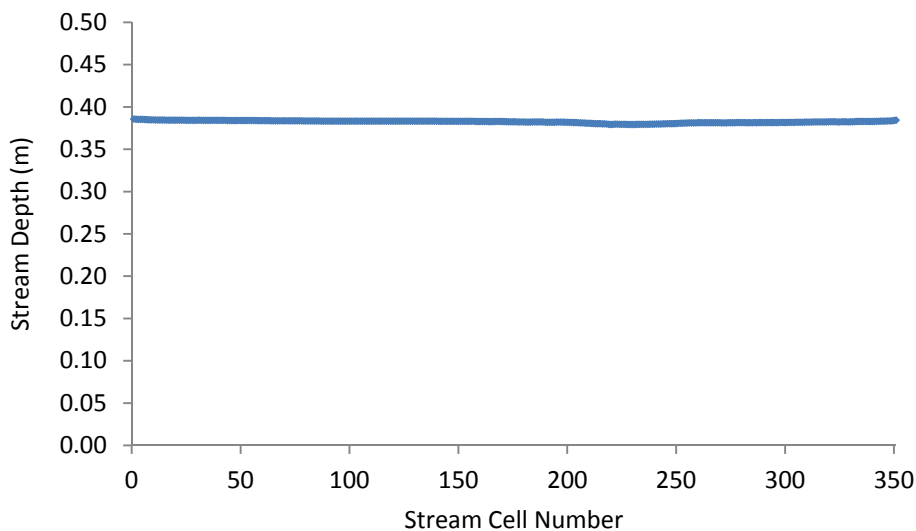


Figure 7: Steady-state stream depth for every stream reach in the model. Stream reaches are sequentially numbered from 0, the furthest upstream reach, to 351, the furthest downstream reach.

Trial and error calibration determined a horizontal hydraulic conductivity of 70 m/d and a vertical hydraulic conductivity of 17.5 m/d in both model layers achieved the best fit between modeled and observed water levels. The 4:1 anisotropy ratio and corresponding hydraulic conductivities fall within the range of suggested values from previous hydrogeologic

interpretation of the aquifer [Burns, 1985; Fox, 2003; Halstead, 2003; Paschall *et al.*, 2006; Donnelly, 2013].

3.5 Steady-State Head Contours

Groundwater is supplied to the study area from three sources: aquifer underflow, streamflow, and precipitation recharge. Conversely, water is discharged from the study area via aquifer underflow, streamflow, and evapotranspiration. The calibrated steady-state model, when head contoured, provides an overview of boundary condition impact on the regional groundwater flow field (Fig. 9) without a time component or changes in storage. More importantly, the head solution serves as the initial conditions, or starting point, for the transient model simulation.

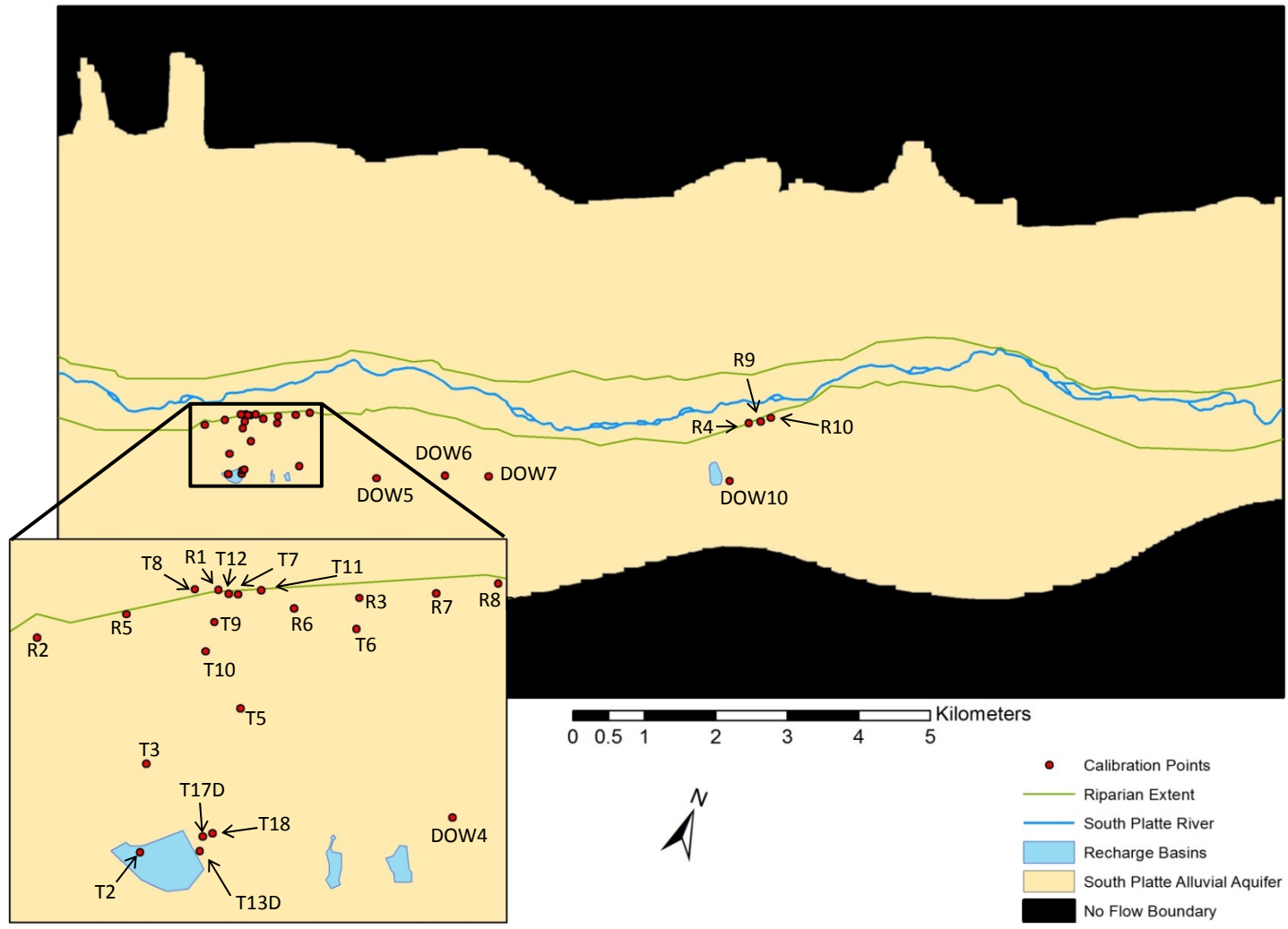


Figure 8: Location of steady-state model calibration points, recharge ponds, South Platte River, no-flow boundaries and the extent of the riparian area. Map projection is NAD 1983 UTM 13N. Data sources for the map: Colorado Division of Water Resources and Colorado Parks and Wildlife.

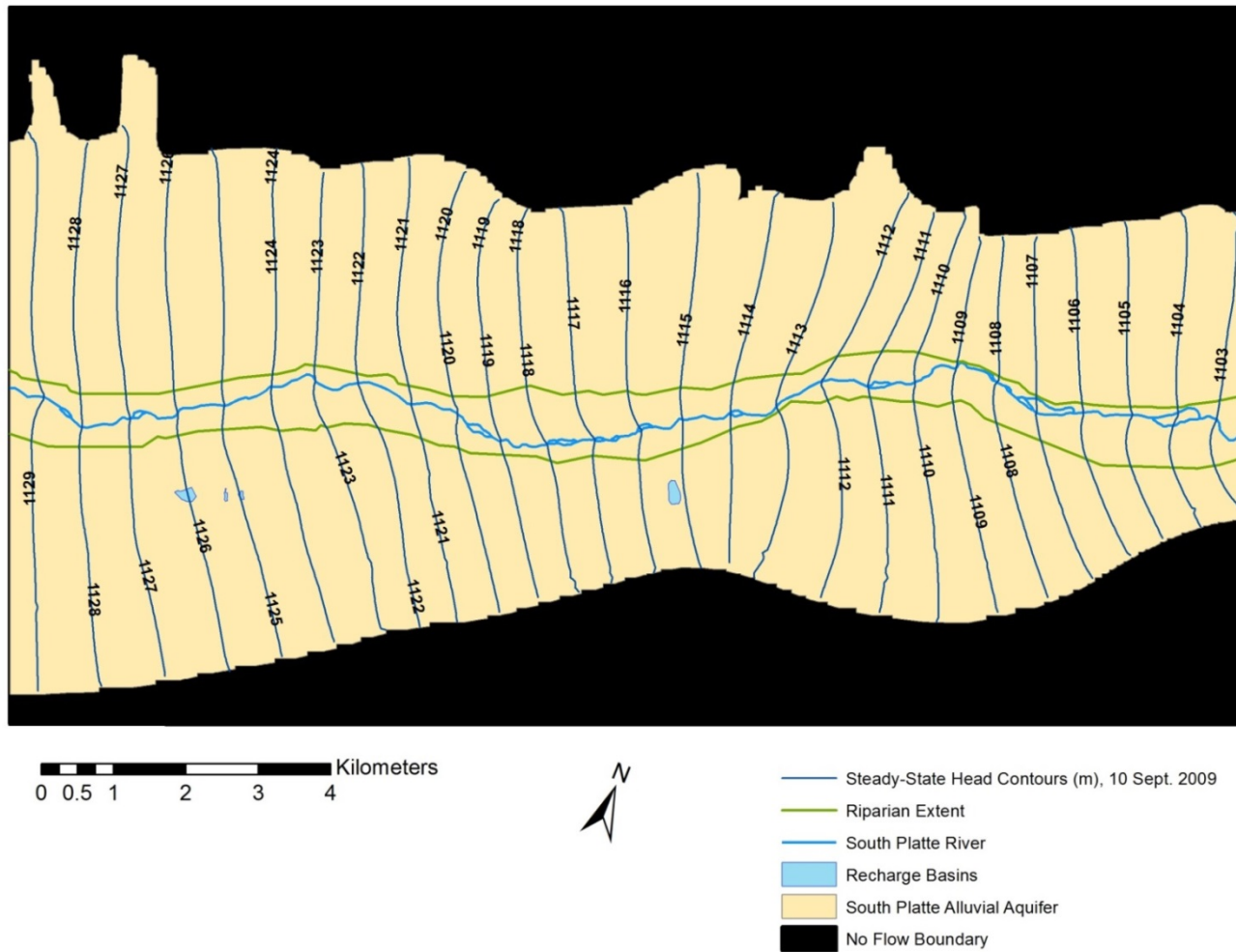


Figure 9: Steady-state head contours in 1m increments, calibrated to water levels observations on 10 September 2009. Contours are labeled in meters above sea level. Map projection is NAD 1983 UTM 13N. Data sources for the map: Colorado Division of Water Resources and Colorado Parks and Wildlife.

3.6 Transient Model Simulation

After steady-state model calibration, a one year transient simulation was run for the period: 1 September 2012 to 31 August 2013. The chosen one year interval contains the lowest rates of streamflow measured at the Crook gaging station over the period of record (2007 to date). The low water period provides the smallest ratio of streamflow to pumped groundwater at Tamarack and the best opportunity to model the effects of groundwater recharge operations on streamflow. Mean daily streamflow for the period, calculated from 15 minute interval stream gaging records, totaled 34,494,300 m³ [CDWR, 2013]. The volume of alluvial groundwater pumped into the recharge ponds during the period was 6,887,200 m³, 20% of total streamflow [J. Altenhofen, personal communication, 2013].

The transient model was designed with 14 stress periods (Tables 6, 7, and A-1). The first three stress periods divide September into three, ten day periods with 240, 120, and 40 time-steps, respectively. The shorter stress periods and greater length of time steps at the beginning of the simulation allows the model to reference the initial steady-state heads on 10 September 2009, with a higher streamflow (489,300 m³/d), and transition down to a much lower streamflow (65,400 m³/d) in September of 2012, without becoming computationally burdensome on the model. The remaining 11 stress periods represent one month of time, with daily time-steps ranging from 28 – 31 days.

Recharge operations during the period consisted of nine pumping wells operating from 1 December 2012 to 31 March 2013, providing groundwater to four recharge ponds (Fig. 9, Tables 3 and 4) [J. Altenhofen, personal communication, 2013]. The recharge ponds are modeled as injection wells in layer one with multiple cells covering the area of the ponds. Recharge

volumes are evenly distributed over each of the injection cells in the respective ponds, to simulate the actual wetted perimeter of the ponds at peak capacity.

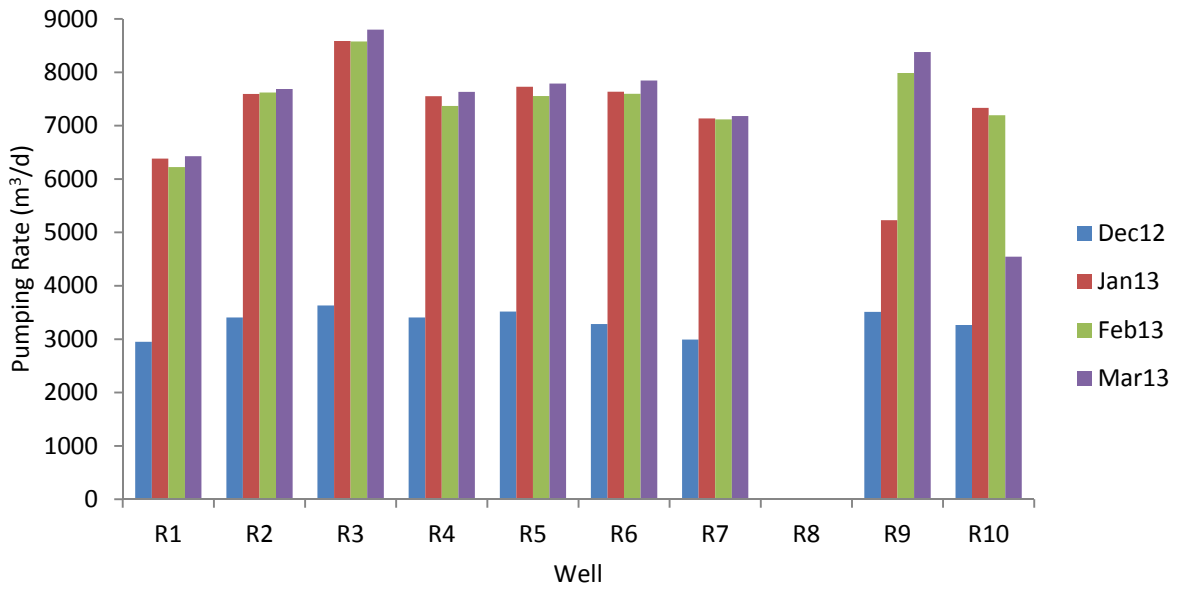


Figure 10: Daily pumping rates (m^3/d) for the recharge wells at Tamarack, utilized in the transient simulation.

Table 6: Total volume (m³) pumped per stress period for each groundwater recharge well.

Stress Period (Month & Year)	R1 (m ³)	R2 (m ³)	R3 (m ³)	R4 (m ³)	R5 (m ³)	R6 (m ³)	R7 (m ³)	R8 (m ³)	R9 (m ³)	R10 (m ³)
1 (Sep 2012)	0	0	0	0	0	0	0	0	0	0
2 (Sep 2012)	0	0	0	0	0	0	0	0	0	0
3 (Sep 2012)	0	0	0	0	0	0	0	0	0	0
4 (Oct 2012)	0	0	0	0	0	0	0	0	0	0
5 (Nov 2012)	0	0	0	0	0	0	0	0	0	0
6 (Dec 2012)	91483	105636	112566	105569	109005	101772	92,782	0	108869	101268
7 (Jan 2013)	197841	235461	266158	234111	239570	236749	221,201	0	162061	227310
8 (Feb 2013)	174239	213431	240210	206327	211572	212734	199,318	0	223598	201445
9 (Mar 2013)	199258	238310	272799	236660	241454	243223	222,554	0	259726	140923
10 (Apr 2013)	0	0	0	0	0	0	0	0	0	0
11 (May 2013)	0	0	0	0	0	0	0	0	0	0
12 (Jun 2013)	0	0	0	0	0	0	0	0	0	0
13 (Jul 2013)	0	0	0	0	0	0	0	0	0	0
14 (Aug 2013)	0	0	0	0	0	0	0	0	0	0

Table 7: Total volume (m³) of water delivered to each recharge pond per stress period.

Stress Period (Month & Year)	Recharge Pond 1 (m ³)	Recharge Pond 3a (m ³)	Recharge Pond 3b (m ³)	Recharge Pond 6 (m ³)
1 (Sep 2012)	0	0	0	0
2 (Sep 2012)	0	0	0	0
3 (Sep 2012)	0	0	0	0
4 (Oct 2012)	0	0	0	0
5 (Nov 2012)	0	0	0	0
6 (Dec 2012)	306124	153560	153560	315707
7 (Jan 2013)	672871	362053	362053	623482
8 (Feb 2013)	599242	326131	326131	631380
9 (Mar 2013)	679023	369288	369288	637309
10 (Apr 2013)	0	0	0	0
11 (May 2013)	0	0	0	0
12 (Jun 2013)	0	0	0	0
13 (Jul 2013)	0	0	0	0
14 (Aug 2013)	0	0	0	0

3.7 Transient Head Contouring

The transient modeling results can be evaluated both qualitatively and quantitatively. Qualitative analysis consists of two-dimensional head contour mapping to visualize the large scale effects of groundwater recharge on the aquifer system at a point in time. Heads were contoured for the last day of recharge operations, after the system had been cumulatively pumped for four months and the effects on the system were most pronounced (Fig. 11). Both clusters of pumping wells have cones of depression that intercept the stream, resulting in streamflow capture. Water quickly infiltrates the ponds and elevates the water table beneath them, becoming a visible groundwater mound. Two weeks after the pumps are turned off (Fig. 12), the groundwater mounds have dissipated into pressure waves that are now seen migrating to

the northeast along the regional flow gradient. The aquifer, in the vicinity of the pumping well clusters that experienced drawdown, no longer has visible cones of depression and the lines of equipotential have returned perpendicular to the stream, indicating a recovery after only two weeks. Two months after groundwater recharge was stopped (Fig. 13), the pressure wave is no longer distinctly visible on the contour map.

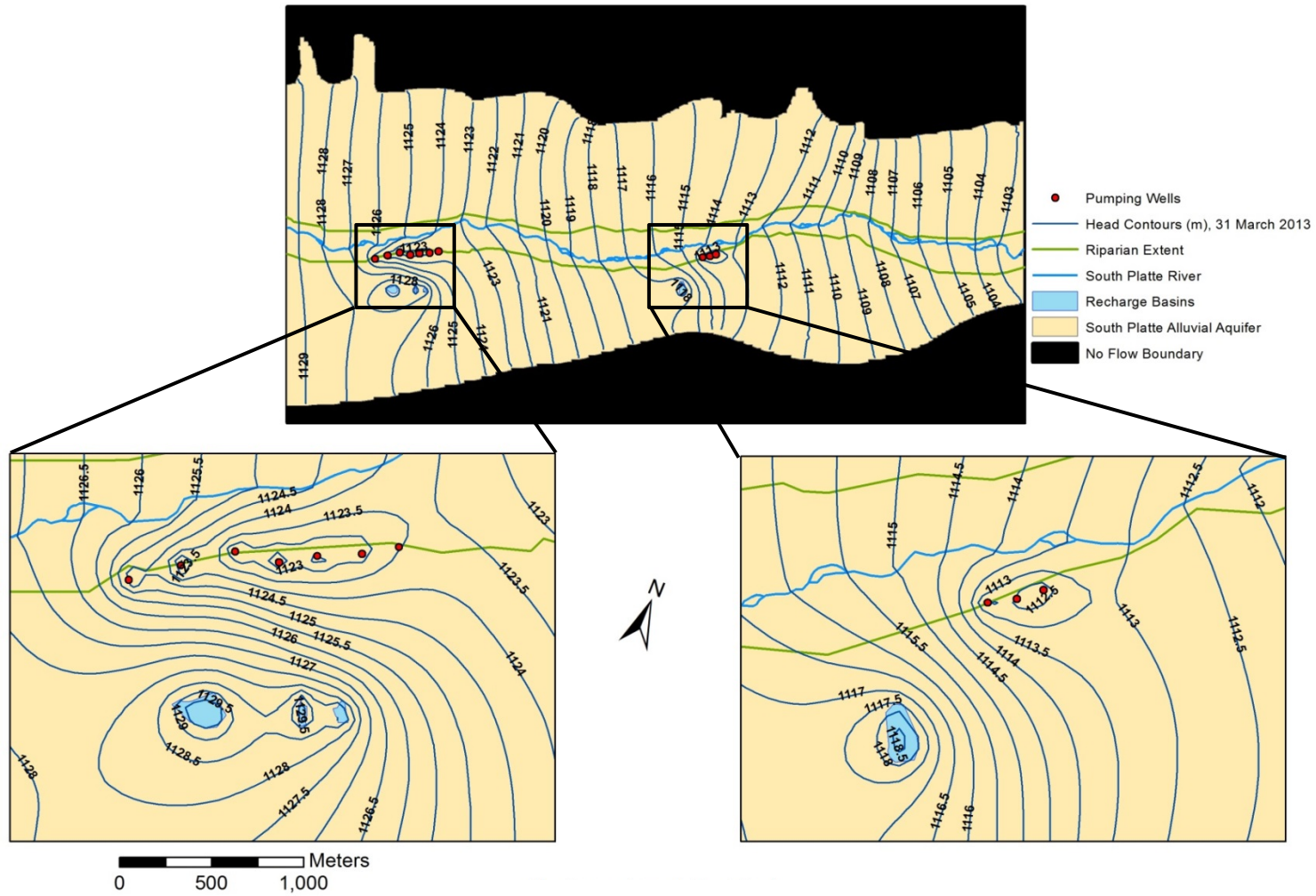


Figure 11: Simulated head contours on 31 March 2013, the last day of recharge operations. Contours are labeled in 1 meter increments on the base map and 0.5 meter increments on the inserts. All contours are labeled meters above sea level.

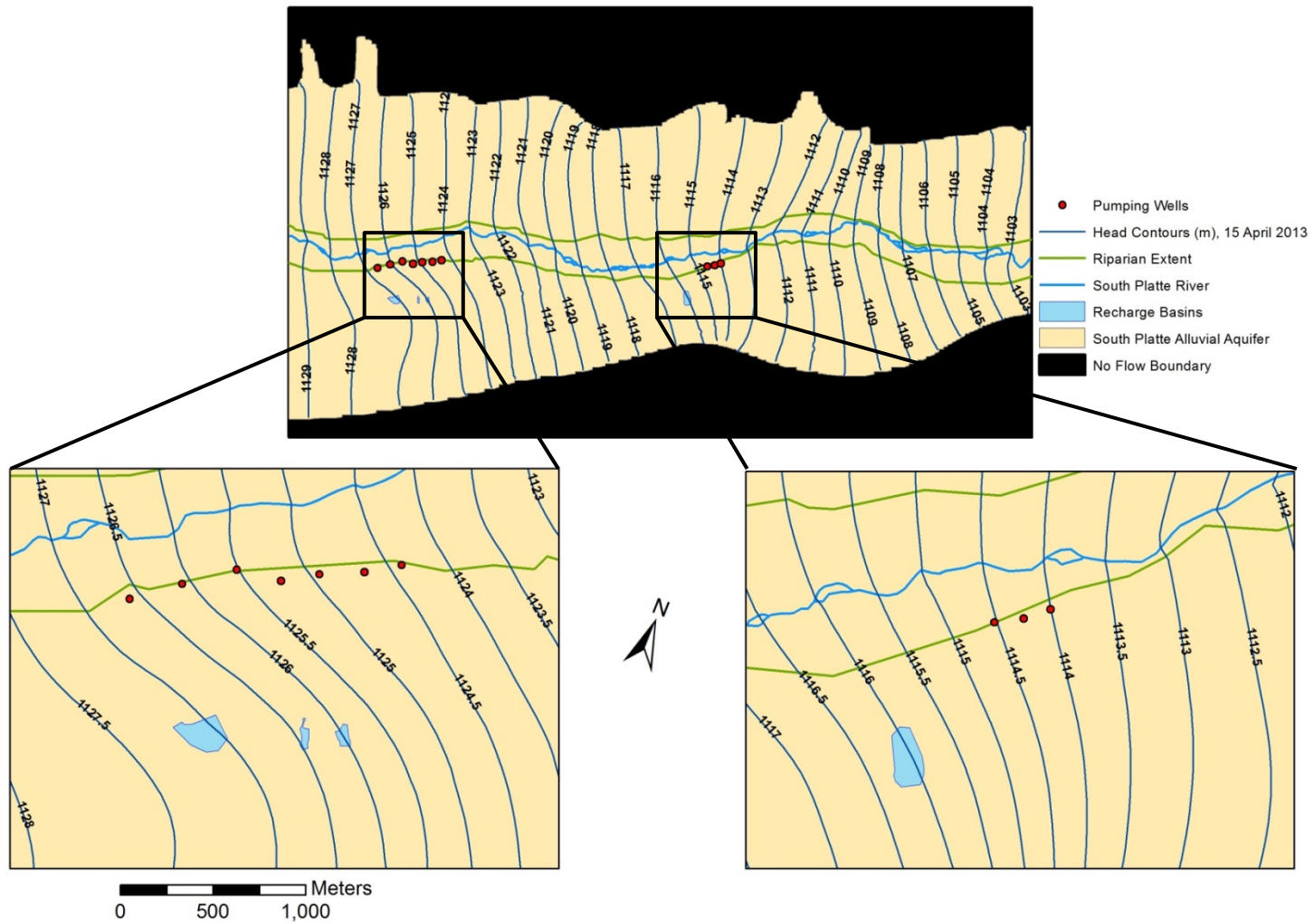


Figure 12: Simulated head contours on 15 April 2013, two weeks after the end of recharge operations. Contours are labeled in 1 meter increments on the base map and 0.5 meter increments on the inserts. All contours are labeled meters above sea level.

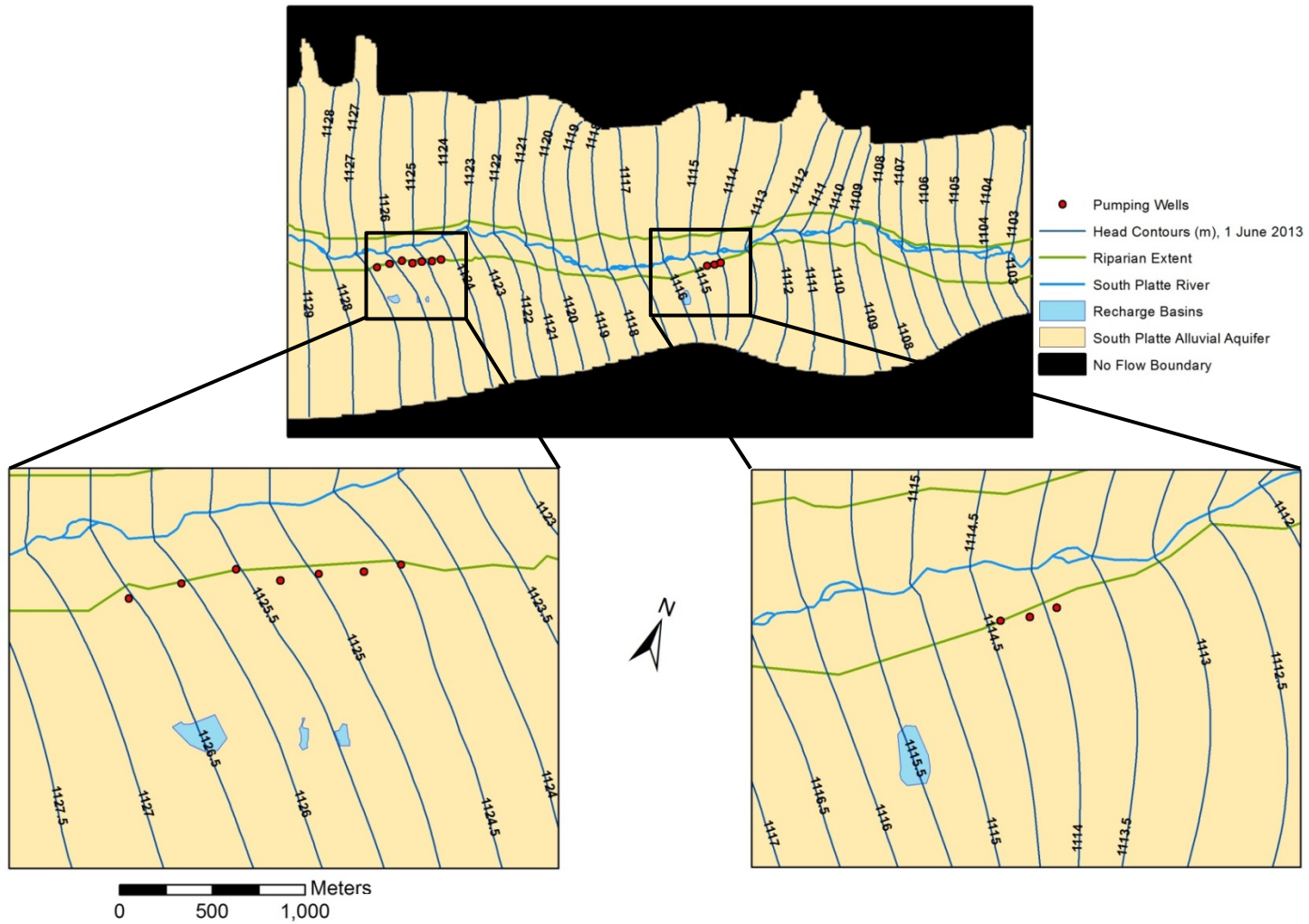


Figure 13: Simulated head contours on 1 June 2013, two months after the end of recharge operations. Contours are labeled in 1 meter increments on the base map and 0.5 meter increments on the inserts. All contours are labeled meters above sea level.

3.8 Transient Model Water Budget

The transient model water budget is written for each stress period by MODFLOW and can be used to evaluate the aquifer system in relation to hydrologic stresses and aquifer recovery, by providing volumetric accounting of inputs and outputs. The two significant hydrologic stresses in this study, groundwater pumping and ET, cause significant changes in the overall water balance during transient simulation. During a month with managed groundwater recharge the decline in hydraulic heads near the pumping wells results in the release of water from aquifer storage (Fig. 14). In a warm month with riparian ET, the water budget is much different. Outflow from aquifer storage is near zero and stream leakage outflow is lower than stream leakage inflow, indicating that ET is consuming mostly streamflow (Fig. 15).

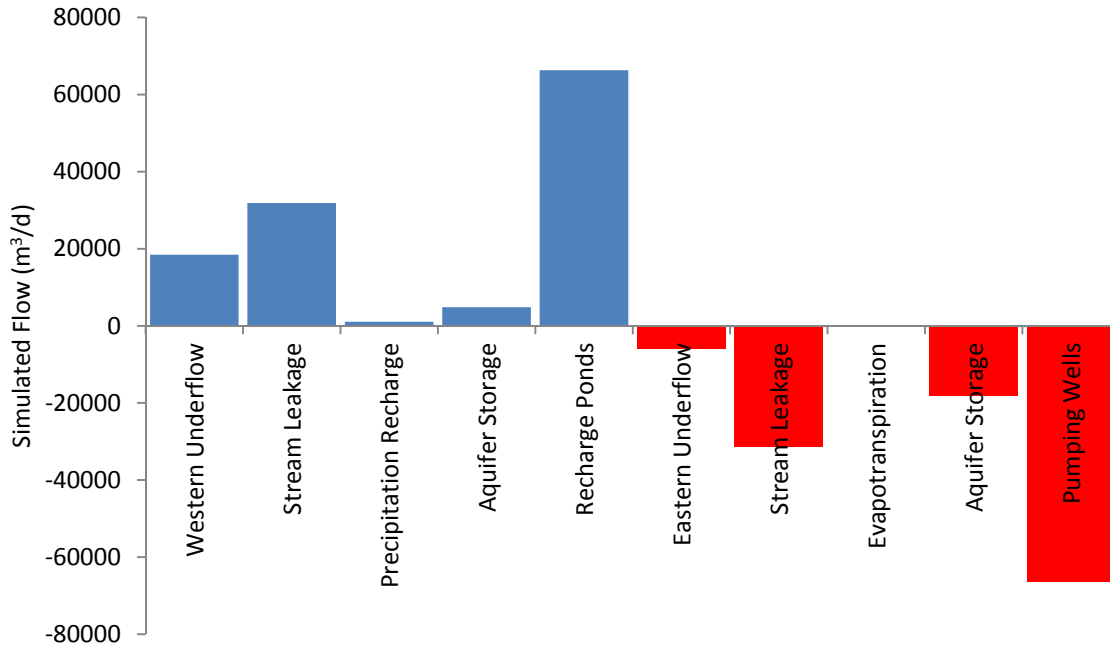


Figure 14: March 2013 transient model water budget with aquifer inflows in blue and outflows in red for the eastern and western boundary underflows, stream leakage, precipitation recharge, aquifer storage, evapotranspiration, pumping wells, and recharge ponds.

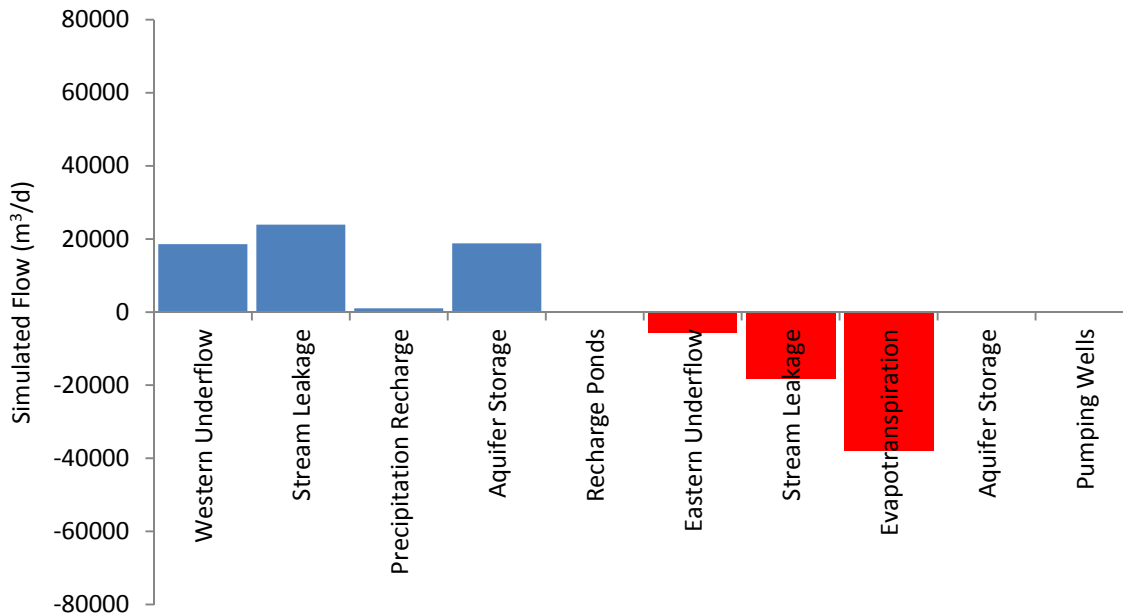


Figure 15: July 2013 transient model water budget with aquifer inflows in blue and aquifer outflows in red for the eastern and western boundary underflows, stream leakage, precipitation recharge, aquifer storage, evapotranspiration, pumping wells, and recharge ponds.

3.9 Stream-Aquifer Interaction

To evaluate the influence of recharge operations, a second, identical transient model was constructed without pumping and injection wells. The two model outputs allow for a side-by-side comparison of water budgets to quantitatively compare the system with and without pumping. Stream-aquifer interaction was investigated for all 351 stream boundary cells by plotting the groundwater/surface water flux rate and stream depth for the last day of each stress period. Every stress period was plotted and is available in the appendix. March is of particular interest because it is the fourth and final month that groundwater recharge operations took place and also the lowest volume of streamflow in the transient model. This combination of low streamflow and cumulative pumping results in the largest stress to the aquifer system during this study. July is also of interest because it is a target month for streamflow accretion due to low flows in the South Platte River.

After four months of groundwater pumping the effect on the stream is apparent, beginning near stream reach 50, where the stream passes in close proximity to the western cluster of pumping wells (Fig. 16). Beginning with stream reach 50, groundwater pumping causes water to be removed from the stream, resulting in reduction in streamflow, hence stream depth. The removal of water from the stream is modeled as a positive flux into the aquifer that was not simulated in the non-pumping model (Fig. 17). Once past the western well cluster and out of the influence of the pumping wells, the stream begins to gain again until reaching the eastern cluster of wells at reach 226, where pumping again depletes the stream.

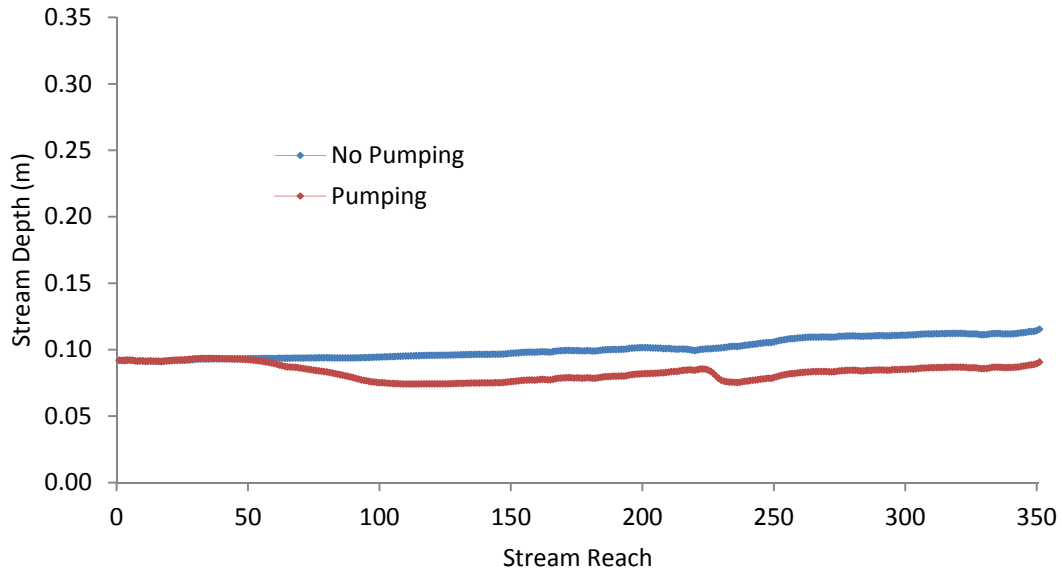


Figure 16: Simulated stream depth, with and without pumping, for each stream reach, 31 March 2013. Stream reaches are sequentially numbered from 0, the furthest upstream reach, to 351, the furthest downstream reach.

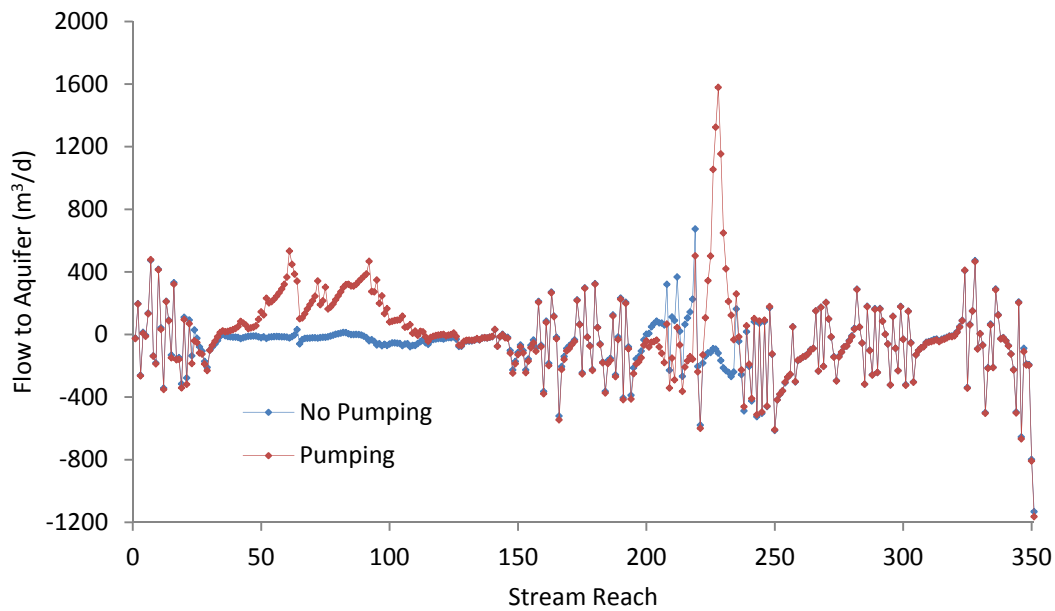


Figure 17: Simulated groundwater/surface water flux rate, with and without pumping, for each stream reach, 31 March 2013. Stream reaches are sequentially numbered from 0, the furthest upstream reach, to 351, the furthest downstream reach.

Simulated stream depth was plotted for the last day of July, three months after groundwater recharge operations were stopped. Simulated stream depth was higher in the downstream reaches of the model with pumping than in the model without pumping, indicating streamflow accretion due to groundwater recharge. There is a small difference in depth where the model with pumping has lower flux into the aquifer than the model without pumping (Fig. 18). Streamflow accretion begins after stream reach 50 where the first recharge pond is located and becomes more evident further downstream.

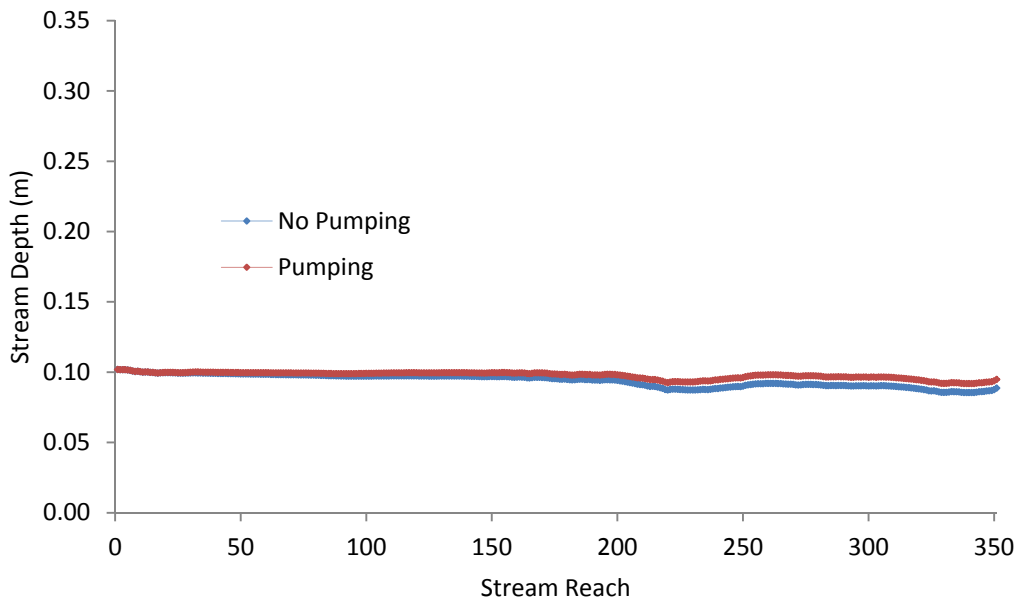


Figure 18: Simulated stream depth, with and without pumping, for each stream reach, 31 July 2013. Stream reaches are sequentially numbered from 0, the furthest upstream reach, to 351, the furthest downstream reach.

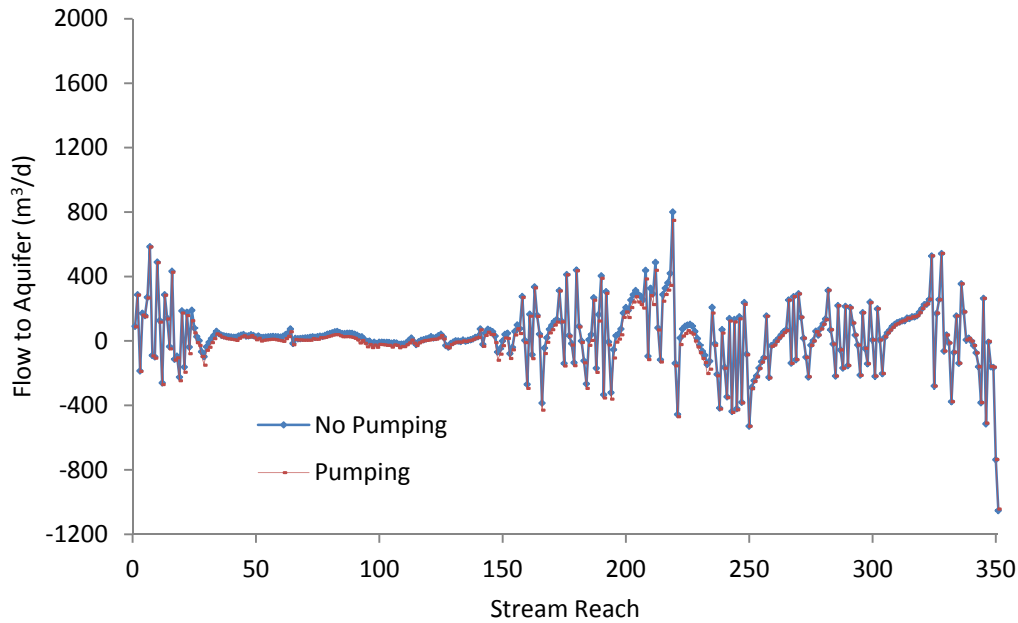


Figure 19: Simulated groundwater/surface water flux rate, with and without pumping, for each stream reach, 31 July 2013. Stream reaches are sequentially numbered from 0, the furthest upstream reach, to 351, the furthest downstream reach.

The stream depth and groundwater/surface water flux analysis for 31 July 2013 indicate the aquifer system is responding to groundwater recharge operations as designed and in the target time period. However, data for a single day are not enough to determine the quantity of additional streamflow that can be expected from groundwater recharge. To examine the hydrograph over space, the GAGE package [Merritt and Konikow, 2000] was used to designate five streamflow modeling locations. Stream gaging locations (Fig. 20) include: one upgradient and one downgradient of the two pumping well clusters, and one at the Tamarack property boundary (Red Lion Bridge). This allowed for the spatial determination of groundwater recharge effects on streamflow.

In Stream Reach 20, the hydrographs are nearly identical for both the pumping and non-pumping transient simulations indicating no streamflow accretion or depletion from groundwater pumping operations (Fig. 21). At Red Lion Bridge, the pumping model hydrograph exhibits

both phases of groundwater recharge operations (Fig. 22). Stream depletion is prominent from December to March, when the non-pumping model simulates higher streamflow; streamflow accretion occurs from April to August with higher streamflow.

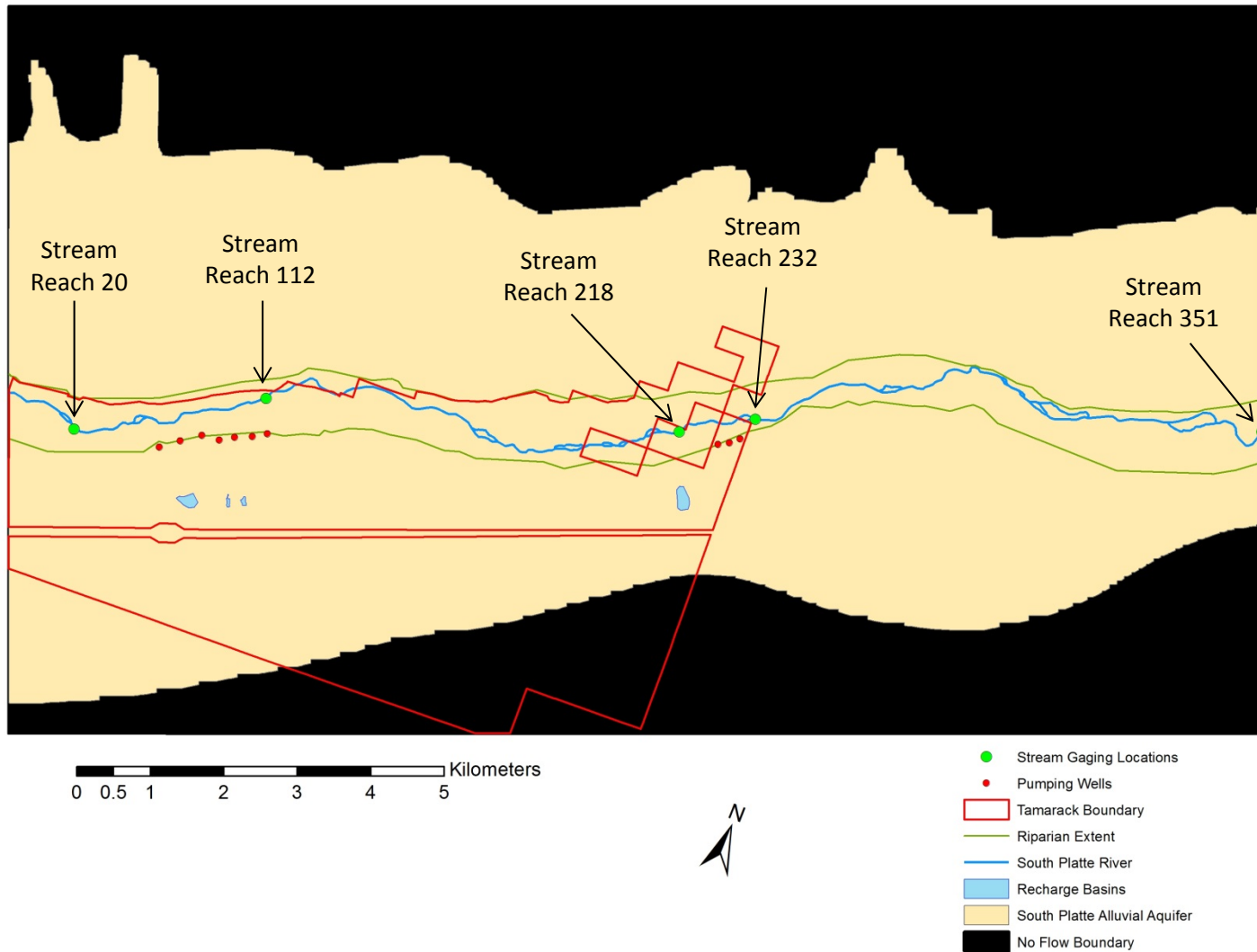


Figure 20: Location of stream streamflow gaging stations (at Stream Reaches 20, 112, 218, 232, and 351) used to compute streamflow hydrographs with the GAGE package. Also included are the Tamarack property boundary, locations of the recharge ponds, pumping wells, South Platte River, no-flow boundaries and the extent of the riparian community.

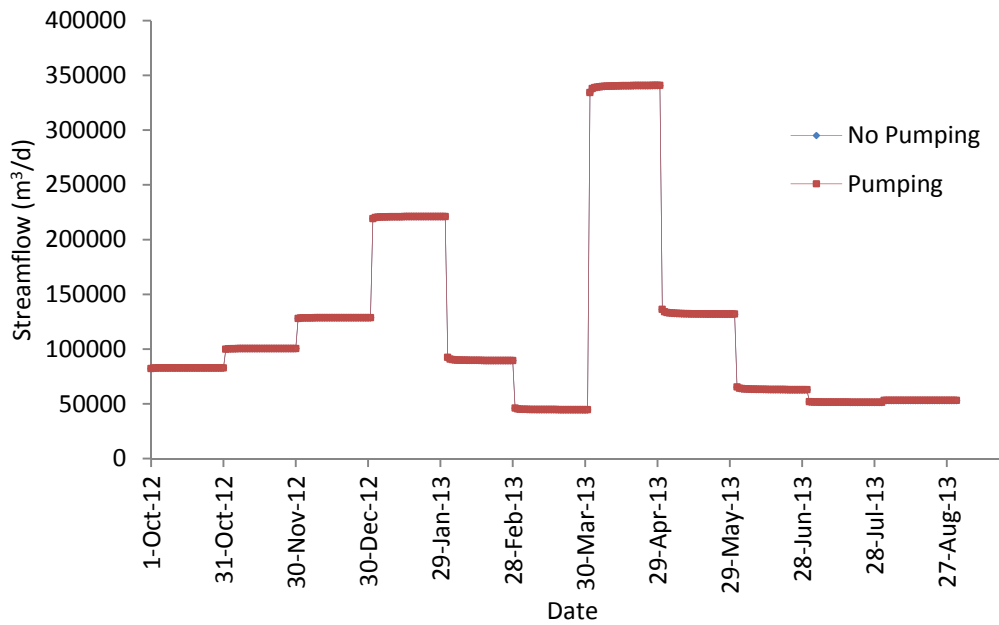


Figure 21: Transient hydrographs at stream reach 20 for both the pumping and non-pumping transient models (m³/d).

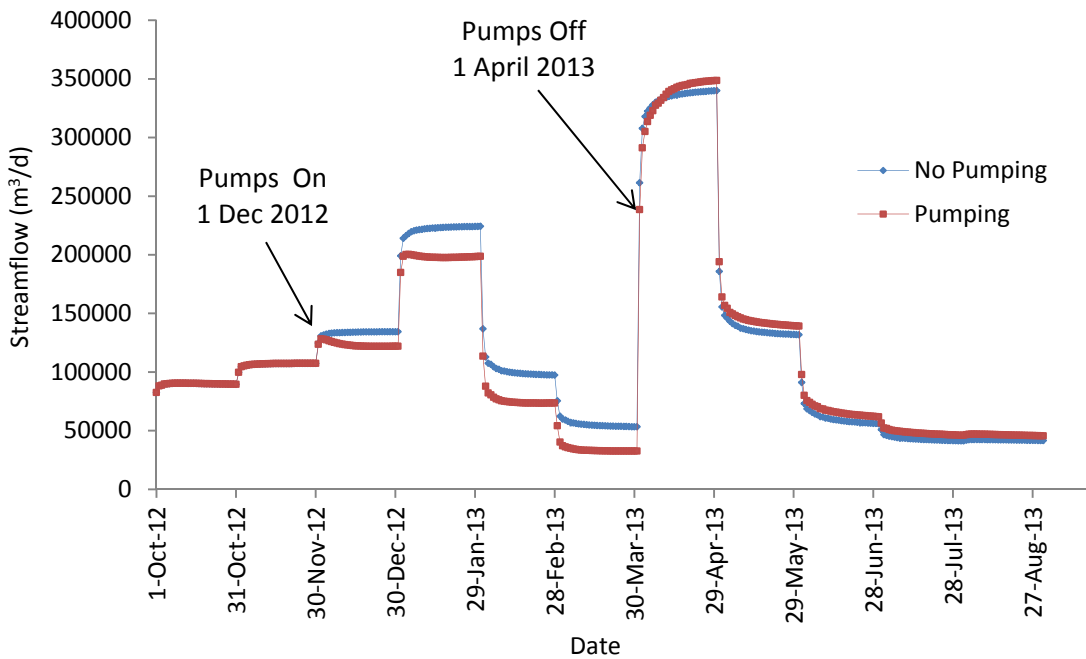


Figure 22: Transient hydrographs at the Red Lion Bridge (stream reach 232) for both the pumping and non-pumping transient models (m³/d).

To examine the change in streamflow due to groundwater recharge operations, the non-pumping hydrograph was subtracted from the pumping hydrograph for all stream gaging locations (Figs. 23, 24, 25, 26, and 27). All four modeled locations exhibit streamflow accretion starting between 10 April 2013 and 13 April 2013, indicated when the difference in streamflow between the pumping simulation and the non-pumping simulation becomes positive, and the effects of groundwater pumping no longer result in streamflow depletion. Streamflow accretion is then evident through the last day of simulation, 31 Aug 2012. The model was terminated before all accretion waters were added to streamflow.

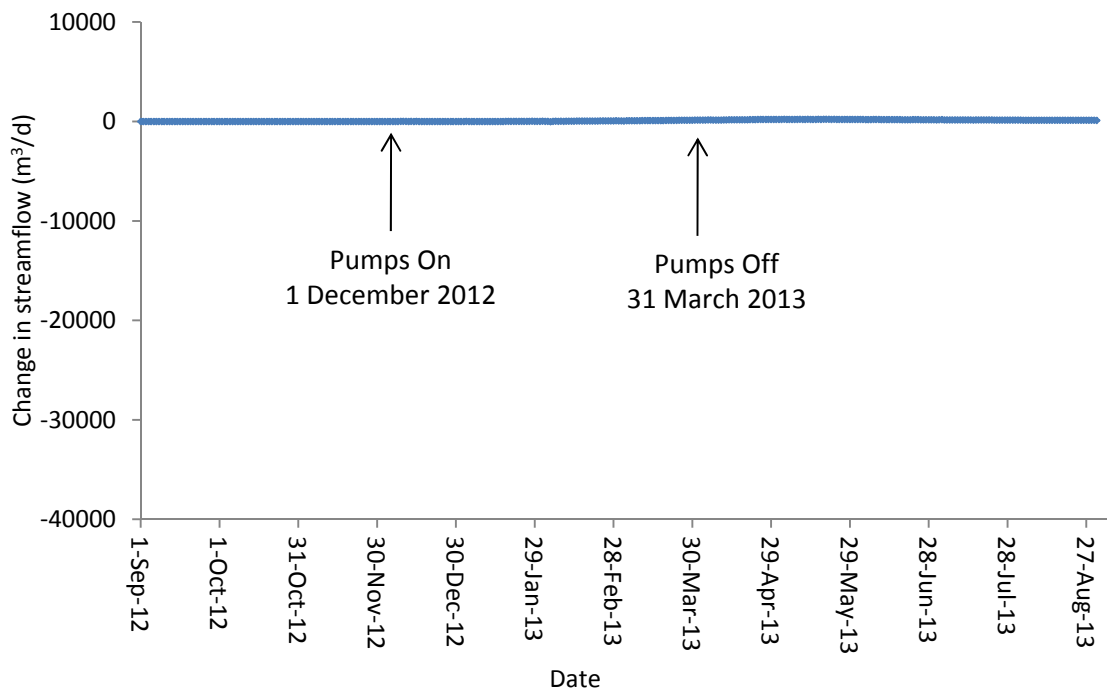


Figure 23: Change in streamflow (m^3/d) at Stream Reach 20, calculated by subtracting the non-pumping model hydrograph from the pumping model hydrograph (shown in Fig. 22).

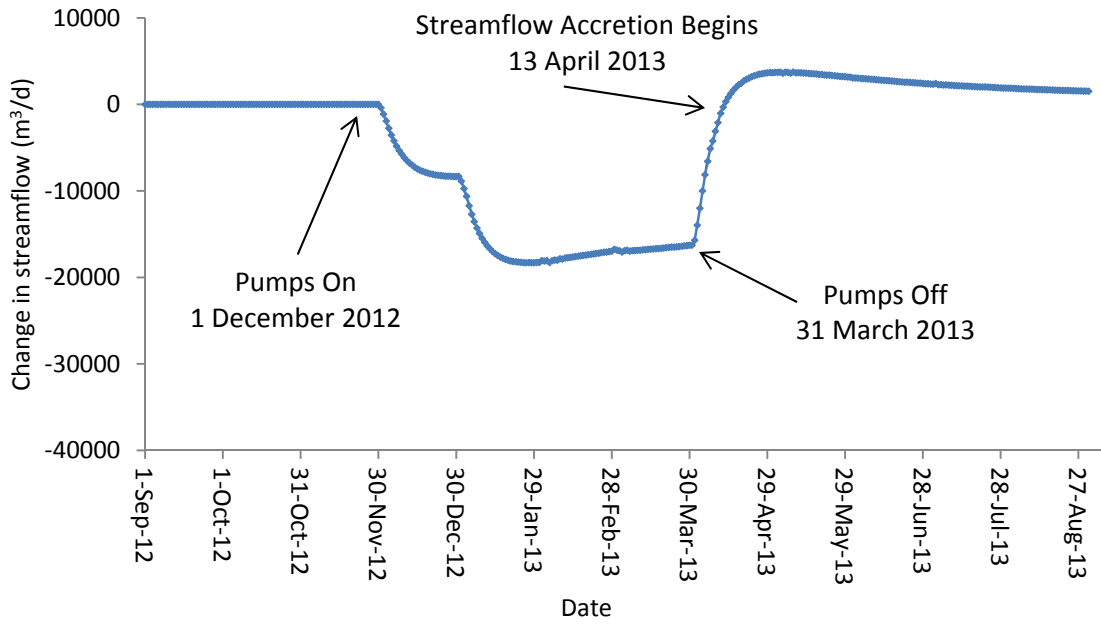


Figure 24: Change in streamflow (m³/d) at Stream Reach 112, calculated by subtracting the non-pumping model hydrograph from the pumping model hydrograph (shown in Fig. 22).

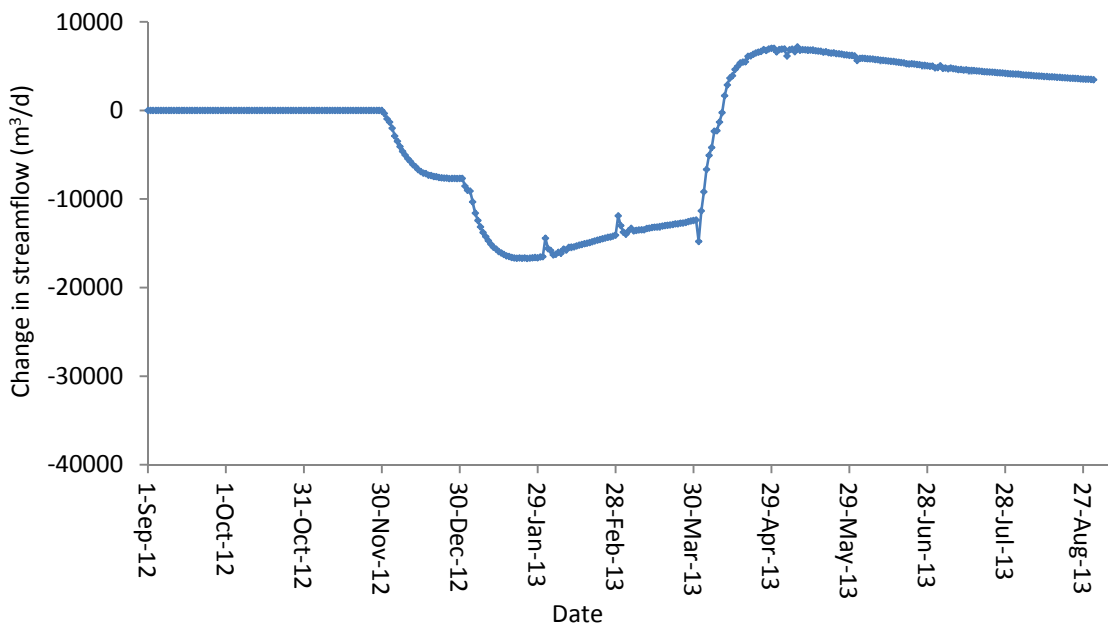


Figure 25: Change in streamflow (m³/d) at Stream Reach 218, calculated by subtracting the non-pumping model hydrograph from the pumping model hydrograph (shown in Fig. 22).

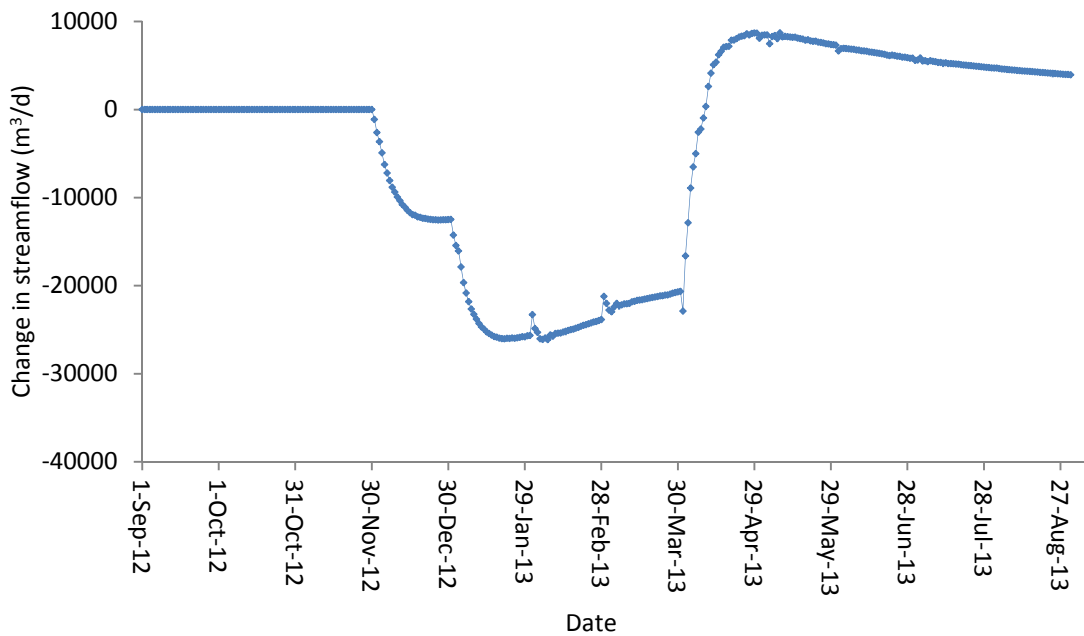


Figure 26: Change in streamflow (m^3/d) at the Red Lion Bridge (stream reach 232) calculated by subtracting the non-pumping model hydrograph from the pumping model hydrograph (shown in Fig. 22).

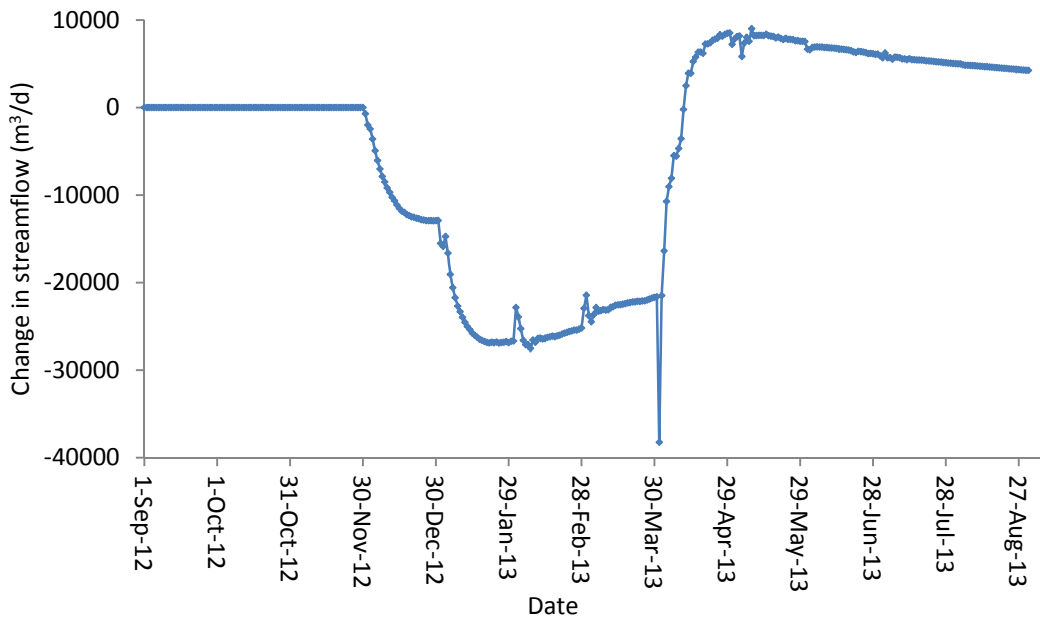


Figure 27: Change in streamflow (m^3/d) at the eastern model boundary (Stream Reach 351), calculated by subtracting the non-pumping model hydrograph from the pumping model hydrograph (shown in Fig. 22).

Streamflow accretion values at the Red Lion Bridge (Stream Reach 232) from 10 April 2013 to 31 August 2013 were then converted to units of (m³/s) and evaluated in proportion to the streamflow gaging records at the Crook station (Fig 28). The ratio of simulated average daily streamflow accretion to actual average daily streamflow ranges from 2 – 10%, with the greatest proportion occurring in the first month after groundwater recharge operations ended (Table 8). The total volume of simulated streamflow accretion during this period at the Red Lion Bridge (Stream Reach 232) is 878,000 m³, 13% of total volume of groundwater pumped into the recharge ponds. Total streamflow accretion at the eastern model boundary, approximately 8 km downstream of the Red Lion Bridge, increased by less than 1%, to 881,000 m³. This indicates that most streamflow augmentation is occurring before the stream leaves the Tamarack property. Streamflow accretion was occurring at the end of model simulation, 31 August 2013, so not all accretions are accounted for in this study.

Table 8: Simulated mean daily streamflow accretion (m³/s), mean daily streamflow (m³/s), and streamflow accretion percent contribution to total streamflow for the period 10 April 2013 – 31 August 2013 at the Red Lion Bridge (stream reach 232).

Month and Year	Average Daily Streamflow Accretion (m ³ /s)	Average Daily Streamflow (m ³ /s)	Streamflow Accretion (% of Total Streamflow)
April 2013	0.08*	4.29**	2.0
May 2013	0.09	1.54	5.8
June 2013	0.07	0.75	9.3
July 2013	0.06	0.62	9.7
August 2013	0.05	0.64	7.8

*only includes days of streamflow accretion (21 days)

**only 21 days of streamflow corresponding with streamflow accretion

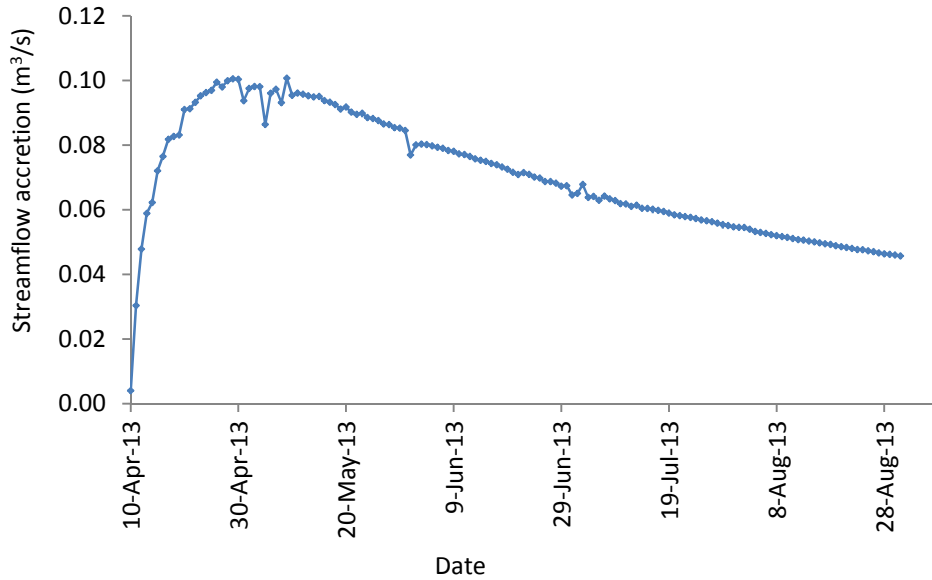


Figure 28: Total simulated streamflow accretion (m^3/s) at the Red Lion Bridge (stream reach 232) from 10 April 2013 to 31 August 2013.

3.10 Advective Transport Simulation

Advective transport was simulated in MODPATH using forward particle tracking to map the transport pathways and travel times of groundwater away from the recharge basins by placing one particle in every grid cell of the recharge ponds (Fig. 29). In total, 56 particles were released into pond 1, 11 into pond 3a, 11 into pond 3b, and 19 into pond 6. Particles were introduced in the top of layer one to all four recharge ponds on the first day of pumping on 1 December 2012, and simulated through the last day of the transient stress period on 31 August 2013.

Recharge pond 1 is the only pond with particles traveling in every direction away from the pond with the pumping induced forced gradient. Once the pumps are turned off, the particles change direction to the northeast, under the influence of the regional flow field. Particles originating in recharge ponds 3a, 3b and 6 do not exhibit the same multidirectional flow field as basin 1 under the forced gradient conditions. Particles from 3a, 3b and 6 never travel in a westerly direction, instead always traveling east, northeast, or southeast. Particles originating in

pond 3a travel directly east until they encounter the groundwater mound that forms under pond 3b. The particles are then forced either north or south around pond 3b along the forced gradient. Similar to pond 1, once the pumps are turned off, the particles change direction to the northeast, under the influence of the regional flow field. All 97 particles traveled less than one kilometer during the 9 month simulation.

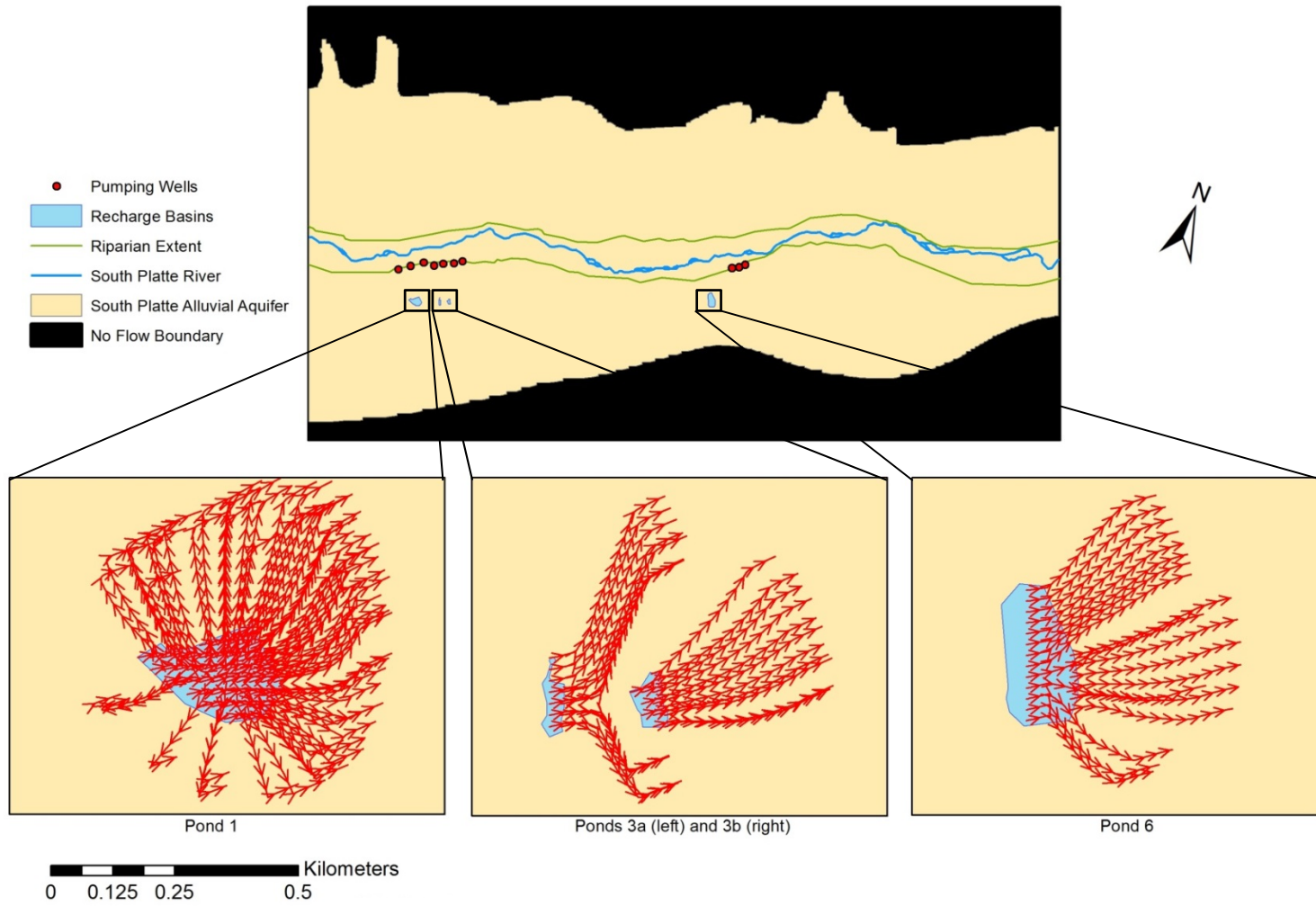


Figure 29: Transient model forward particle tracking for the period: 1 December 2012 – 31 August 2013.

CHAPTER 4

DISCUSSION

4.1 Steady-State Model Calibration and Flow Field

A detailed numerical model was created using MODFLOW to characterize the groundwater flow field at the Tamarack project. The unconfined alluvial aquifer and South Platte River form a dynamic system which never reaches a true steady-state condition, required as the initial conditions for a transient groundwater simulation. To address this issue, the streamflow hydrograph for the entire period of record was analyzed to find a relatively stable period, corresponding with groundwater level observations that could be used for steady-state model calibration. The selected date for steady-state model calibration was 10 September 2009, with 28 observed groundwater levels from the network of monitoring wells at Tamarack. Model calibration was quantitatively evaluated through the use of hydraulic head residual statistics and simulated streamflow gain or loss. The head residual mean error (ME) of -0.08 m is the arithmetic mean of all residuals and provides an indication of model bias towards over simulating heads, particularly in the area near the river (Table 3), but does not provide further meaningful interpretation of the data because the large positive and negative residuals cancel to produce this value. A better indication of the magnitude of the errors was achieved by using the mean absolute error (MAE) of 0.31 m, which is the arithmetic mean of the absolute value of the residuals. To further constrain the error in the model, MAE was by divided by the range of data (13.04 m) resulting in a model error of 2.4%. The Nash-Sutcliffe model efficiency statistic was also used to evaluate the predictive power of the model. A coefficient of 0.99 indicates the model is accurate at predicting the measured head values. To date, there is no standard protocol

for evaluating model calibration, so the judgment between model fit and reality is still subjective [Anderson and Woessner, 2002]. With an overall error of 2.4% and a high Nash-Sutcliffe efficiency, this model is considered to be well calibrated because it reasonably reproduces field observed hydraulic heads and is not largely biased. Although primary calibration of the steady-state model was obtained through evaluation of head residuals, stream depth was also considered. Supporting the conceptual model, the stream did not have any large gaining or losing reaches under steady-state conditions, when groundwater pumping had not occurred for many months. The stream was considered well calibrated when the fluctuation in stream depth was ± 1 cm over 19 km of stream channel.

The calibrated steady-state model agreed with the conceptual model, indicating regional groundwater flow from west to east at an approximate gradient of 1m/500m and lines of equipotential running north to south, perpendicular to the stream. The use of a uniform hydraulic conductivity and 4:1 anisotropy ratio throughout the model does not indicate the alluvial sediments are homogenous but rather that the heterogeneity suggested by previous research at the site is confined to localized beds and not continuous layers that present a noticeable effect on regional groundwater flow [Bjorkland and Brown, 1957; Warner *et al*, 1986; Beckman, 2007; Lonsert, 2013].

4.2 Transient Model Simulation

After calibration, the steady-state head distribution was utilized as the initial condition for a one year transient simulation to evaluate the effects of managed groundwater recharge on the regional flow field and the South Platte River. The transient model was constructed using a detailed pumping schedule and recharge pond configuration provide by the Northern Colorado Water Conservancy District [J. Altenhofen, personal communication, 2013]. After model

simulation, head contour maps were created for three periods of interest starting on the last day of recharge operations, 31 March 2013. The contour maps helped to evaluate the effects of groundwater recharge on the regional flow field after 4 months of pumping when changes to the system were most evident. On the last day of pumping the contour map showed changes to the groundwater flow field in the form of groundwater mounds that formed beneath the recharge ponds. This confirms the formation of groundwater mounds reported in earlier hydrogeologic work at Tamarack [Beckman, 2007; Gehman, 2009]. The groundwater mounds quickly begin to dissipate after the pumps are turned off and the flow field returns to the regional pattern observed in the steady state model (Fig 9). A few weeks after the pumps were turned off, the groundwater mounds dissipate into migrating pressure waves that move through the system, away from the recharge ponds and toward the river along a northeast trajectory [Beckman, 2007]. After two months, the pressure wave is no longer visible.

4.2.1 Transient Water Budget

The two significant hydrologic stresses in this study, ET and groundwater pumping, cause significant changes in the overall water balance during transient simulation, forcing water to be drawn from the stream (stream leakage) and from aquifer storage, due to the decline in hydraulic head. In this study, groundwater pumping occurs during the winter and early spring months when there is no ET in the riparian community; consequently it is necessary to evaluate the water budget at two different times to understand these impacts on the aquifer. The March 2013 water budget (Fig. 14) presents the last month of recharge operations, after the aquifer has been pumped for four months. Although the volumes of well pumping and recharge pond injection are equal and cancel out, the relocation of water up into the recharge ponds causes heads to be lowered near the pumping wells resulting in water being released from storage. Also

visible in the water budget plots (Figs 14 and 15), but unrelated to pumping, is the difference in volume moving across the eastern and western boundaries as aquifer underflow. This disproportion of aquifer underflow remains constant during periods with no pumping and appears to be a function of the smaller aquifer saturated thickness on the eastern boundary. The July 2013 water budget (Fig. 15) graphically represents a summer month with maximum ET and no groundwater pumping. During the full transient simulation ET is a substantial component of the water budget from June through August, peaking in July and accounting for more than 60% of the total outflow from the system (Appendix Table A-4). Outflow from storage is near zero and stream leakage outflow is lower than stream leakage inflow, indicating that ET is consuming mostly streamflow during this period. In July, 30% of total inflow is going to storage, indicating the aquifer is still recovering from four months of groundwater pumping (Appendix Table A-4).

4.2.2 Stream-Aquifer Interaction

The smaller scale effects of groundwater recharge were examined in individual stream cells. In order to evaluate the stream cells for accretions and depletions, a second, identical transient model was constructed without pumping and injection wells that allowed for a side by side comparison. Interaction between the aquifer and stream was investigated by plotting the groundwater/surface water flux rate and stream depth for the last day of each stress period. The groundwater/surface water flux and stream depth plots on the last day of pumping (Figs. 16 and 17) indicate the cones of depression from both pumping well clusters intercept the stream, resulting in stream capture and flux from the stream into the aquifer. This flux is modeled as a positive flow into the aquifer under pumping conditions (Fig. 17). After the pumps are turned off on 31 March, heads in the vicinity of the pumping wells quickly recover to steady-state like conditions, and streamflow accretion begins occurring in less than two weeks. Streamflow

accretion is modeled in the form of small changes in stream depth (Fig. 18) and groundwater flux into the stream (Fig. 19) that were previously undetectable with physical streamflow measurements [Donnelly, 2012]. The modeled groundwater flux from the aquifer to the stream in this study also confirms the presence of a vertical hydraulic gradient in the streambed, measured with in-stream piezometers during the previous hydrologic work. The upward vertical gradient was measured downstream of the western cluster of pumping wells in September of 2010 and was thought to be streamflow accretion from groundwater recharge [Donnelly, 2012].

Hydrographs of the two transient models were plotted at five locations along the stream to examine the quantity of groundwater contribution to streamflow. This was accomplished by utilizing the transient hydrograph, without groundwater pumping, as the reference condition of the stream for the time period. Differences in streamflow were then attributed to managed groundwater recharge at Tamarack. The difference in streamflow between the two models at the Red Lion Bridge (stream cell 232), suggests that streamflow accretion begins on 10 April 2013 and peaks on 26 April 2013, and then slowly diminishes through the end of August, indicating streamflow accretion occurring through the end of the simulation (Fig. 23). Average daily volumes of streamflow accretion at this location were then examined in relation to average daily streamflow to determine the percent groundwater contribution to total streamflow for the target period. The transient simulations show additional groundwater discharge associated with recharge operations contributes 2 – 10% of total streamflow between 10 April 2013 and 31 August 2013 (Table 8). The total volume of streamflow accretion during the transient simulation at the Red Lion Bridge was 878,000 m³, 13% of the 6,887,000 m³ of groundwater pumped into the recharge ponds. Additional analysis of streamflow accretion 8 km downstream, at the eastern model boundary, indicates that the majority streamflow augmentation occurred on the Tamarack

property. Streamflow accretion was occurring at the end of model simulation, 31 August 2013, so not all accretions are accounted for in this study.

4.3 Advective Transport

Particles were introduced to all four recharge ponds and forward tracked from the first day of groundwater recharge operations, 1 December 2012, through the last day of the transient stress period, 31 August 2013. The particles all traveled along the pumping induced forced gradient, analogous to mounding beneath the recharge ponds, until recharge operations were stopped on 31 March 2013. Once the pumps were turned off, the particles immediately changed trajectory to the northeast, in line with the regional flow field. This change in particle trajectory agrees with previous particle tracking at Tamarack which showed that water leaving Recharge pond 1 moved north during pumping and northeast after the pumps were turned off [Beckman, 2007].

All 97 particles traveled less than one kilometer during the nine months of transient simulation. The short distance particles traveled under forced gradient conditions and the regional flow field that follows pumping emphasizes the relative slow velocity of water moving through the porous medium. In comparison, the pressure wave from groundwater recharge, evident in the head contour maps (Figs. 11, 12, 13), moves much faster.

CHAPTER 5

CONCLUSIONS

The steady-state model of Tamarack was well constrained with streamflow gaging records, 28 groundwater calibration points and a confining unit surface map that incorporated recent surface ERT data and numerous boreholes. This allowed for steady-state model calibration to be achieved with a low model error and high Nash-Sutcliffe efficiency. The model adequately represented the necessary initial condition for a one year transient simulation to evaluate the effects of managed groundwater recharge on streamflow accretion in the South Platte River.

The transient model suggests that recharge operations at Tamarack are producing a quantifiable contribution to streamflow in the intended target period of April to September. However, the total volume of streamflow accretion simulated in this study at the Red Lion Bridge is 878,000 m³, only 13% of the 6,887,000 m³ of groundwater pumped into the recharge ponds. Streamflow accretion was occurring at the end of the model simulation on 31 August 2013 so not all accretions are accounted for, but the center of mass had already passed in late April and the contribution to streamflow was diminishing. Further downstream analysis indicates the majority of streamflow augmentation occurred on the Tamarack property.

The transient model water budget indicates that evapotranspiration is a significant component of the water budget during summer months, coinciding with the target period for streamflow augmentation. Further research is necessary to understand the effects of evapotranspiration on streamflow augmentation.

CHAPTER 6

RECOMMENDATIONS

Further field investigations and groundwater modeling at Tamarack would improve current understanding of the dynamic groundwater-surface water system at Tamarack.

Recommendations for future studies include:

1. A longer model simulation to better characterize aquifer changes over time. Pumping and injections wells in the model conserve mass, therefore a model simulation many years in length would benefit the overall water budget by allowing the changes in storage to equilibrate. A longer simulation would also provide more conclusive particle tracking results by further determining the influence of the confining unit topography on recharge water.
2. A second model, without the detailed confining unit surface made possible with recent surface ERT data, would provide better insight into the effects of the buried paleo channel topography on the hydraulic head solution, streamflow accretion, and particle tracking. The results of a side by side comparison of model outputs would also better determine whether expanded ERT data, to better characterize the confining unit, would help to improve understanding of the overall water budget.
3. Recent water level observations in the network of monitoring wells at Tamarack and QA/QC of the streamflow data at the Crook gage would improve future model calibration and results. Monthly water level observations would be ideal, in order to calibrate both the steady-state and transient models.

4. The consumptive use of surface and groundwater by the riparian community is poorly understood. An investigation of riparian evapotranspiration that includes vegetation density, rooting depth, and transpiration rates would benefit the calculation of vegetative consumptive use and provide a more clear understanding of the regional water budget and the effects on streamflow augmentation by conjunctive use at Tamarack.
5. Improved understanding of streambed properties in the South Platte River would help to better estimate groundwater/surface water flux at Tamarack. Established flux rates can be used as calibration targets to better constrain a numerical model.

LITERATURE CITED

- Altenhofen J. 2013. Northern Colorado Water Conservancy District. Personal communication. Berthoud, CO.
- Anderson M., Woessner W. 2002. Applied groundwater modeling: simulation of flow and advective transport. California: Academic Press, Inc. 381 pp.
- Beckman N. 2007. Quantifying groundwater and surface water mixing at a conjunctive use site. Colorado State University Thesis. Department of Forest, Rangeland, and Watershed Stewardship. 179 p.
- Bjorklund L., Brown R. 1957. Geology and ground water resources of the Lower South Platte River Valley between Hardin, Colorado and Paxton, Nebraska. Washington, D.C.: U.S. Geological Survey. Water Supply Paper 1378. 366 p.
- Blomquist W., Heikkila T., Schlager E. 2001. Institutions and conjunctive water management among three western states. *Natural Resources Journal*. Vol 41. p. 653-684.
- Bredehoeft J. 2012. Modeling groundwater flow- the beginnings. *Groundwater* Vol 50, No 3. p. 468-474.
- Burns A. 1985. Hydrologic description of the Tamarack Wildlife Area and vicinity, Logan County, Colorado, and simulated effects of possible water management activities. USGS water-resources investigations report 85-4014. 42 pp.
- Colorado Division of Water Resources (CDWR). 2013. Colorado surface water conditions. South Platte River near Crook, CO (PLACROCO). Accessed: 16 October 2013
http://www.dwr.state.co.us/SurfaceWater/data/detail_graph.aspx?ID=PLACROCO&MTYPE=DISCHRG
- Cooper D. 2013. Colorado State University. Personal communication. Fort Collins, CO.
- CPW vs. State of Colorado. 2012. Court decree #1196CW1063. CO Weld County District Court 19th JD. Filing date July 12, 2012. Filing ID 45309980.
- Cypher J. 2008. Hydrogeologic modeling of a 1,4-dioxane plume in a glacial aquifer system; Washtenaw County, Michigan. Wayne State University Thesis. Department of Geology. 141 p.
- Domenico P., Schwartz F. 1990. Chemical and physical hydrogeology. New York: John Wiley and Sons. 824 pp.

Donnelly E. 2012. Effects of conjunctive use on streamflow at the Tamarack Ranch State Wildlife Area, Northeastern Colorado. Colorado State University Thesis. Department of Ecosystem Science and Sustainability. 126 p.

ESRI. 2013. World Map Imagery. Accessed: 1 Oct 2013.
<http://www.arcgis.com/home/item.html?id=10df2279f9684e4a9f6a7f08febac2a9> .

Fetter C. 1980. Applied Hydrogeology. New Jersey: Prentice Hall. Fourth edition. 598 pp.

Fox G. 2003. Modeling of stream/aquifer interaction during alluvial well depletion. Colorado State University Doctor of Philosophy dissertation. Department of Civil Engineering. 217 p.

Freeman D. 2010. Implementing the Endangered Species Act on the Platte Basin Water Commons. Boulder, CO: University Press of Colorado. 482 p.

Freeze A., Cherry J. 1979. Groundwater. New Jersey: Prentice-Hall. 604 pp.

Garner H. 2013. Colorado Division of Water Resources. Personal Communication: Denver, CO.

Gazal R., Scott R., Goodrich D., Williams D. 2006. Controls on transpiration in a semiarid riparian cottonwood forest. *Journal of Agricultural and Forest Meteorology*. Vol. 137. p 57 – 67.

Gehman C., Harry D., Sanford W., Stednick J., Beckman N. 2009. Estimating specific yield and storage change in an unconfined aquifer using temporal gravity surveys. *Water Resources Research*. Vol. 45.p. 1-15.

Halstead M., Flory V. 2003. Tamarack modeling project (draft report and technical memorandums), Division of Wildlife, Colorado Department of Natural Resources, Denver, Colorado. 20 p.

Harbaugh A., Banta E., Hill M., McDonald M. 2000. MODFLOW-2000 User Guide to Modularization Concepts and the Ground-Water Flow Process: U.S. Geological Survey Open-File Report 00-92. 121 p.

Hobbs G. 1999. Colorado's 1969 Adjudication and Administration Act: Settling In, 3 U. Den. Water L.Rev.1. University of Denver Water Law Review. Vol.3, Issue 1. 19 p.

Horton J., Kolb T., Hart S. 2001. Physiological response to groundwater depth varies among species with river flow regulation. *Ecological Applications*, 110 (4). p. 1046-1059.

Hurr R., Schneider P. 1973. Hydrogeologic characteristics of the valley-fill aquifer in the Sterling reach of the South Platte River valley, Colorado. U.S. Geological Survey Open-File Report 73-126, 2 p.

Jenkins C. 1968. Computation of rate and volume of stream depletion by wells. *Groundwater* 6. no. 2: 37-46.

Kittell G., VanWie E., Damm M. 1998. A Classification of the Riparian Vegetation of the South Platte and Republican River Basins, Colorado 1998 Final Report. Colorado Natural Heritage Program. Colorado State University. 327 p.

Kokes L. 2013. Colorado Parks and Wildlife. Personal communication. Denver, CO.

Landmeyer J. 2011. Introduction to phytoremediation of contaminated groundwater: historical foundation, hydrologic control, and contaminant remediation. New York: Springer. 415 pp.

Larroque F., Treichel W., Dupuy A. 2008. Use of unit response functions for management of regional multilayered aquifers: application to the North Aquitaine Tertiary system (France). *Hydrogeology Journal*. Vol. 16. Issue 2. P 215-233.

Lonsert R. 2013. DC electrical resistivity constraints on hydrostratigraphy in the South Platte alluvial aquifer in northeast Colorado. Colorado State University Thesis. Department of Geosciences. 35 p.

Maidment D. 1993. Handbook of hydrology. New York: McGraw-Hill. 2,947 pp.

McDonald M., Harbaugh A. 1988. A modular three dimensional finite difference ground water flow model: Techniques of Water-Resources Investigations of the United States Geological Survey. Book 6. Chapter A1. 586 p.

Merritt M., Konikow L., 2000. Documentation of a computer program to simulate lake-aquifer interaction using MODFLOW groundwater flow model and the MOC3D solute transport model: U.S. Geological Survey Water Resource Investigations Report 00-4167. 146 p.

Miller C., Durnford D., Halstead M., Altenhofen J., Flory V. 2007. Stream depletion in alluvial valleys using the SDF semianalytical model. *Ground Water* 45(4): 506-514.

Paschall D., McCuury G., Bliss M. 2006. South Platte Decision Support System (SPDSS) Phase 3 Task 42.3 South Platte Alluvium Region Aquifer Configuration Technical Memorandum. Denver, CO. 39p.

Platte River Recovery Implementation Program (PRRIP). 2013. Accessed: 24 May 2013. <https://www.platteriverprogram.org/AboutPRRIP/Pages/Default.aspx>

Poceta J. 2005. Electrical resistivity imaging of eolian and alluvial sediments along the South Platte River, northeastern Colorado. Colorado State University Thesis. Department of Geosciences. 64 p.

Pollock, D., 2012, User guide for MODPATH version 6. A particle-tracking model for MODFLOW: U.S. Geological Survey Techniques and Methods, book 6, chap. A41, 58 p.

Prudic D., Konikow L., Banta E. 2004. A new stream- flow routing (SFR1) package to simulate stream-aquifer interaction with MODFLOW-2000: U.S. Geological Survey Open-File Report 2004-1042. 104 p.

Remson I., Hornberger G., Molz F. 1971. Numerical Methods in Subsurface Hydrology. New York: Wiley-Interscience. 389 pp.

Rumbaugh J., Rumbaugh, D. 2011. Groundwater Vistas version 6. Copyright 1996-2011. Environmental Simulations, Inc.

Scott G. 1978. Map showing geology, structure, and oil and gas fields in the Sterling 1 degree x 2 degree quadrangle, Colorado, Nebraska, and Kansas. U.S. Geological Survey miscellaneous investigations series map I-1092, (sheet 1 of 2).

Scott M., Shafroth P., Auble G. 1999. Responses of Riparian Cottonwoods to Alluvial Water Table Declines. Environmental Management. Vol. 2, No. 3. p. 347-358

Stenzel R., Cech T. 2013. Water Colorado's real gold: a history of the development of Colorado's water, the Prior Appropriation Doctrine and the Division of Water Resources. Colorado: Richard Stenzel Publishing. 462 pp.

U.S. Geological Survey. 2013. National elevation data set (NED). Accessed: 30 January 2013. <http://ned.usgs.gov/>

Williams C., Cooper D. 2005. Mechanisms of riparian cottonwood decline along regulated rivers. Ecosystems Journal. 8: 382-395.

Warner J., Sunada D., Hartwell A. 1986. Recharge as augmentation in the South Platte River Basin. Fort Collins: Colorado State University. Completion report 144. 124 p.

APPENDIX A – Detailed Model Input Variables and Transient Water Budget

Appendix A contains the input variables used to define boundary conditions and model parameters in the steady-state and transient models, as well as the water budget for both the pumping and non-pumping transient models.

APPENDIX A

Table 9: Transient model stress period set-up and model input variables. Stress period setup includes the month and year of each period, the period length in days, and the number of time steps per stress period. Model input variables include upgradient streamflow in (m³/d), stream depth (m), stream width (m), streambed hydraulic conductivity (K) in (m/d), evapotranspiration (ET) rate in (mm/d), evapotranspiration (ET) extinction depth (m), specific storage (Ss), specific yield (Sy), porosity, aquifer horizontal hydraulic conductivity (Kh) in (m/d), and aquifer vertical hydraulic conductivity (Kv) in (m/d).

Stress Period (Month & Year)	Stress Period Length (d)	Time Steps	Upgradient Streamflow (m ³ /d)	Stream Depth (m)	Stream Width (m)	Streambed K (m/d)	ET Rate (mm/day)	ET Extinction Depth (m)	Ss	Sy	Porosity	Aquifer Kh (m/d)	Aquifer Kv (m/d)
1 (Sep 2009)	10	240	489318	0.43	25	18	0.0021	3	0.00007	0.2	0.2	90	17.5
2 (Sep 2012)	10	120	244659	0.28	25	18	0.0021	3	0.00007	0.2	0.2	90	17.5
3 (Sep 2012)	10	40	65446	0.18	25	18	0.0021	3	0.00007	0.2	0.2	90	17.5
4 (Oct 2012)	31	31	83366	0.19	25	18	0.0003	3	0.00007	0.2	0.2	90	17.5
5 (Nov 2012)	30	30	101060	0.20	25	18	0	3	0.00007	0.2	0.2	90	17.5
6 (Dec 2012)	31	31	129393	0.22	25	18	0	3	0.00007	0.2	0.2	90	17.5
7 (Jan 2013)	31	31	222119	0.27	25	18	0	3	0.00007	0.2	0.2	90	17.5
8 (Feb 2013)	28	28	89938	0.19	25	18	0	3	0.00007	0.2	0.2	90	17.5
9 (Mar 2013)	31	31	44867	0.17	25	18	0	3	0.00007	0.2	0.2	90	17.5
10 (Apr 2013)	30	30	342123	0.34	25	18	0	3	0.00007	0.2	0.2	90	17.5
11 (May 2013)	31	31	133087	0.22	25	18	0.0021	3	0.00007	0.2	0.2	90	17.5
12 (Jun 2013)	30	30	64590	0.18	25	18	0.0027	3	0.00007	0.2	0.2	90	17.5
13 (Jul 2013)	31	31	53304	0.17	25	18	0.0030	3	0.00007	0.2	0.2	90	17.5
14 (Aug 2013)	31	31	55103	0.17	25	18	0.0030	3	0.00007	0.2	0.2	90	17.5

Table 10: Pumping well geographic location, depth, and screen location. Coordinate system: NAD 1983, UTM 13N

Pumping Well	X Coordinate (m)	Y Coordinate (m)	Elevation below surface (m)	Depth of Well (m)	Screened Interval Elevation (m)	Screened Interval Length (m)
R1	687728	4523920	1111.89	16.76	1119.52- 1113.42	6.1
R2	687248	4523560	1111.01	19.20	1118.63- 1112.53	6.1
R3	688154	4524060	1091.09	37.49	1116.38-1110.29	6.1
R4	694317	4526390	1081.63	41.76	1106.01- 1099.91	6.1
R5	687484	4523740	1111.42	17.07	1119.04- 1112.95	6.1
R6	687973	4523950	1096.79	31.09	1110.81- 1104.72	6.1
R7	688375	4524160	1096.13	31.09	1104.36- 1098.26	6.1
R8	688548	4524270	1095.82	31.39	1104.96- 1098.87	6.1
R9	694457	4526470	1068.03	55.78	1094.39-1088.29	6.1
R10	694573	4526570	1063.36	58.83	1101.30- 1095.21	6.1

Table 11: Transect of faux bedrock points along the eastern model boundary used in Kriging, to create the confining unit surface.

Faux Point	X Coordinate (m)	Y Coordinate (m)	Depth of Western Point (m)	Depth of Eastern Point (m)	Distance Weighting Factor (West)	Distance Weighting Factor (East)	Faux Depth (m)
1	70098	4532071	8.721	11.125	0.63	0.37	9.615
2	700351	4531501	6.984	13.961	0.63	0.37	9.577
3	700584	4530910	10.776	9.809	0.63	0.37	10.417
4	700795	4530277	16.431	26.570	0.63	0.37	20.199
5	701090	4529560	24.966	26.570	0.63	0.37	25.562
6	701343	4528926	88.199	26.570	0.63	0.37	65.297
7	701639	4528251	35.467	7.315	0.63	0.37	25.005

Table 12: Simulated water budgets (m³/d) for the pumping and non-pumping transient models

Transient Simulation: No Pumping Inflow (m ³ /d)							Transient Simulation: No Pumping Outflow (m ³ /d)					
Stress Period	Western Underflow	Stream Leakage	Storage	Recharge	Wells	Total	Eastern Underflow	Stream Leakage	Storage	ET	Wells	Total
1	18701	29315	235	1039	0	49290	-7319	-14994	-22	-26644	0	-48979
2	18932	16892	20777	1039	0	57640	-6900	-23857	-19	-26640	0	-57416
3	19278	12445	31192	1039	0	63954	-6344	-30791	-10	-26633	0	-63777
4	19333	12805	7749	1039	0	40925	-6285	-30113	-113	-3805	0	-40315
5	19323	12755	4538	1039	0	37655	-6351	-30248	-400	0	0	-36999
6	19292	13380	2727	1039	0	36439	-6447	-28971	-538	0	0	-35956
7	19112	15112	1500	1039	0	36763	-6755	-26110	-3231	0	0	-36096
8	19381	12133	6030	1039	0	38582	-6341	-31598	-47	0	0	-37986
9	19588	11650	7113	1039	0	39390	-6095	-32705	-2	0	0	-38802
10	19005	18253	1264	1039	0	39561	-7039	-22354	-9490	0	0	-38883
11	19466	17257	7602	1039	0	45364	-6326	-23217	0	-15219	0	-44764
12	19917	23601	14234	1039	0	58791	-5741	-18219	0	-34230	0	-58190
13	20121	27170	12226	1039	0	60556	-5504	-16397	0	-38027	0	-59928
14	20209	28805	9646	1039	0	59699	-5421	-15636	0	-38025	0	-59082
Transient Simulation: Pumping Inflow (m ³ /d)							Transient Simulation: Pumping Outflow (m ³ /d)					
1	18701	29315	235	1039	0	49290	-7319	-14994	-22	-26644	0	-48979
2	18932	16892	20777	1039	0	57640	-6900	-23857	-19	-26640	0	-57416
3	19278	12445	31192	1039	0	63954	-6344	-30791	-10	-26633	0	-63777
4	19333	12805	7749	1039	0	40925	-6285	-30113	-113	-3805	0	-40315
5	19323	12755	4538	1039	0	37655	-6351	-30248	-400	0	0	-36999
6	19277	23080	2677	1039	29966	76038	-6398	-25710	-13309	0	-29966	-75383
7	18928	39361	1232	1039	65176	125736	-6664	-23601	-29664	0	-64176	-125105
8	18811	34724	4481	1039	67246	126301	-6214	-29181	-23004	0	-67246	-125645
9	18453	31839	4819	1039	66287	122437	-5954	-31409	-18114	0	-66287	-121764
10	17348	14732	17570	1039	0	50689	-7034	-27360	-15666	0	0	-50060
11	17628	14545	18425	1039	0	51637	-6343	-28039	-1487	-15222	0	-51092
12	18187	20209	22434	1039	0	61869	-5768	-20867	-396	-34238	0	-61269
13	18590	23941	18803	1039	0	62374	-5534	-18190	-43	-38034	0	-61801
14	18881	26040	15196	1039	0	61156	-5449	-17031	0	-38031	0	-60510

APPENDIX B – Groundwater-Surface Water Flux and Stream Depth Plots

Appendix B contains plots of simulated groundwater-surface water flux and simulated stream depth, with and without pumping, for each stress period in the transient model.

APPENDIX B

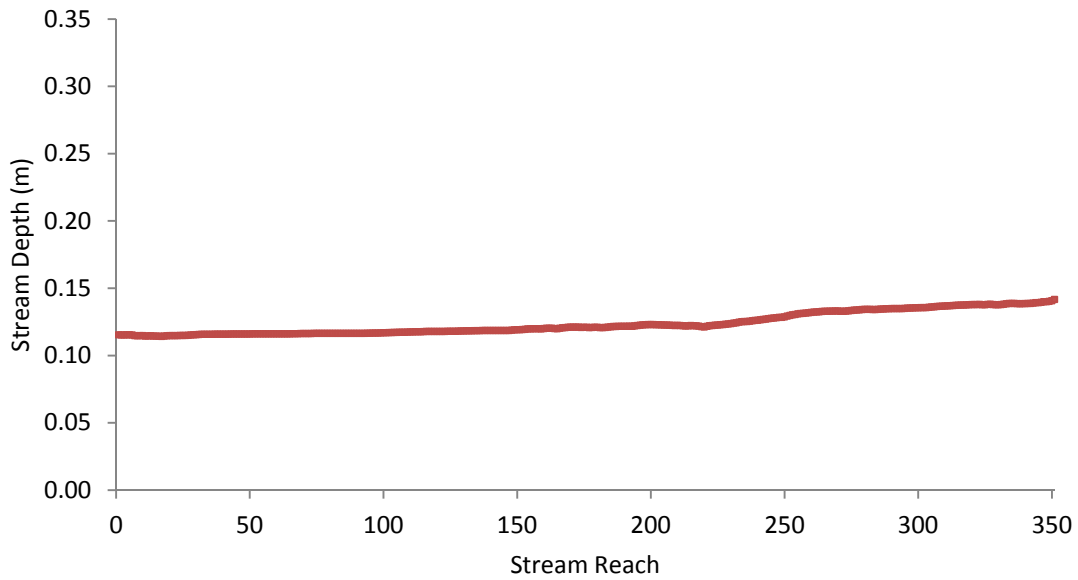


Figure 30: Simulated stream depth, with and without pumping, for each stream reach, 30 September 2013. Stream reaches are sequentially numbered from 0, the furthest upstream reach, to 351, the furthest downstream reach

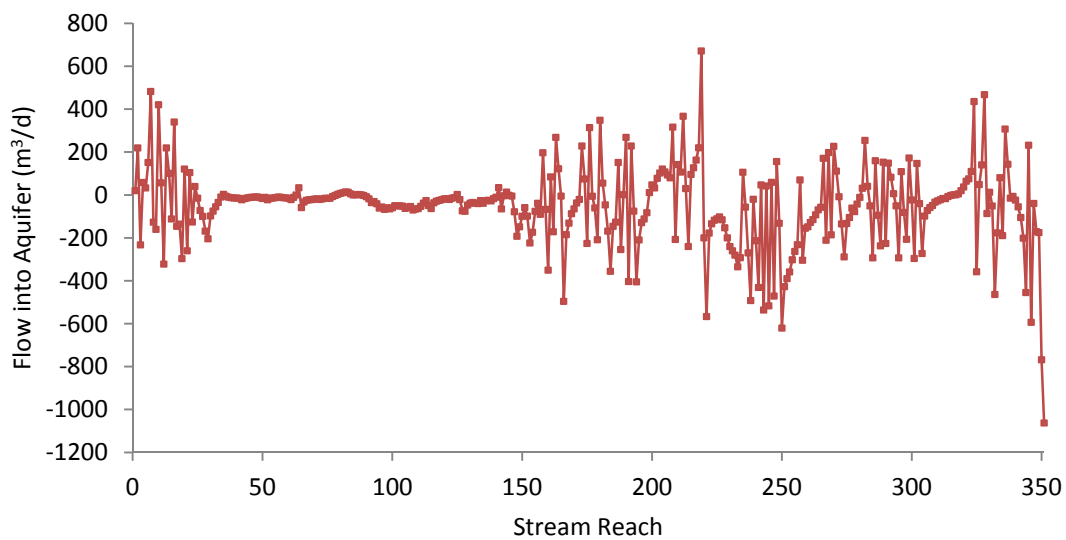


Figure 31: Simulated groundwater/surface water flux rate, with and without pumping, for each stream reach, 30 September 2013. Stream reaches are sequentially numbered from 0, the furthest upstream reach, to 351, the furthest downstream reach.

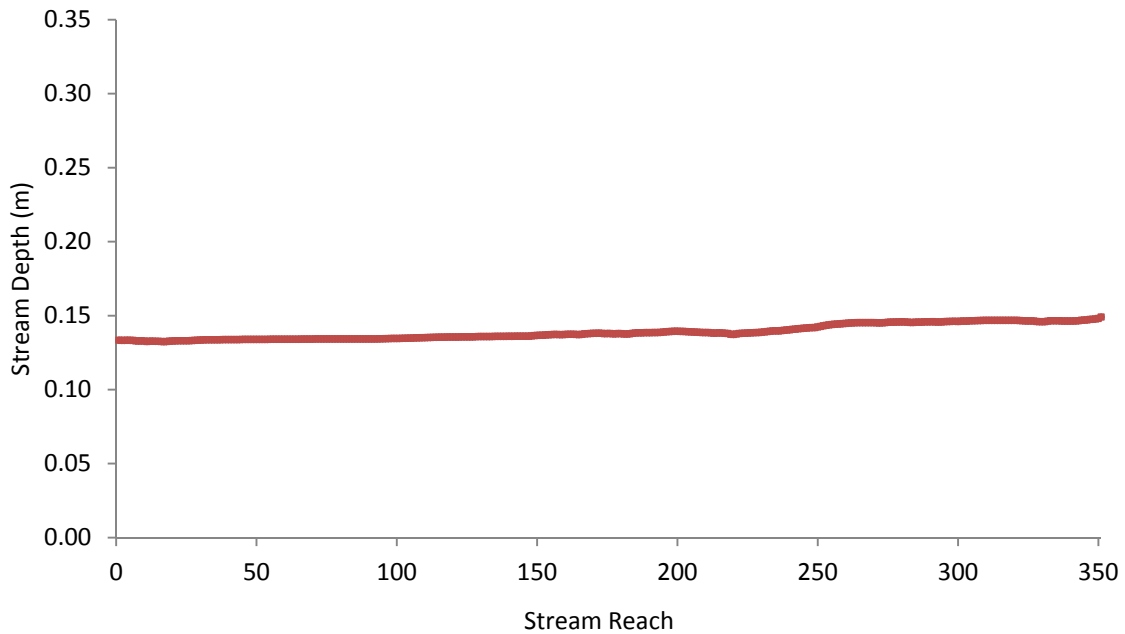


Figure 32: Simulated stream depth, with and without pumping, for each stream reach, 31 October 2013. Stream reaches are sequentially numbered from 0, the furthest upstream reach, to 351, the furthest downstream reach

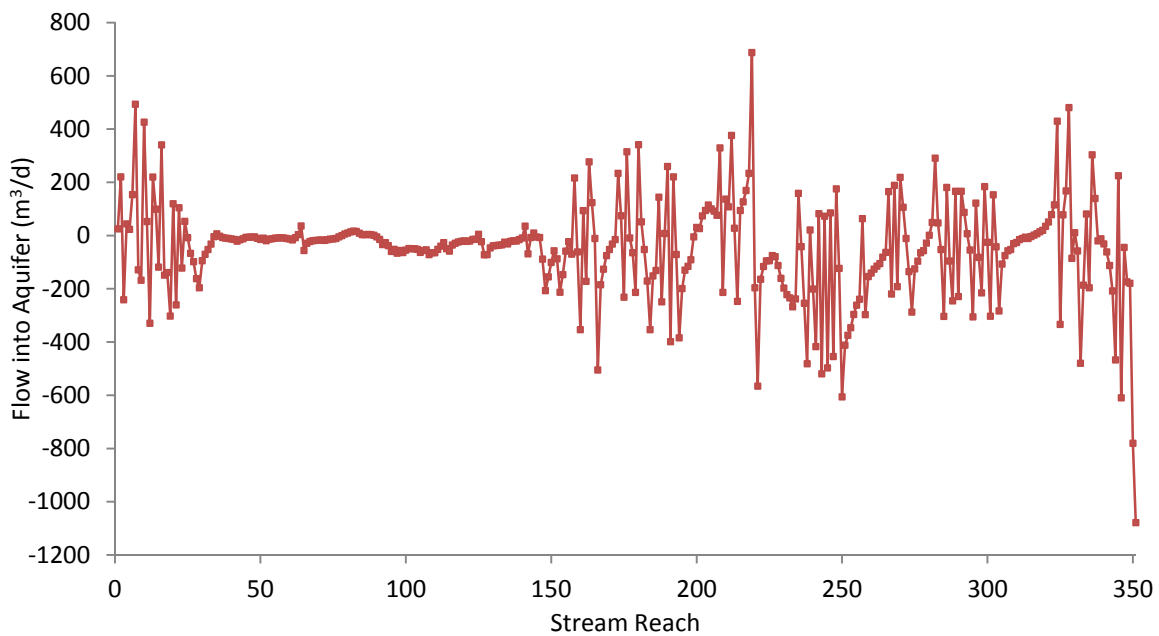


Figure 33: Simulated groundwater/surface water flux rate, with and without pumping, for each stream reach, 31 October 2013. Stream reaches are sequentially numbered from 0, the furthest upstream reach, to 351, the furthest downstream reach.

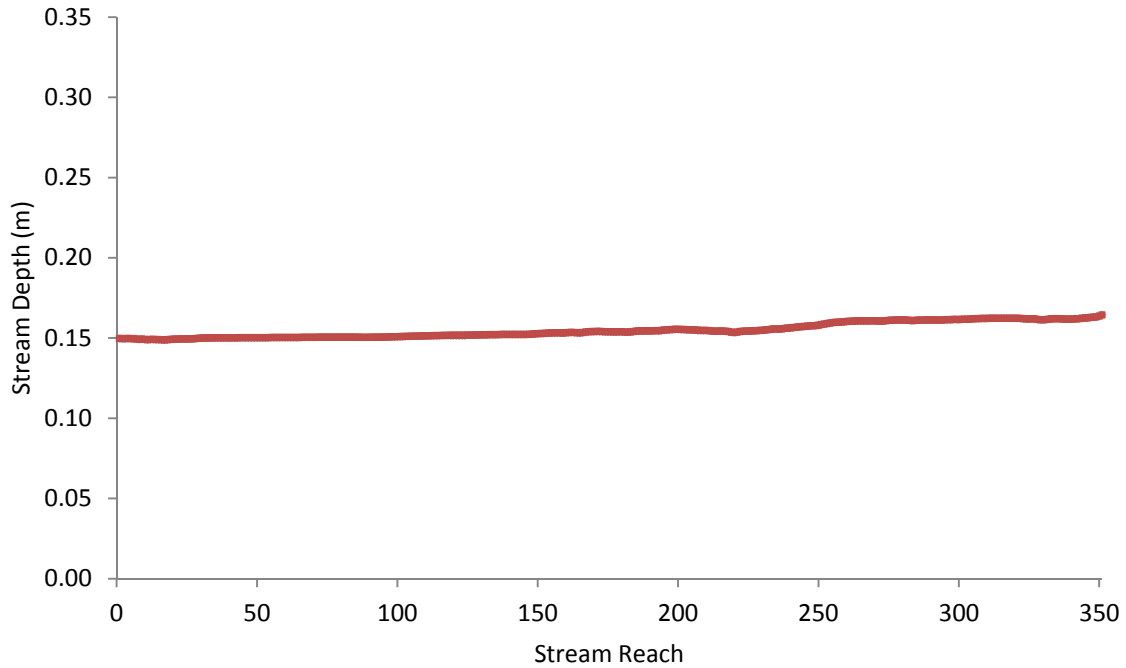


Figure 34: Simulated stream depth, with and without pumping, for each stream reach, 30 November 2013. Stream reaches are sequentially numbered from 0, the furthest upstream reach, to 351, the furthest downstream reach

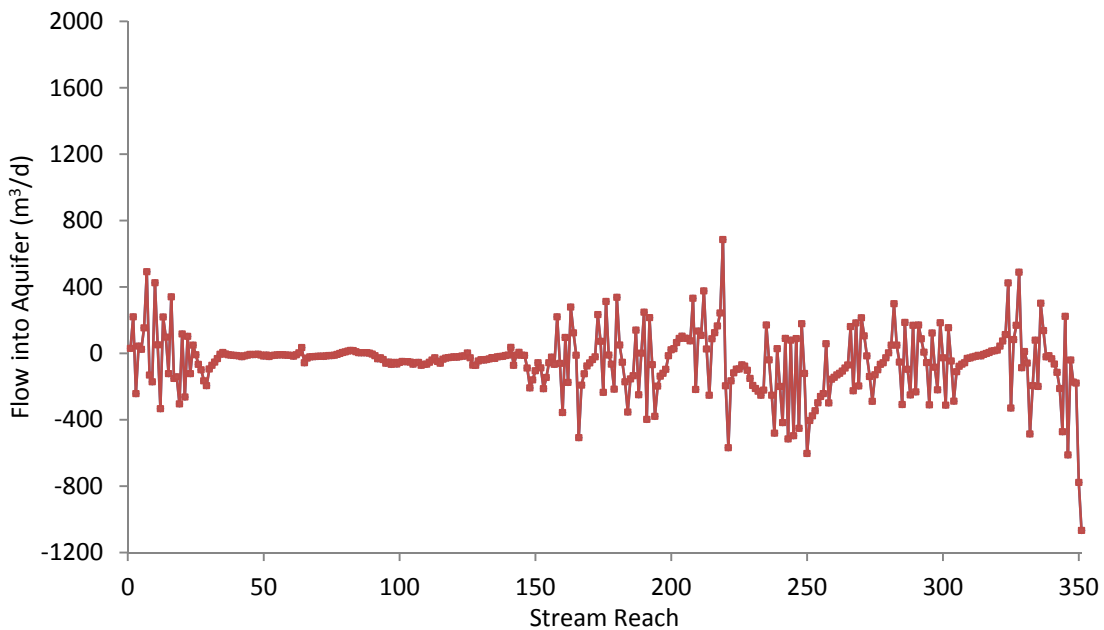


Figure 35: Simulated groundwater/surface water flux rate, with and without pumping, for each stream reach, 30 November 2013. Stream reaches are sequentially numbered from 0, the furthest upstream reach, to 351, the furthest downstream reach.

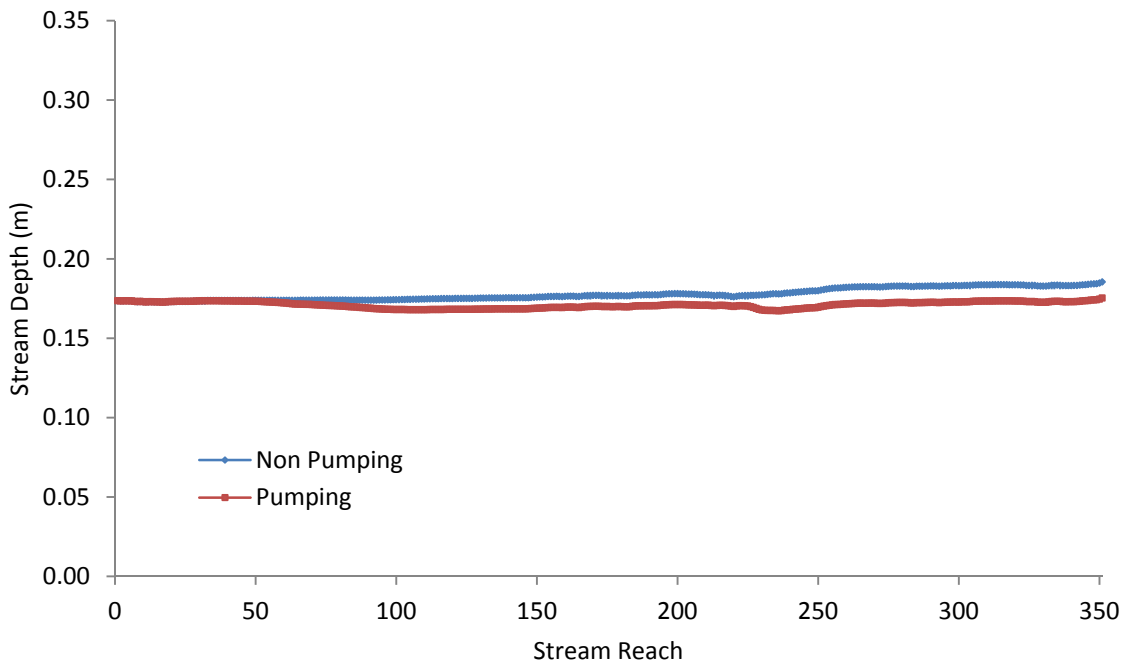


Figure 36: Simulated stream depth, with and without pumping, for each stream reach, 31 December 2013. Stream reaches are sequentially numbered from 0, the furthest upstream reach, to 351, the furthest downstream reach

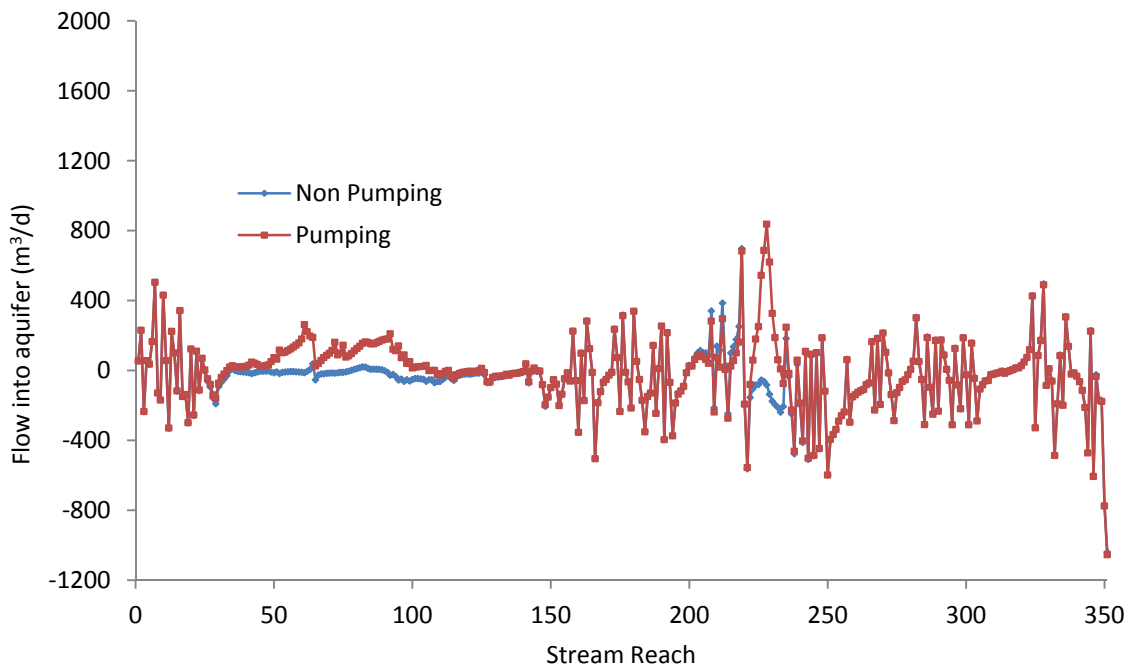


Figure 37: Simulated groundwater/surface water flux rate, with and without pumping, for each stream reach, 31 December 2013. Stream reaches are sequentially numbered from 0, the furthest upstream reach, to 351, the furthest downstream reach.

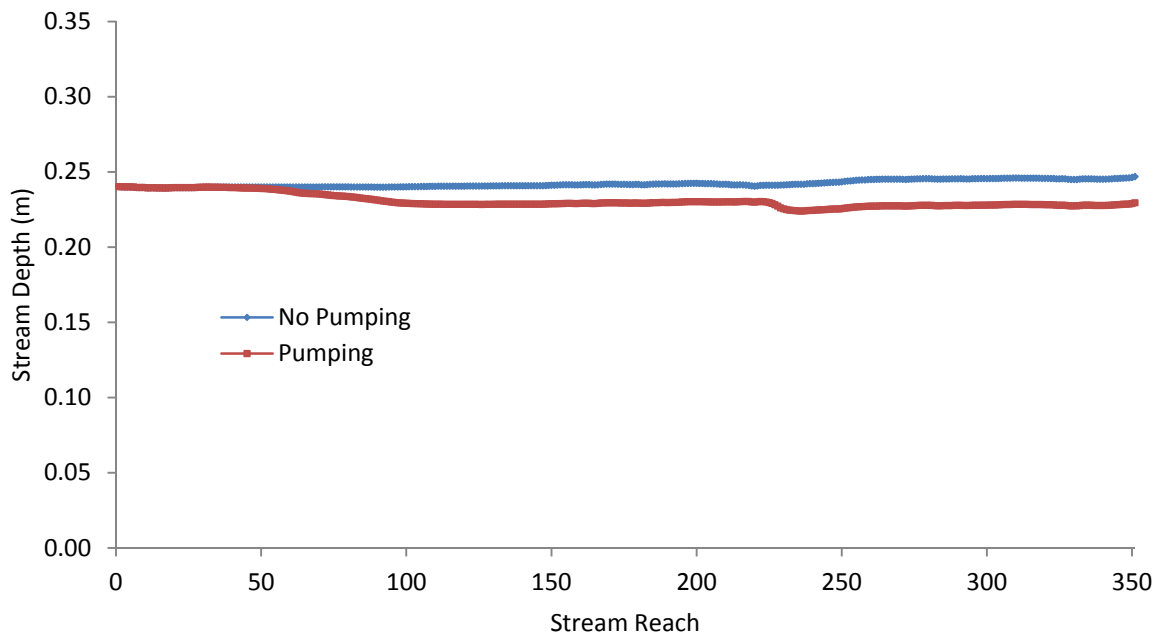


Figure 38: Simulated stream depth, with and without pumping, for each stream reach, 31 January 2013. Stream reaches are sequentially numbered from 0, the furthest upstream reach, to 351, the furthest downstream reach

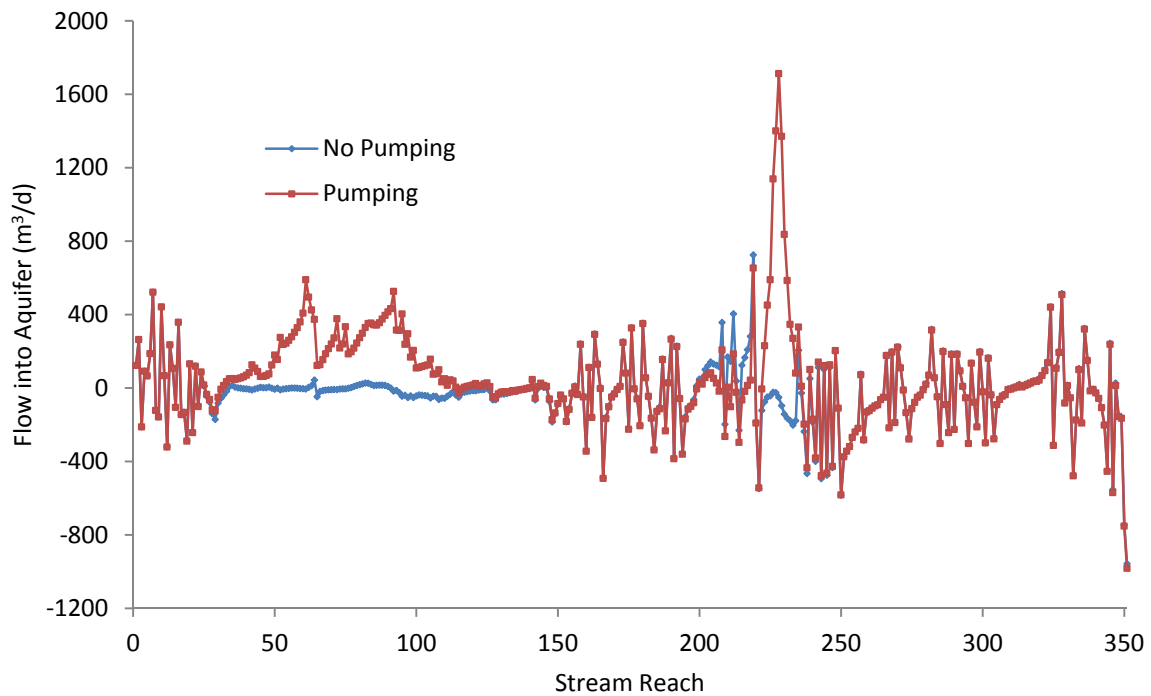


Figure 39: Simulated groundwater/surface water flux rate, with and without pumping, for each stream reach, 31 January 2013. Stream reaches are sequentially numbered from 0, the furthest upstream reach, to 351, the furthest downstream reach.

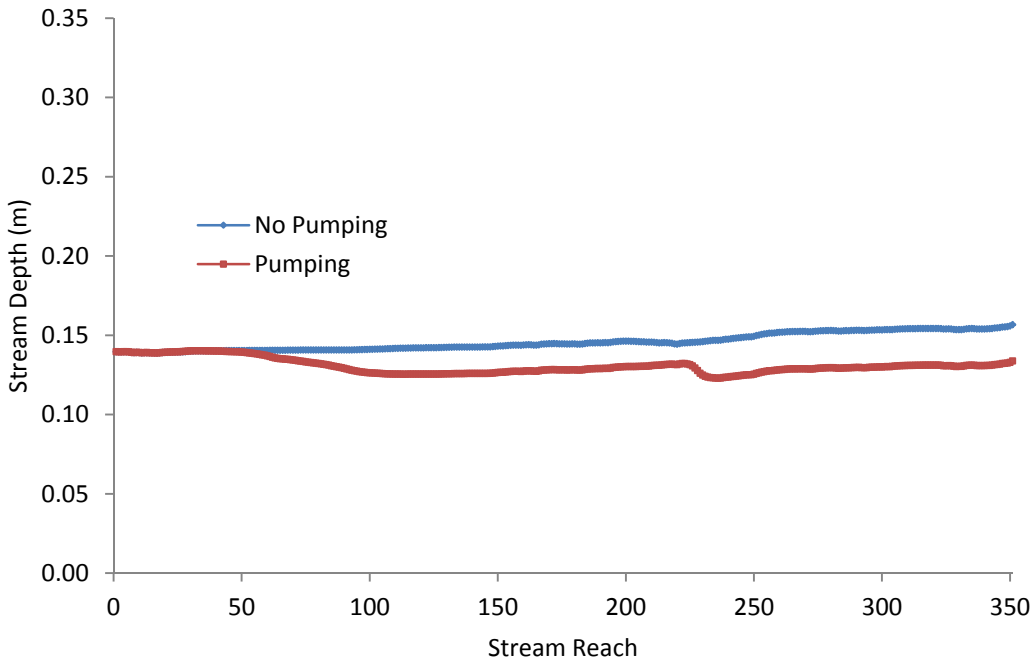


Figure 40: Simulated stream depth, with and without pumping, for each stream reach, 28 February 2013. Stream reaches are sequentially numbered from 0, the furthest upstream reach, to 351, the furthest downstream reach

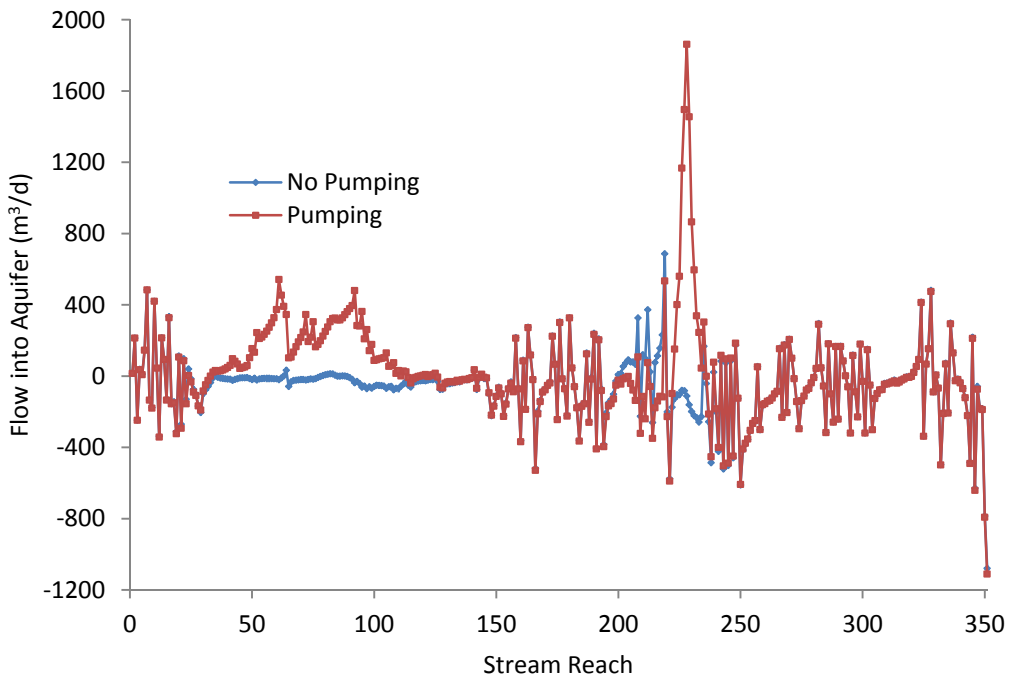


Figure 41: Simulated groundwater/surface water flux rate, with and without pumping, for each stream reach, 28 February 2013. Stream reaches are sequentially numbered from 0, the furthest upstream reach, to 351, the furthest downstream reach.

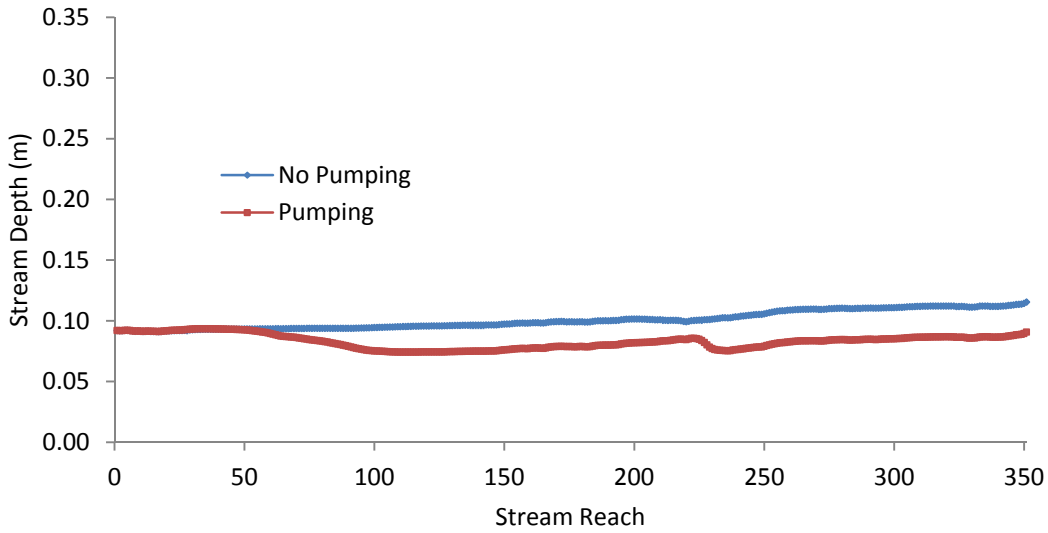


Figure 42: Simulated stream depth, with and without pumping, for each stream reach, 31 March 2013. Stream reaches are sequentially numbered from 0, the furthest upstream reach, to 351, the furthest downstream reach

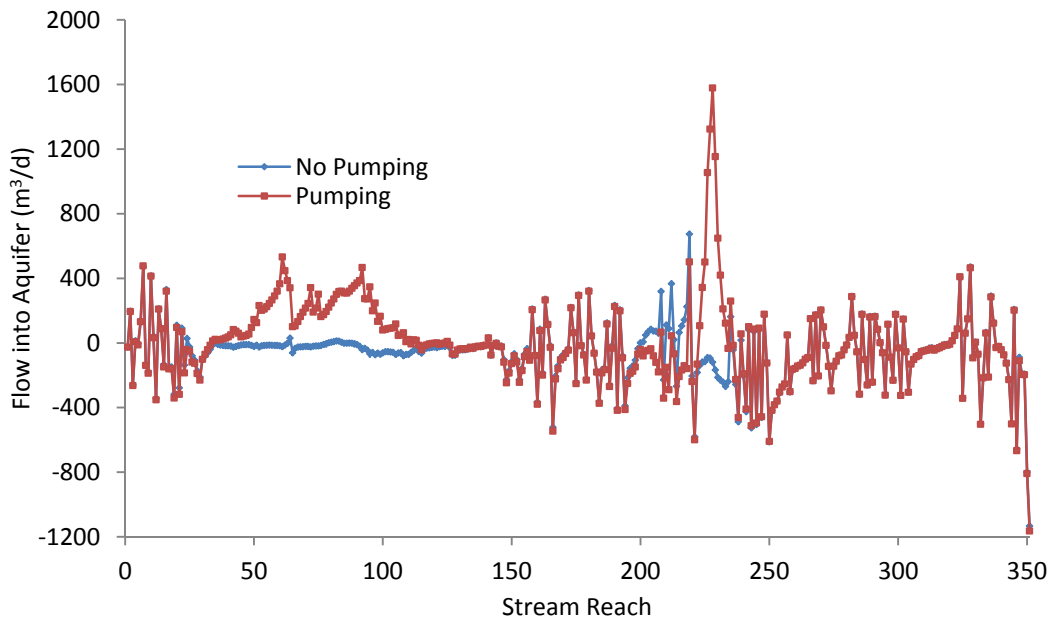


Figure 43: Simulated groundwater/surface water flux rate, with and without pumping, for each stream reach, 31 March 2013. Stream reaches are sequentially numbered from 0, the furthest upstream reach, to 351, the furthest downstream reach.

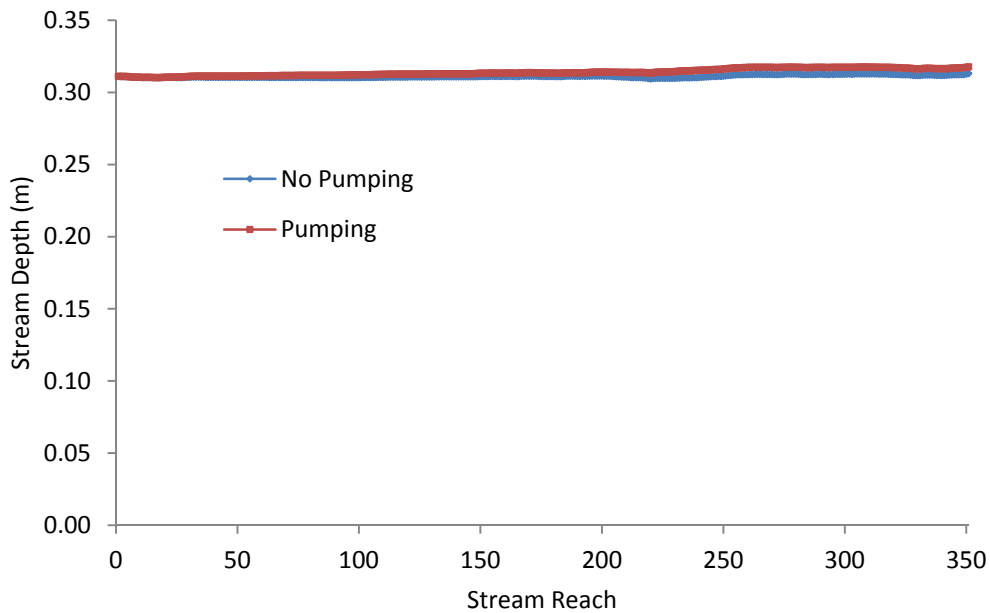


Figure 44: Simulated stream depth, with and without pumping, for each stream reach, 30 April 2013. Stream reaches are sequentially numbered from 0, the furthest upstream reach, to 351, the furthest downstream reach

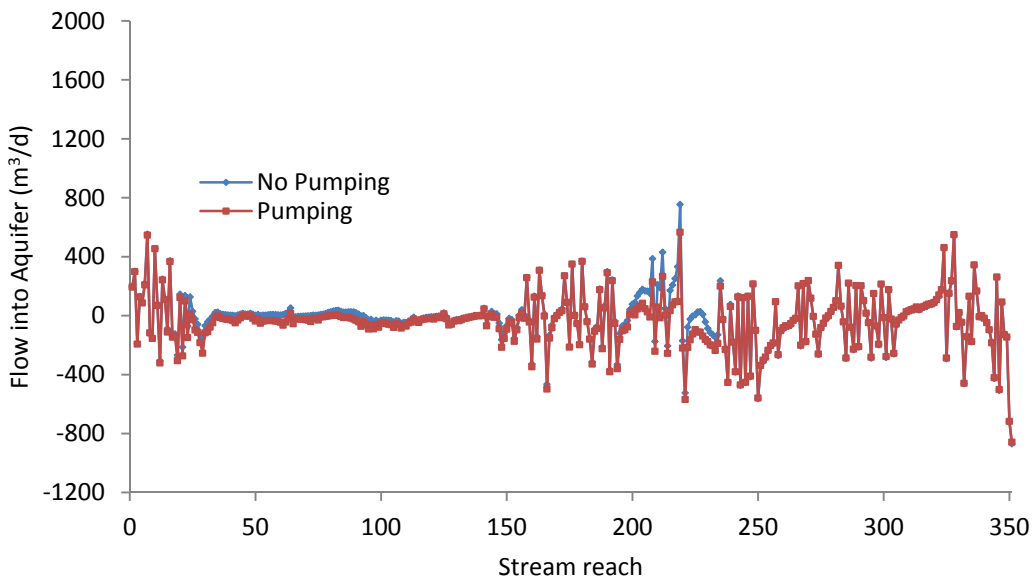


Figure 45: Simulated groundwater/surface water flux rate, with and without pumping, for each stream reach, 30 April 2013. Stream reaches are sequentially numbered from 0, the furthest upstream reach, to 351, the furthest downstream reach.

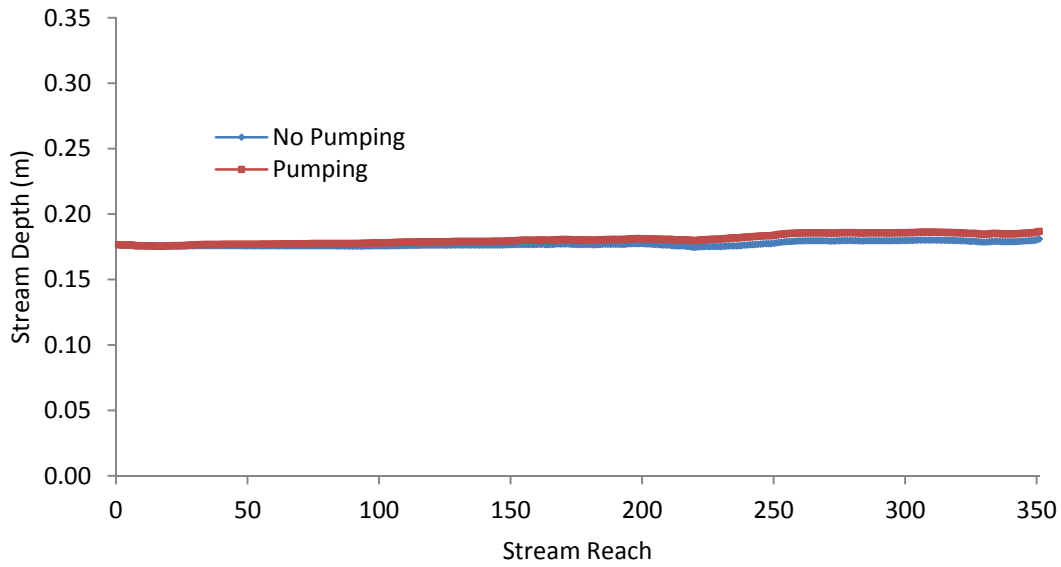


Figure 46: Simulated stream depth, with and without pumping, for each stream reach, 31 May 2013. Stream reaches are sequentially numbered from 0, the furthest upstream reach, to 351, the furthest downstream reach

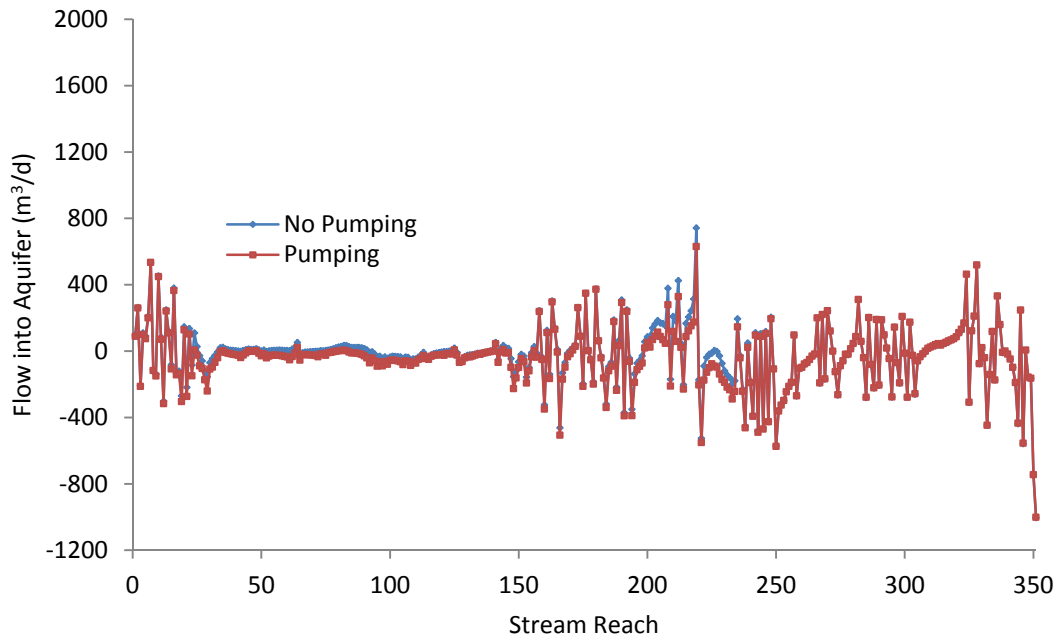


Figure 47: Simulated groundwater/surface water flux rate, with and without pumping, for each stream reach, 31 May 2013. Stream reaches are sequentially numbered from 0, the furthest upstream reach, to 351, the furthest downstream reach.

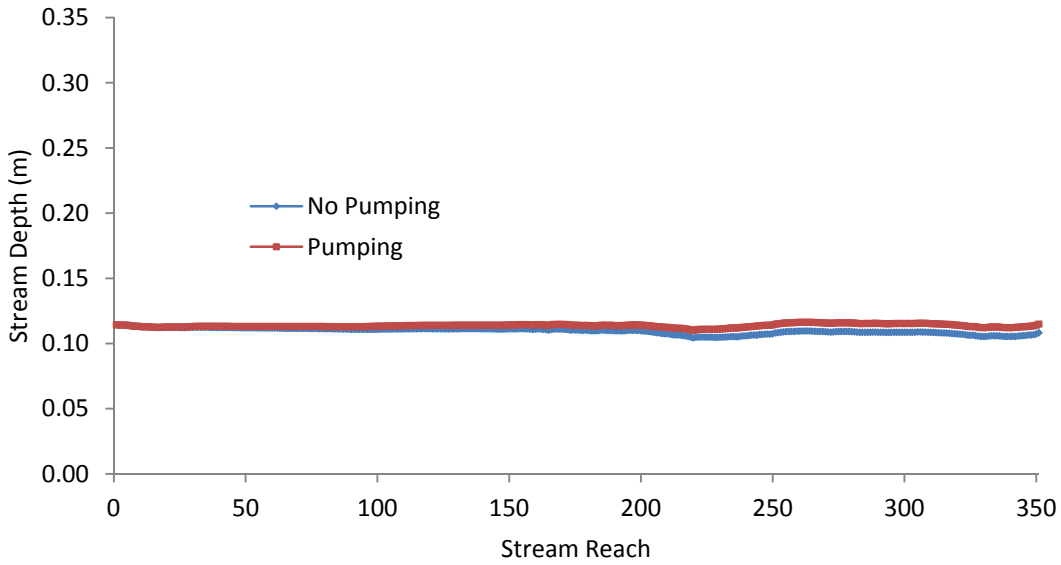


Figure 48: Simulated stream depth, with and without pumping, for each stream reach, 30 June 2013. Stream reaches are sequentially numbered from 0, the furthest upstream reach, to 351, the furthest downstream reach

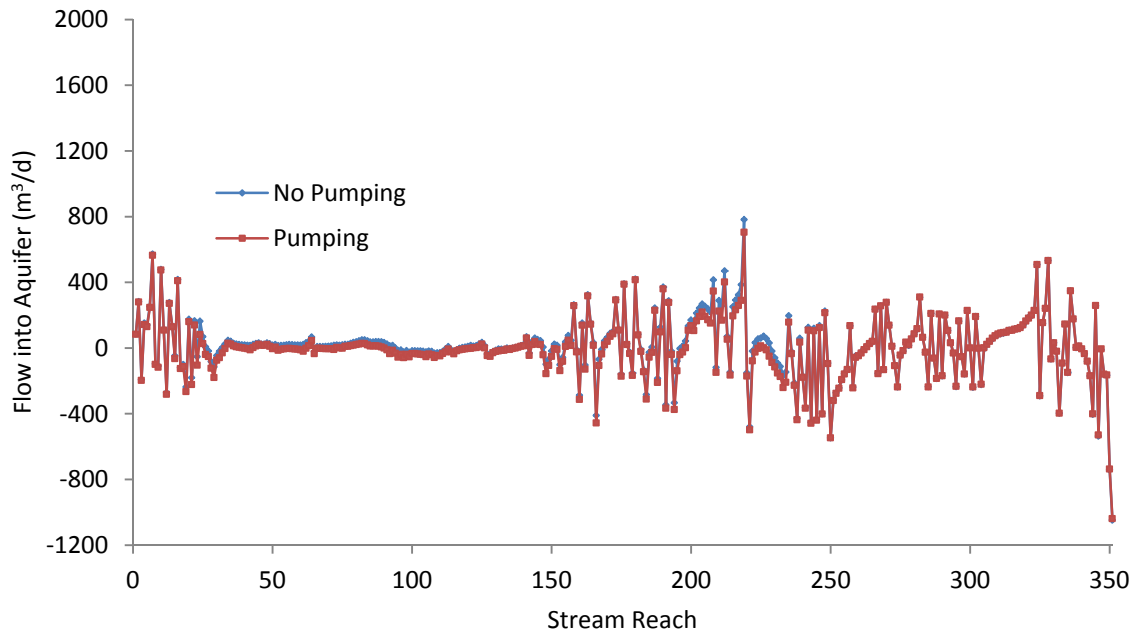


Figure 49: Simulated groundwater/surface water flux rate, with and without pumping, for each stream reach, 30 June 2013. Stream reaches are sequentially numbered from 0, the furthest upstream reach, to 351, the furthest downstream reach.

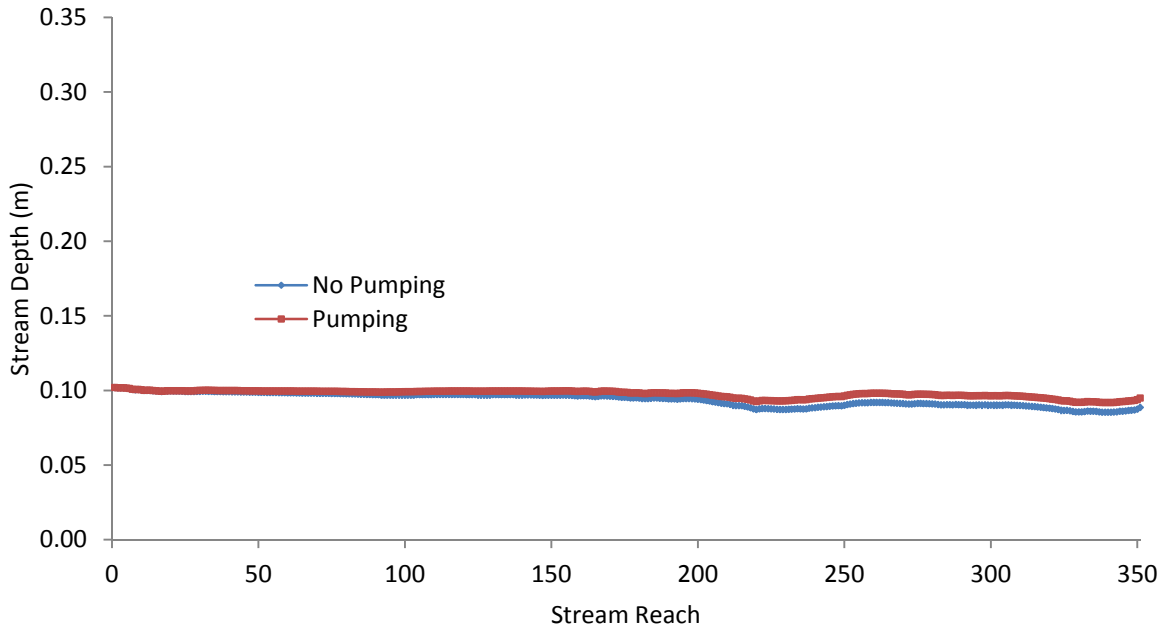


Figure 50: Simulated stream depth, with and without pumping, for each stream reach, 31 July 2013. Stream reaches are sequentially numbered from 0, the furthest upstream reach, to 351, the furthest downstream reach

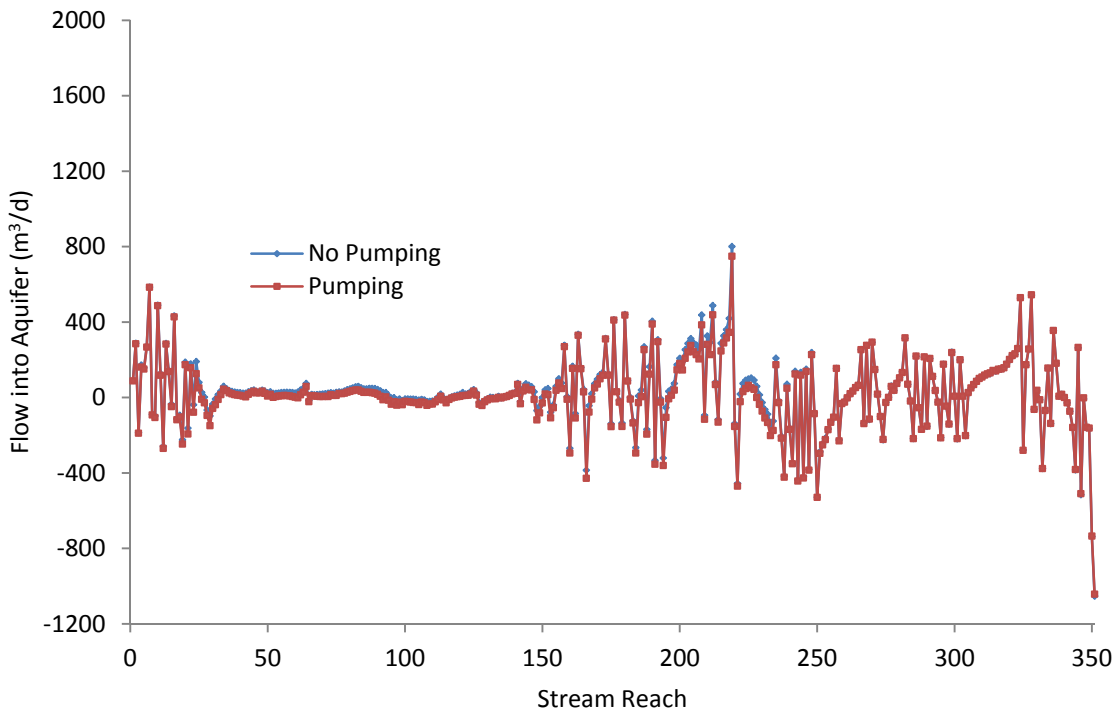


Figure 51: Simulated groundwater/surface water flux rate, with and without pumping, for each stream reach, 31 July 2013. Stream reaches are sequentially numbered from 0, the furthest upstream reach, to 351, the furthest downstream reach.

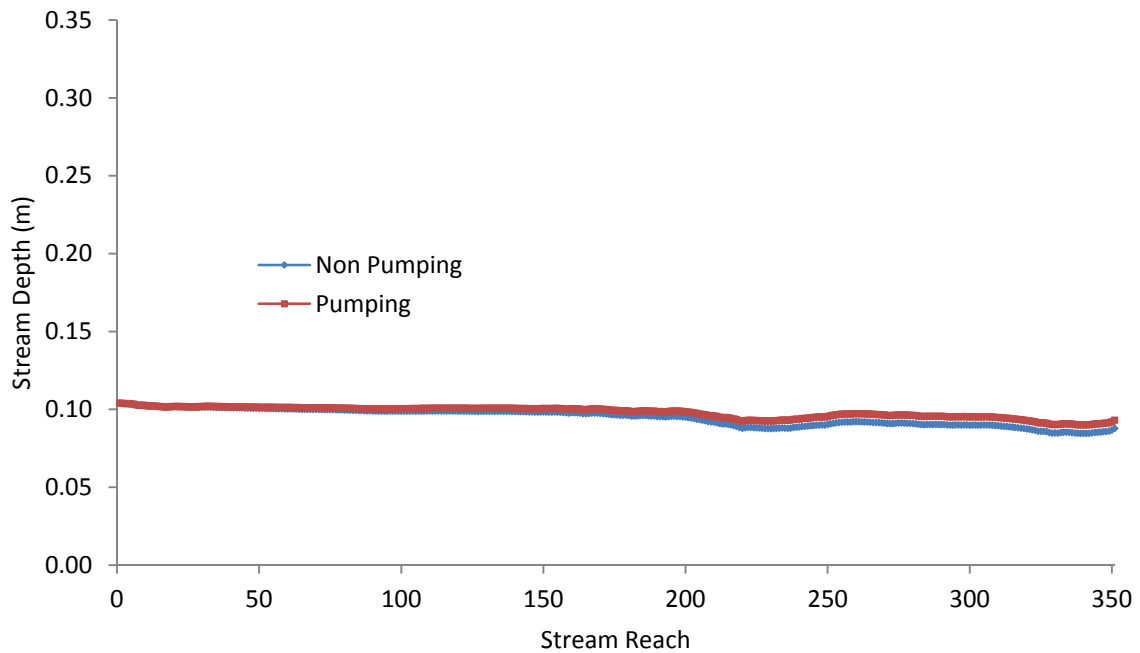


Figure 52: Simulated stream depth, with and without pumping, for each stream reach, 31 August 2013. Stream reaches are sequentially numbered from 0, the furthest upstream reach, to 351, the furthest downstream reach

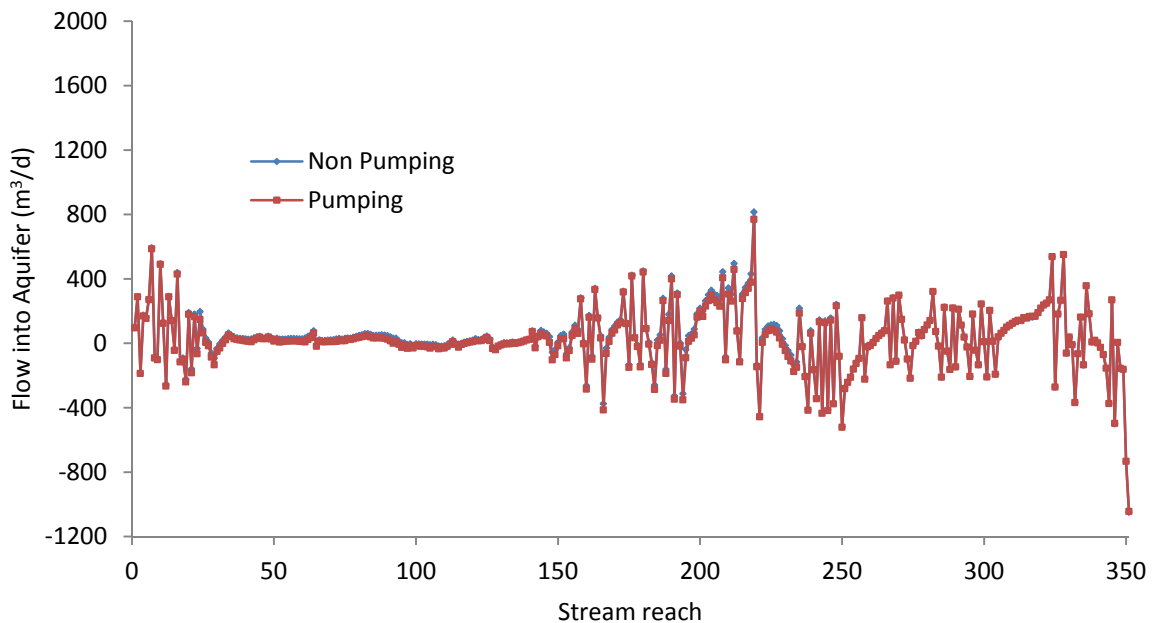


Figure 53: Simulated groundwater/surface water flux rate, with and without pumping, for each stream reach, 31 August 2013. Stream reaches are sequentially numbered from 0, the furthest upstream reach, to 351, the furthest downstream reach.